A THEORETICAL AND FIELD STUDY OF LOAD TRANSMISSION THROUGH GROUNDED ICE RUBBLE

ALFRED R. MARSHALL, B.Eng

A THEORETICAL AND FIELD STUDY OF LOAD TRANSMISSION THROUGH GROUNDED ICE RUBBLE

by

© Alfred R. Marshall, B.Eng

A thesis submitted to the School of Graduate Studies
in partial fulfillment of the requirements for the degree of
Master of Engineering

Faculty of Engineering and Applied Science
Memorial University of Newfoundland
St. John's, Newfoundland
Canada

September 1990

ISBN 0-315-65363-9

Aerial view of Caisson Retained Island (CRI) at Kaubvik, May 1987.

To Lisa

ABSTRACT

Oil exploration from artificial Islands in the Beaufort Sea has shown that grounded ice rubble fields often accumulate around such structures, preventing moving ice from acting directly against the structure. A simple, rigid body model, has commonly been used to estimate the load "seen" by the structure, with the result that no loading is expected until global rubble sliding occurs. It was realized that such an approach is not entirely realistic and so a collaborative field program was carried out, followed by theoretical modelling. The field work was done at a drilling location in the southern Beaufort Sea on ESSO's Caisson Retained Island (CRI). The three groups involved were ESSO Resources Canada Ltd., National Research Council of Canada (NRC) and Memorial University of Newfoundland (M.U.N.). The M.U.N. data and subsequent theoretical work is presented here, with the ESSO and NRC data summarized in the site description.

Memorial University collected data from pressure sensor rosettes, a strain array, thermocouple arrays, rubble profiling, and ice property measurements. The most important data came from the pressure sensor rosettes and the thermocouple arrays. These indicated that average sea ice pressures against the rubble reached 350 kPa, and that a substantial and rapidly formed refrozen layer existed within the rubble, with a thickness exceeding 3 m near the rubble field periphery.

Based on the field measurements, a theoretical model was developed to investigate the role of the rubble refrozen layer in load transmission through rubble. The rubble field was modelled as a system of springs and dampers to represent the elastic, frictional, and viscous stiffness of the various load paths. The deformations and load distributions were calculated using a commercial finite element package called ABAQUS. Each material property was assumed to have a range of values, the limits of which were determined from the literature, theoretical considerations and field measurements.

The sensitivity of the output to each of the inputs was examined and the following was concluded;

1. From the analysis it appears that the elastic response of the rubble leads to the highest loads on the embedded structure because the transmitted load tends to decrease with time (creep).
2. The ice rubble properties that are the most important for further study are the delayed elastic and shear properties of un-refrozen rubble, as well as their variability within natural rubble fields.
3. Significant loads may be transmitted through ice rubble to a structure before global sliding of the rubble field occurs.
4. The presence of the refrozen layer gives the potential for substantial loads to be imposed on the structure during rubble field movement.
5. Possible future improvements to the ABAQUS computer model include the incorporation of; refrozen layer discontinuities, berm slope, non-rigid structure behaviour, kinetic and static friction values (rather than an average), and water and ice mass. Furthur research is also required on ice/rubble failure modes to esablish design pressures at the rubble field boundaries.
6. The sample 3D calculations show that viscous deformation may also be important, although it is also clear that the 3D method presented needs improvement.

KEY WORDS

Sea ice, sea-ice, ice rubble, ice loads, landfast ice, rubble fields, Kaubvik, artificial islands, Beaufort Sea, pressure sensors, strain array, thermocouple array, refrozen layer, consolidated layer, ABAQUS, computer model.

ACKNOWLEDGEMENTS

It has taken three years to complete this thesis, during which time many people have helped in some way. I would like to take this opportunity to thank them, as well as to acknowledge their contributions, and I can only hope that I have lived up to their expectations. To begin with, I would like to thank my supervisor, Dr. Ian J. Jordaan for inviting me to take part in this project, and for his time, guidance, generous financial support, and benevolent sharing of academic credit. I would also like to thank Dr. Richard F. McKenna, who acted as an unofficial supervisor, unselfishly providing advice, assistance, and encouragement. For their financial support, I am grateful to the Natural Sciences and Engineering Research Council for funding the field work, and the Provincial Government of Newfoundland for awarding me career development funding. I would like to express my gratitude to those members of the field project team with whom I have had the most contact, Dr. Ken R. Croasdale, Charles Der, Dr. Mohammed Sayed, Dr. Bob W. Frederking, Dr. Jean-Paul Nadreau, and Eugene Guy; thank you for your advice and patient replies to all my questions. Finally, I would like to thank some of my fellow graduate students, Sanjay Singh, David Finn, John Cross, and Jing Xiao for helping me with later field measurements at Hogan's Pond.

Contents

List of Figures

List of Tables

SYMBOLS AND NOMENCLATURE

A_r	Rubble field area (m^2)
a_T	Delaved elasticity exponent (/s)
b	Constant (0.34)
C	Constant
C_C	Un-refrozen rubble compaction creep modulus (m^2/s N)
C_d	Drag coefficient
C_{RL}	Refrozen layer creep modulus (m^3/s N^3)
C_S	Un-refrozen rubble shear creep modulus (m^3/s N^3)
D	Structure diameter (m)
D_C	Compaction creep damper (N s/m)
D_{RL}	Refrozen layer viscous damper (N^3 s/m)
D_S	Shear creep damper (N^3 s/m)
d	Grain diameter (mm)
d_1	Reference grain diameter (1 mm)
E	Young's Modulus (N/m^2)
E_C	Un-refrozen rubble compaction modulus (N/m^2)
E_i	Young's Modulus for ice (saline ice) (N/m^2)
E_{xt}	Rubble field extent (m)
F	Force (N)
F_a	Applied force (N)
F_L	Force per meter width (N/m)
F_s	Force on structure (N)
G	Shear Modulus (Pa)
G_r	Un-refrozen rubble shear modulus (N/m^2)
g	Acceleration due to gravity ($9.81\ m/s^2$)
H	Sail height (m)
H_i	Average height of rubble above water (m)
H_k	Average depth of rubble below water (m)
H_s	Average sail height (m)
H_w	Water depth (m)
K	Constant
n	Power law flow exponent (usually ≈ 3 for ice)
N_s	Number of sails
P	Porosity (%)
Q	Activation energy (J/mole)
q	Heat flow rate (J/s)
q_l	Latent heat of freezing (J/kg)
R	Universal gas constant (J/mole K)
$S_{1,2}$	Shift function for Sinha's equation
S_C	Compaction spring constant (N/m)

S_{ij}	Stress vector (N/m^2)
S_{RL}	Refrozen layer spring constant (N/m)
S_S	Shear spring constant (N/m)
T_{1and2}	Temperatures (K)
T_f	Freeboard thickness (m)
T_{RL}	Refrozen layer thickness (m)
T_s	Submerged thickness (m)
t	Time (s)
t_i	Ice thickness (m)
v	Velocity (m/s)
W_g	Grounding weight of keel on seabed (N)
W_s	Sail weight at underside of refrozen layer (N)

γ	Shear strain
$\dot{\gamma}$	Shear strain rate (/s)
δ_{Avg}	Average displacement (m)
δ_c	Deformation at the center of the indenter (m)
δ_{RL}	Displacement of refrozen layer (m)
ΔT_g	Thermal gradient (°C/m)
ϵ_e	Elastic strain
ϵ_d	Delayed elastic strain
ϵ_v	Viscous strain
$\dot{\epsilon}_{ij}$	Strain rate vector
$\dot{\epsilon}_{v1}$	Reference strain rate (/s)
λ	Thermal conductivity (W/m k)
μ_{ii}	Ice/ice friction coefficient
μ_{is}	Ice/seabed friction coefficient
μ_{RR}	Refrozen/Un-refrozen rubble friction coefficient
ν	Poisson's Ratio
ρ_i	Density of ice (saline) (kg/m^3)
ρ_w	Density of sea water (kg/m^3)
σ	Applied stress (N/m^2)
σ^1	Reference stress (1 MPa)
σ_n	Normal stress (N/m^2)
τ	Shear stress (N/m^2)
τ_f	Failure shear stress (N/m^2)

1 INTRODUCTION

Continuing demand for oil and gas has pushed the search for these resources into harsher and more remote areas of the world, including the Arctic. Petroleum is often found offshore but the presence of sea ice in the Arctic has made it difficult to use conventional fixed or floating exploration platforms. Consequently artificial island technology was developed to provide year round stable drilling platforms. In 1973 the first artificial island was built in the shallow waters of the Southern Beaufort Sea. This was little more than a leveled-off pile of fill material (sand/gravel) placed in 2-3 m of water. Since then, artificial island technology has progressed from sand bag retained islands to the latest generation of caisson and caisson retained islands. Caisson retainment reduces the volume of fill material and practically eliminates erosion and the risk of ice ride-up. All these developments were required as exploration advanced into deeper water and more mobile ice. The increased ice movement encountered by such islands resulted in a phenomenon not originally encountered, the formation of grounded ice rubble piles around the island.

Ice rubble is a compact mass of ice blocks, fragments, snow and slush that is created when a moving ice sheet fails continuously against a fixed object. If the rubble is unable to clear around the structure (wide structure) it will accumulate as a pile. The pile extends above and below the waterline and can become well enough grounded to resist subsequent ice movements from other directions. If such grounding occurs a "field" of rubble piles may accumulate around the structure.

Initially, it was feared that grounded ice rubble fields might increase global loads on structures by increasing the effective structure diameter. However, subsequent experience and field measurements have indicated that pressures are reduced, and it has become generally accepted that such formations are in fact protective. Nevertheless, full scale properties and pressure distributions were not well enough known to allow a thorough engineering analysis of load transmission through such grounded ice rubble.

The use of external caissons in artificial island construction, not only reduces construction time and costs but also makes island instrumentation much easier. By 1986 ESSO's Caisson Retained Island (CRI) was equipped with 40 external ice pressure sensors, 10 geotechnical sensors, and internal straingauging, making it an ideal platform for the study of island/ice interaction. For this reason, during the winter of 1986/87, ESSO Resources Canada Ltd. collaborated with the National Research Council of Canada (NRC) and Memorial University of Newfoundland (M.U.N.) to conduct an ambitious field study of a grounded ice rubble field. This was done at ESSO's CRI while on location at Kaubvik in the Southern Beaufort Sea. The collaborative program was set up to document thoroughly a full scale case history of sea ice/rubble/structure interaction. The collected data was to be publicly available and was intended to guide subsequent theoretical work on load transmission through grounded ice rubble. A wide variety of data was collected and the field work was arranged so that each group was responsible for collecting, processing, and documenting a certain portion of the data. This data was subsequently released in three separate data reports; Croasdale et al, 1988 (ESSO), Frederking et al, 1988 (NRC), Jordaan et al, 1988 (M.U.N.), followed by a summarizing paper by Marshall et al, 1989.

2 OBJECTIVES

As outlined in the introduction the Kaubvik study was the work of many individuals from several groups. The author's specific responsibilities were to;

- Assist with the field work,
- Process, analyze, and document the field data collected by M.U.N.,
- Review all the data and other literature, and
- Develop a theoretical model for calculating force transmission through grounded ice rubble.

The objectives for this thesis were thus to;

1. Present the M.U.N. data and analysis,
2. Summarize the associated literature,
3. Describe a theoretical method for calculating load transmission through ice rubble,
4. Compare the theoretical calculations with the case study.

The presence of the separate M.U.N. data report gave the author the luxury of being able to concentrate in this thesis on the data more directly concerned with the subsequent theoretical work, since reference for less critical details can be made to Jordaan et al, 1988.

3 LITERATURE REVIEW

3.1 Previous Island-Ice Measurement Programs

The first artificial island in the Beaufort Sea was constructed by ESSO in 1973 (Albery et al, 1984), only 13 winters prior to the Kaubvik program. Instrumentation to measure ice forces and movements around islands immediately became important and most, if not all islands had some sort of ice monitoring program. Many of these programs, however, were set up to collect specific design data such as maximum ice pressure, or for safety purposes such as warning of ice pressure build-up (Templeton III, 1979). Actually analyzing movement events and ice pressures, by correlating them with ice failure modes, wind data, currents, and other environmental forces was of secondary importance; and in many cases grounded rubble did not form. The results of many of these programs are also confidential and this somewhat reduces the literature to be reviewed. The publicly available literature on previous island/ice field measurement programs has been reviewed and is summarized chronologically in table 1.

The main objective of many of these measurement programs was to collect design related data, such as ice thickness, movement, pressure, and global loads on structures. The large number of groups involved resulted in the use of a wide variety of instrument types and measurement procedures, which sometimes produced conflicting results. An enormous amount of data was generated which cannot be comprehensively condensed here. It is, however, intended to summarize enough information so that the important features of the Kaubvik data can be assessed. The sources listed in table 1, provide the following types of data:

Table 1: Summary of island/ice field measurement programs described in the open literature.

YEAR	ISLAND NAME	TYPE	SOURCES
1974	Adgo F-28	sand/gravel	Nelson et al, 1974
1975	Adgo P-25	sand/gravel	Metge, 1976; Nelson et al, 1976
1975	Netserk B-44	sand/gravel	Metge, 1976; Nelson et al, 1976; Kry, 1977
1976	Netserk F-40	sand/gravel	Strilchuk, 1977
1977	Arnak L-30	sand/gravel	Semeniuk, 1977
1977	Kannerk G-42	sand/gravel	Semeniuk, 1977; Favrat, 1982
1980	Fairway Rock	natural	Kovacs et al, 1981
1979-80	Issungnak	sand/gravel	Fenco Consultants Ltd., 1981; Frederking et al, 1982; McGonigal, 1981; McGonigal et al, 1986; Shinde, 1981; Shinde et al, 1982; Vaudrey, 1980
1980-83	Hans Island	natural	Danielewicz et al, 1981,1982, 1983, 1988; Metge et al, 1981
1982-84	Tarsuit	caisson	DePaoli et al, 1983; Pilkington et al, 1983; Sanderson, 1984
1982-85	Adams Island	natural	Frederking et al, 1983, 1984, 1986a, 1986b, 1886c; Sayed et al, 1986a, 1988; Stander, 1985
1984	Kadluk	caisson	Johnson et al, 1985
1985	Amerk 0-09	caisson	Sayed et al, 1986b; K.R Croasdale & Assoc. Ltd, 1985
1985	Mukluk	sand/gravel	Cox et al, 1988
1985-86	Molikpaq	caisson	Wright et al, 1986
1986	Minuk	sand/gravel	K.R. Croasdale & Assoc. Ltd, 1986

Ice Pressures:	Small pressure sensors, large pressure panels, biaxial pressure sensors, structure mounted panels, strain gauging of structural members.
Ice Movements:	Wire line reels, radar, traditional survey methods, electronic distance measurements, time lapse photography
Rubble Movements:	Electronic distance measurements, standpipe installations,inclinometers.
Ice/Rubble Strains:	Electronic distance measurements (large scale), small strain arrays.
Rubble Geometry:	Aerial photography, level surveys, auger drilling, electromagnetic sensing, thermistor strings.
Other:	Anemometers (wind speed, profile, direction), tide gauges, current meters, borehole jacks, small scale properties measurements, water temperature, geotechnical measurements, island mounted inclinometers.

The collected data is variable in almost every respect. Prior to 1982, useful pressure data within rubble was only obtained at two locations, Netserk B-44, and Arnak L-30. This, and subsequent data from caisson structures, indicates that external ice loading does result in pressure at the structure, but it is generally reduced. Measurements at Tarsuit also showed measurable pressure at depths greater than 4 m below the waterline. At many of the sites no significant rubble field formed; these locations fall into two classes.

1. Islands close to shore, in shallow water, which are not subject to large ice movements.
2. Steep-sided structures in deep water where accumulations of rubble are unable to ground firmly.

Thus, the structures most prone to generate extensive rubble fields are those with gentle slopes, and far enough offshore (>10 km) to be subject to large ice movements. Structures in this category are sand/gravel islands and shallow caissons on underwater berms.

Table 2: Results from auger and thermistor measurements of refrozen layer thickness.

AUGER	THERMISTOR STRING	DIFFERENCE
1.66 m	1.92 m	+ 16 %
1.70 m	1.30 m	- 24 %
2.69 m	1.26 m	- 53 %

The largest rubble field reported to have formed around an artificial island was 1500 m x 800 m and formed at Issungnak during the winter of 1979-80. As part of the Issungnak field program, however, a rubble accumulation at a natural shoal was also studied and this reached 8900 m x 6900 m.

Refrozen layer thickness was measured at Issungnak by "feel" during auger profiling, and by using in situ thermistor strings. The maximum thickness in February 1980, measured by auger, was 3.7 m. The difference between the thermistor data and the auger data was also measured at three locations with the results presented in table 2.

It is apparent from these results that the two measurement methods can produce very different results. The use of thermistor strings also allowed the measurement of refrozen layer growth rate. On average these were:

Nov - March 6.0 mm/day (growth)

March - June -16.0 mm/day (melting)

The largest rubble sails were measured at Fairway Rock and Mukluk Island, both of which had rubble piles up to 15 m high. On average, the maximum sail height at other locations was less than 12 m.

Rubble movements were monitored at three locations, Issungnak, Tarsuit, and Amerk (ESSO's CRI). Movements were detected at all locations with short term (hours-days) movements as large as 0.3 m. At Tarsuit, movements were described as being tens of cm at the rubble field periphery, and less near the caisson.

Island movement was measured at Adgo P-25 using inclinometers which indicated that a total movement of 5 cm occurred. This was calculated by M. Metge (1976) to require an average global force of 984 kN/m from the surrounding ice.

Interpretation of ice pressure sensor data is not completely straight forward and various assumptions are usually made, in order to calculate such parameters as global load. For example, average pressure can be obtained by combining the output from several sensors. This is used together with ice thickness measurements to calculate the maximum average thrust, but because bottom ice is relatively "warm" and soft, a reduced thickness is often used in the calculation. The maximum pressure recorded in floating sea ice was measured at Netserk B-44, where a peak pressure reached 1.5 MPa. A maximum average pressure of 1.1 MPa was calculated from data collected at Arnak L-30. In general, however, maximum pressure during any season rarely exceeded 1 MPa. At several locations in landfast ice, the maximum thrust was associated with thermal expansion of the ice.

Ice movements were monitored as part of most of the field programs. This was considered important because standard indenter equations allow direct calculation of ice forces from the indentation geometry and ice velocity. Increasing ice velocity is associated with increasing ice forces. During non-landfast conditions, ice movements can easily be of the order of kms/day, but upon becoming landfast, the ice is greatly restrained. Wind, currents, tides, and temperature have all been found to influence landfast ice movement, with the magnitude of movement also being influenced by location. At Adams Island, 3 km offshore, average ice velocities were less than 10 cm/day, while at Netserk F-40, some 32 km offshore, average velocities were of the order of 1 m/day. Attempts to correlate driving forces with ice movement have given variable results. At Adgo F-28, movements were claimed to correlate with wind, although no significant movement occurred during two of the larger wind events. At some locations tide effects dominated, while at others, thermal expansion appeared to be the major contributor to ice movement. An interesting mechanism called tidal jacking, was proposed to account for movements at Adams Island. Tidal jacking would appear to be a process whereby water-filled, wedge-shaped cracks, formed by bending failure of the ice sheet near the shore, freeze, thereby causing the ice to move horizontally during tide reversal. It is apparent from the literature that the process of landfast ice movement is complex and cannot yet be accurately predicted.

3.2 Load Transmission Models

The force required to move (cause sliding failure of) a grounded ice rubble field over a level seabed is universally calculated as;

$$F = W_g \cdot \mu_{is} \tag{1}$$

where:

μ_{is} = ice/seabed friction coefficient

W_g = grounding weight and can be calculated as follows;

$$W_g = \left(1 - \frac{P}{100}\right) [H_i \cdot \rho_i - H_k(\rho_w - \rho_i)] \cdot g \cdot A_r \tag{2}$$

where

P = rubble porosity (%)

H_i = average height of sail ice above water (m)

H_k = average depth of keel ice below water (m)

ρ_i = density of ice (saline) (kg/m^3)

ρ_w = density of sea water (kg/m^3)

g = acceleration due to gravity (9.81 m/s^2)

A_r = Horizontal area of rubble field (m^2)

If one assumes that P, ρ_i, ρ_w, g, and μ_{is} are basically constants, the ability of a rubble field to resist sliding depends on three geometric variables, H_s, H_k, and A_r. Sliding resistance increases with greater sail height, shallower water, and larger area. This is straight forward but it should be noted that area is very important. Sea ice loads against a structure (or rubble field) are in essence calculated as follows;

$$F = F_L \cdot D \tag{3}$$

Where F_L is force per metre diameter and D is the structure (or rubble field) diameter. The applied force therefore varies in direct proportion to the diameter while the sliding resistance is proportional to the diameter squared. Thus any grounding pressure will produce a stable rubble field, provided that the field is large enough.

Sliding stability calculations of early sand/gravel islands treated the rubble-island system as a single unit in order to calculate global sliding resistance. This approach has since been expanded in order to calculate load (F_s) transmitted to a structure through grounded rubble (Kry, 1977, 1980; Allyn et al, 1979, 1982; Bercha et al, 1980, K.R. Croasdale and Associates, 1985). This method uses a rigid body assumption for the rubble field and shall be referred to here as the simple theory. The rigid body assumption implies that no load will reach the structure until global rubble sliding occurs, at which point;

$$F_s = \text{Total external force} - \text{Rubble field sliding resistance}$$

This method of calculation has been used in various ways. K.R. Croasdale & Associates (1985) used a two-dimensional approach and considered only the rubble directly between the structure and the applied load. Kry, Bercha and others took a three-dimensional approach, considering the entire rubble field. The three-dimensional approach led to concerns that a poorly grounded rubble field could increase global loads on a structure by increasing the effective structure diameter. Allyn and others extended the three-dimensional approach by including the berm slope, edge failure and friction (shear) along the sides of the rubble field in a computer program which calculated the loads on a circular sand/gravel island. Sayed et al (1984) included an assumption about ice rubble properties. They assumed that newly formed ice rubble is a vertically and horizontally homogeneous Mohr-Coulomb material at critical equilibrium. The stress distribution within the rubble was calculated for a narrow rubble field against a structure (two-dimensional case) but although this approach was more complex than previous models, the calculated loads were still zero until the applied load exceeded the total rubble sliding resistance.

None of these analyses take into account the possibility that rubble field deformations under loading may generate forces against an embedded structure before the sliding resistance is reached. In order to overcome the limitations of the rigid body assumption, several groups have resorted to numerical methods for calculating load distributions.

Evgin and Morgenstern (1984) led the way, using finite element analysis to examine the behaviour of an eight sided, caisson retained, island (Tarsuit) when subjected to ice loads. They included the case of an intact ice sheet resting on grounded ice rubble, and from their results they concluded that the presence of a rubble field reduces the amount of displacement and increases the overall maximum force an island can withstand. However, upon examining their methods it is apparent that this conclusion is subject to several qualifications. It appears that only one 2D elastic case was examined, for which an arbitrary value for rubble elasticity was used. It also appears that the possibility of sliding at the refrozen/un-refrozen interface and rubble/seabed interface was not considered; and the intact ice sheet (refrozen layer) was assumed to be the same thickness as the surrounding sea ice. This study clearly brought forth the concept that an ice rubble field can be treated as a non-rigid body, but generalizations from the results must be made very cautiously.

In 1986, Williams et al used numerical computer simulation to calculate ridge and rubble building forces. They used a discrete element method to solve incrementally the dynamic equilibrium equations for each of the rubble blocks as well as for the advancing ice sheet. This method is similar to finite element analysis except that it is used for systems of discrete bodies. There were two examples presented, of ice rubble accumulation in front of a structure, both starting with an intact ice sheet. Each example was run for only 100 seconds and although no grounded rubble field formed (at most two blocks were grounded) it is obvious that longer runs would have produced more grounded rubble. This approach requires the input of material properties, as well as initial and boundary conditions. Deformations within the rubble are thus calculated and, with correct inputs, this method should give reasonable results for newly formed rubble.

Finally, in 1988, Canadian Marine Engineering Ltd. carried out a finite element analysis to examine load transfer through a grounded rubble field with a refrozen layer. Only the 2D, rigid structure case was examined with an 80 m wide rubble field. It is interesting to note that the refrozen layer was assumed not to reach the outer edge of the rubble field. Two cases were presented, the difference being the horizontal extent of the refrozen layer (75 m and 78 m). The Young's Modulus for the consolidated (refrozen) layer was assumed to be 0.2 GPa, some ten times larger than the value used for the un-refrozen rubble. Some effort was made to determine these properties from theoretical considerations, as well as from small scale test data. Unfortunately, problems were encountered with the rubble/seabed slider elements and so they were removed. The rubble was thus fixed to the seabed, and so it was estimated that the finite element analysis results were in error by more than an order of magnitude. The geometry and justification of material properties were more advanced than those used by Evgin and Morgenstern (1984), but the slider element problems and limited cases examined meant that few generalizations could be made.

4 SITE DESCRIPTION

4.1 General

Section 4.1 gives an overview of the environmental conditions in the Southern Beaufort Sea with site specific details provided where ever possible, while section 4.2 reviews the data collected by ESSO and NRC during the winter of 1986/87.

4.1.1 Weather

At Tuktoyaktuk the average air temperature is below 0 degrees between late September and early May. The average February air temperature is -29 degrees and winter temperatures are persistently rather than extremely cold. There is little precipitation and the average annual snowfall at Sachs Harbour is 75 cm/yr. Prevailing winds are from the northwest and east-southeast with the one hour averaged, 50 year return period wind, being 105 kmh. The worst month for storms is October (storms present 8% of the time) and during the remainder of the time low pressure systems are present 2-3% of the time, meaning that the Beaufort Sea is not a stormy area (Pilkington et al, 1983).

4.1.2 Water movement

Water movement in the Southern portion of the Beaufort sea is influenced by the westward moving Beaufort Gyre, the northeasterly flow of the MacKenzie River, and the easterly flow of the Trans-Polar Drift. Water current velocities are usually very low and only extreme currents exceed 50 cm/sec (1 knot). Wind induced water movement at the surface may mask the general water flow and may induce strong short term currents. Tidal fluctuations are generally small and average 15 cm, although in 1944 an extreme storm surge caused water levels to rise 3 m at Tuktoyaktuk (Pilkington et al, 1983).

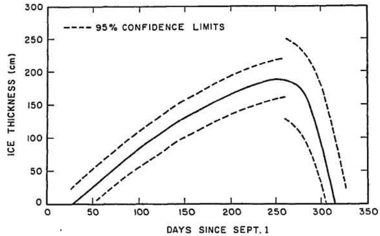

Figure 1: Ice thickness versus time after September 1. Data is from Thesiger Bay (Sachs Hr.) (from Parker, 1987)

4.1.3 Ice Conditions

Freeze-up usually starts by the first week in October and the maximum ice thickness of 2 m is reached by the middle of May (see figure 1). The measured ice thickness at Kaubvik was 1.5 m by April 10, 1987 which is less than usual for the time of year.

The Kaubvik site is usually landfast by midwinter and then remains landfast until the spring breakup at the end of June (McKenna et al, 1988). Between the start of freeze-up and landfast conditions the site is subject to moving first-year pack ice with occasional multi-year floes and ridges. It is thus during the initial non-landfast conditions, when ice movement is of the order of kilometers per day (Spedding, 1979), that rubble fields form.

During the winter of 1986/87 Kaubvik became landfast by the second week in January. Landfast ice, although generally stable, does move and movement rates in 20 m water depths can reach 3 m/hr (McKenna et al, 1988). These major movements have been associated with coastal storms (Agerton et al, 1979).

4.1.4 Bathymetry

The average width of the continental shelf is 70 km and extends to the 50 m depth contour. Kaubvik is 30 km from the nearest shore, in 18.5 m of water, and is thus well inside the outer edge of the continental shelf.

A circular, flat topped berm 10 m high was built underwater, onto which the caisson ring was set down. The outside design diameter of the berm was 380 m, sloping up to a 148 m diameter level surface for the caissons. After construction of the berm a bathymetric survey was carried out giving the berm contour map in figure 2.

4.1.5 Geotechnical

Core samples of the sea bed at Kaubvik were tested before construction of the berm in order to calculate island settlement rates and sliding resistance. The bottom sediments consist mostly of soft clay with some sand layers. The berm material was obtained from Issigak and consisted of sand and fine gravel with a lower bound shear friction angle expected to be 34° (Shinde, 1988).

4.1.6 Caisson Structure

ESSO's CRI is one of the earliest arctic caisson islands and was first used at Kadluk during 1983/84. In 1986 it was stationed at Kaubvik, some 120 km northwest of Tuktoyaktuk (69° 52.5' north, 135° 25' west). The CRI consists of 8, water ballasted, steel caissons arranged in a ring and held together by tensioned wire ropes as shown in figure 3. Each caisson is 49.2 m long, 13.2 m wide and 12.2 m high, with a mass of 5000 tonnes (K.R. Croasdale and Associates Ltd, 1985). The central core of the island is filled with sand which provides the working surface for drilling operations, as well as sliding resistance against ice forces. The design global ice pressure is 1700

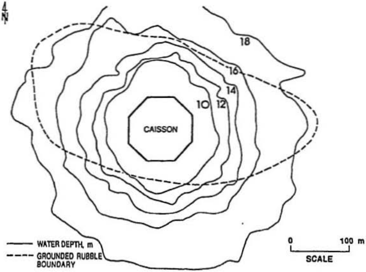

Figure 2: Bathymetric contour map of berm at Kaubvik (from Frederking et al, 1988).

kPa (global load of approximately 45 000 tonnes) and the design local ice pressure is 4800 kPa (Croasdale et al, 1988).

When the caisson ring is set down it is precisely positioned so that caisson 1 faces directly north (Croasdale et al, 1988). The CRI was originally designed to include 33 ice load sensors, various geotechnical sensors, as well as structural response sensors (Hawkins et al, 1983). By the winter of 1986/87 32 ice load sensors and 10 geotechnical sensors were active.

4.2 Other Kaubvik data

In order to present a complete case study description, the other two project data reports (Croasdale et al, 1988 and Frederking et al, 1988) are summarized here. As with the M.U.N. data, the main emphasis is to describe the results that are relevant to the subsequent theoretical work.

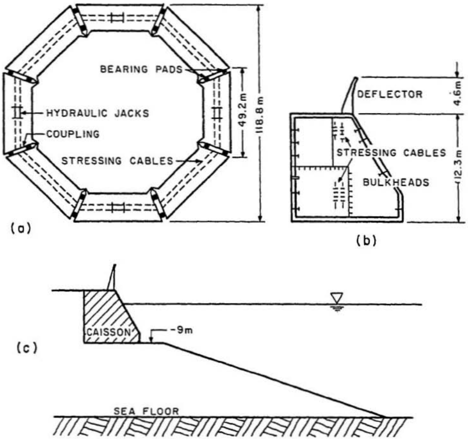

Figure 3: Details of the CRI showing a) plan view of the caisson ring, b) cross section through a caisson, and c) cross section through a completed island (from K.R. Croasdale and Associates, 1985).

4.2.1 ESSO Data

ESSO Resources Canada Ltd was responsible for operating the CRI mounted sensors. The sensors of concern for this project were the external ice pressure sensors and the sand core geotechnical sensors. Analysis of the collected geotechnical data showed that ice forces did not significantly affect the measured pore pressures, so the following summary only deals with the ice pressure data.

By the winter of 1986-87 there were two types of ice pressure sensor, microcells and shearbar panels. Microcells are small (0.02 m^2) and were designed to measure point pressures while the shearbar panels (1.05 m^2) were designed to measure pressures averaged over a larger area. During the field period, 27 microcells and 5 shearbar panels were operating, with the greatest concentration of sensors being in the northern quadrant. Although pressures from the north (open ocean) were expected to be the greatest, all caissons had some sensors and the southern caissons had a total of 8 operational microcells (see figure 4). The microcells were mounted at the waterline and welded flush with the outer caisson plating. The microcells have the following specifications:

Type : Strain gauged cantilever diaphragm
Diameter : 16.5 cm
Full Scale rating : 6895 kPa
Accuracy : 5% full scale (340 kPa)

Until drilling operations ceased in early January, the southern microcell data was sampled every 10 seconds. Immediate processing was done to reduce data volume and only the 5 minute peak, average, and variance values were actually stored. After shutdown of drilling operations a battery powered remote data acquisition system was installed which recorded pressures at a fixed logging rate, without any preprocessing. This system operated until May.

Although there were no shearbar panels in the southern quadrant it is interesting

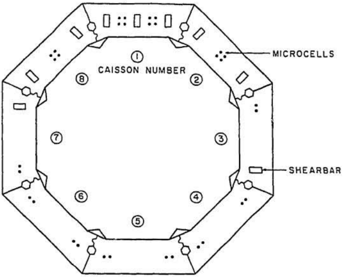

Figure 4: Plan view of CRI showing ice pressure sensor locations (from Croasdale et al, 1988).

to compare the output from the two sizes of sensor. Figure 5 contains the maximum peak CRI pressure recorded during the entire winter (caisson 8). The drop in pressure fluctuations after October 26 appears to indicate the presence of an ice rubble accumulation. In comparison, the maximum peak pressure measured by a shearbar panel on caisson 8 was less then 0.5 MPa (see figure 6). This is due to the difference in sensor area. During ice failure, direct ice-structure contacts are transient and localized. The small microcells can frequently have transient ice contact over a large percentage of the sensor area, whereas the shearbars will average these small contacts over a much larger area. The microcell output is therefore more erratic but the time averaged pressures on both should be the same. During non-failure events (ice creep) the output from both should be similar.

Once ice rubble had formed against the CRI no compressive failure of the rubble or refrozen layer was observed at the CRI/rubble contact. Pressures measured by the microcells during the latter part of the winter should thus be relatively independent

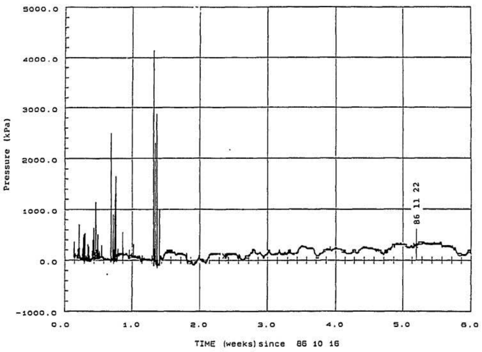

Figure 5: Microcell output covering the period of highest maximum pressure (from Croasdale et al, 1988).

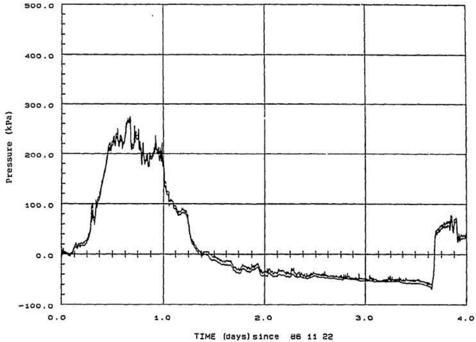

Figure 6: Shearbar data showing one of the high pressure events. Note that although the pressure magnitude is similar to that measured by the microcell on the same date, the shearbar shows the event much more clearly because of the increased sensitivity (lower full scale)(from Croasdale et al, 1988).

of sensor size. The time of greatest interest is the period coinciding with the M.U.N. data, March 12 - May 5. During this time, however, very little activity was detected at the southern quadrant. It appears from the plots (see appendix 1) that the resolution of the data was ± 60 kPa which makes it difficult to detect small pressure variations. Consequently, most of the late winter data is straight line and close to zero (see appendix A). The most dramatic exception occurred on April 15th, when both sensors active on caisson 4 measured pressures exceeding 1.0 MPa. This lasted about 2 hours and although no similar change in pressure was observed at any of the other caissons, it appears to be an actual event rather then an equipment malfunction. Similarly, early winter pressure events were usually detected by more than one sensor but often not by all the expected sensors. Interpretation of this data with regard to average pressures is therefore not so straightforward.

In conclusion, no pressures over 300 kPa were recorded at any of the southern caissons during the M.U.N. field period, except for the April 15th (julian day 105) event, and in general, pressures were less than 100 kPa. The low pressures, combined with 60 kPa resolution, make it difficult to compare the microcell data with other data on an event by event basis.

4.2.2 NRC Data

The National Research Council of Canada was responsible for collecting rubble field pressure panel and survey data. Field work started in late December 1986 and ended in early May. Fourteen pressure panels were installed in the rubble in 4 groups (arrays). As these were installed while the sea ice was still active (not landfast) three of the arrays were placed to the northwest of the CRI (see figure 7), where rubble formation was most likely. The fourth array was placed to the southeast to coincide with the M.U.N. instruments. As expected, ice movement caused rubble building to

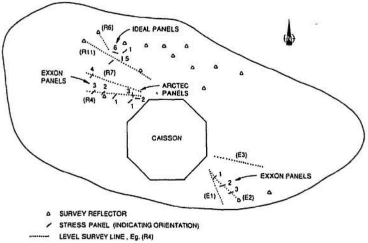

Figure 7: NRC panel and survey locations in the late winter rubble field at Kaubvik (from Frederking et al. 1988).

occur twice in the week following panel installation. One event extended the rubble field eastward but the second event occurred along the northwest edge of the rubble field. New rubble even overtopped old rubble, burying the two outermost pressure panels. The resulting internal rubble pressures were successfully recorded and demonstrate that sustained pressures of several hundred kPa can be transmitted into the rubble, see figure 8. As figure 9 shows, however, the distribution of pressures within the rubble was not straightforward. The greatest pressures were actually measured some distance back from the rubble field edge. Many factors could contribute to this, including local refrozen layer bending, incomplete sensor freeze in, a thinner refrozen layer in the newer (external) rubble, or it could indicate that the CRI was a stress concentrator. Ice profile drilling done at that time indicated that the "consolidated layer" was about 2.5 m thick, and although this was measured by "feel", rather than temperature measurement, it is still a good indication that a substantial refrozen

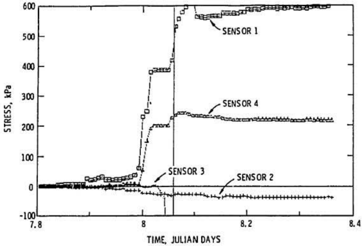

Stress versus time, north-west Exxon panels.

Figure 8: Internal rubble pressures as measured by the Northwest Exxon array during the January 8th event (from Frederking et al, 1988).

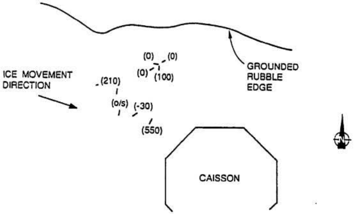

Figure 9: The pressure distribution at one time during the January 8th rubble building event (from Frederking et al, 1988).

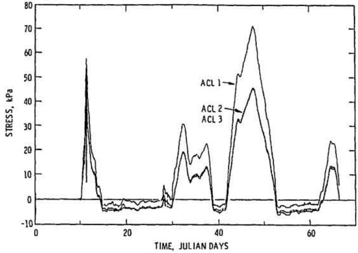

Figure 10: Arctec panel rosette data (from Frederking et al, 1988).

layer existed at that time. The Arctec panel rosette near the caisson recorded almost equal biaxial stress (see figure 10) indicating a maximum principle stress only 20-30 kPa greater than the minimum principle stress.

Some of the panels were divided into horizontal segments and data from these indicated that vertical pressure gradients existed (see figure 11). Unfortunately, over time, zero drift and apparent malfunctions reduced the reliability of the data. The southeast array data of greatest interest is that which coincides with the M.U.N. data (March - May). By that time, some pressure variations are apparent but the magnitudes are considered to be unreliable.

NRC also collected 4 types of rubble survey data; rubble elevations, rubble field movement, rubble profiling, and rubble block size. Standard surveying techniques were used to measure rubble elevation along 7 survey lines (see figure 7). A typical result is shown in figure 12 and from these it was determined that the average sail height southeast of the CRI was 4 m. This was calculated using equation 4 to ensure that average height H_s could be used to calculate average sail weight (assume similar

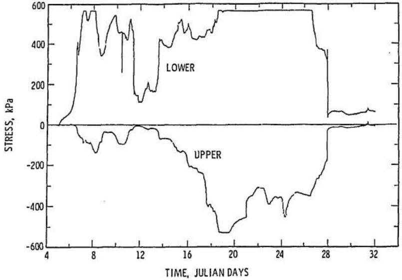

Figure 11: Data from horizontally segmented pressure panel (from Frederking et al, 1988).

sail shapes).

$$H_s = \left(\frac{\Sigma H^2}{N_s}\right)^{0.5} \tag{4}$$

where:

H = Sail height

N_s = Number of sails

The highest sail in the rubble field (not on a survey line) was about 9 m high.

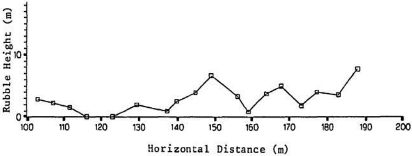

Figure 12: Surveyed rubble elevations southeast of the CRI.

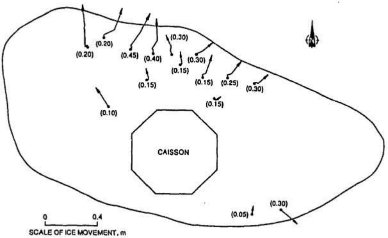

Figure 13: Electronic Distance Measurement survey results showing horizontal movement and (in brackets) settlements over the win (from Frederking et al, 1988.

In order to measure rubble movement, 15 survey posts were mounted in the rubble in early January (usually atop sails). The horizontal and vertical positions of these posts were measured at various times throughout the winter using an electronic distance measuring device (EDM). The results are shown in figure 13, from which it is apparent that the rubble settled at all locations and, with one exception, the rubble moved horizontally in a northerly direction.

The horizontal movement is also, with one exception, away from the CRI and down the berm slope. Horizontal movement of up to 0.33 m was measured but uneven settlement (tilting) of rubble sails may have contributed to this.

Rubble profiling was done by drilling holes into the rubble. This showed that "valleys" between sails generally reached within 0.2 m of sea level, and the consolidated layer in January was 2.5 m thick in places. A floating block at a depth of 5.5 m, 25 m from the CRI also indicated that not all the rubble was completely grounded. The rubble block measurements showed that 0.2 m thick ice formed grounded rubble in 8.5 m deep water, the rubble closest to the CRI was the oldest (thinnest blocks), and rubble formation appeared to have ceased when the sea ice reached a thickness of 0.75 m (thickest blocks).

5 FIELD RESULTS AND DISCUSSION

5.1 General

The rubble field finished growing when the surrounding ice became landfast in early January, with the major accumulations of rubble being to the east and northwest of the CRI. The first field visit was scheduled for March and so, with the CRI so heavily protected on the east and northwest sides, it was decided to concentrate efforts to the south (see figure 14). The rubble mounds to the south were not so extensive or massive, and thermal expansion of the landfast ice sheet during the second half of the winter was expected to result in loading from that direction. A total of three field trips was required, covering a two month period starting in early March 1987. The M.U.N. team collected the following data.

1. Sea ice stresses from 9 mercury filled stress sensors.
2. Creep and strain in the ice rubble from one strain array.
3. Rubble thickness from 8 auger holes.
4. Rubble temperature profiles from two thermocouple arrays.
5. Torque readings from one 10 m instrumented auger hole.
6. Ice properties from 9 cores.

In addition to this, Tuktoyaktuk air temperature, wind speed, and wind direction data were obtained from Environment Canada (see Jordaan et al, 1988).

5.2 Sea Ice Stresses

Nine stress sensors were arranged in three rosettes, with one sensor in each rosette oriented to measure stresses towards a survey point on caisson 4. Each mercury

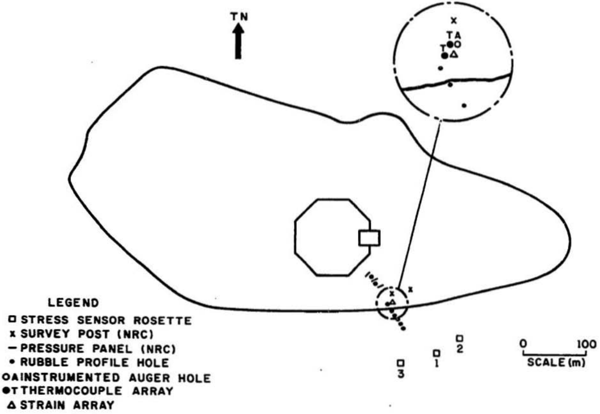

Figure 14: Plan view of CRI and rubble field with the position of the M.U.N. field measurements indicated.

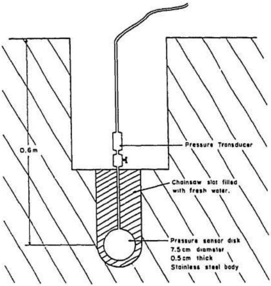

Figure 15: Diagram of mercury filled pressure sensor.

filled, disk shaped, sensor was attached to a pressure transducer which measured the pressure of the mercury (see figure 15). The rosettes were frozen into the sea ice about 240 m southeast of the caisson centre and about 50 m apart. The sensors were thus about 90 m south of the rubble field edge. At the time of installation the sea ice was cored and found to be 1.5 m thick. The neutral axis of such a sheet is located at a depth of approximately 0.6 m (Duckworth et al, 1988) and so this was the chosen deployment depth. An electric chainsaw in an alignment jig was used to cut the slot for each pressure sensor. The slot was filled with fresh water from a vacuum flask, the sensor was lowered to the bottom of the slot, and the water froze within one minute. Two thermocouples were also installed, one in the data logger and one at a depth of 0.6 m in the ice. The data were read and recorded every 2 minutes by a CD248 data logger powered by a thermal generator.

Over the 31 day measurement period the data from the nine stress sensors and 2 thermocouples were read 22,353 times. Unfortunately, an intermittent fault which

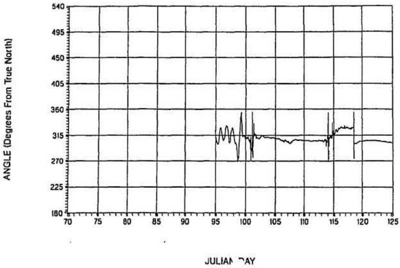

Figure 16: The principal stress angle for array 2.

has been attributed to the data logger, caused large negative values to be recorded on occasion, mainly with rosette number three. This only affected the stress sensor channels and resulted in a loss of 16% of the stress readings, leaving a total of 168,000 stress readings and 44,700 temperature readings. During subsequent data processing the erroneous negative pressures were discarded. Plots of stress versus time were made for each sensor and the principal maximum and minimum stresses, stress angle, and shear stress for each rosette were calculated (see Jordaan et al, 1988). The largest measured stress was 550 kPa which corresponded to a maximum principal stress of 570 kPa. The principal stress direction for all three rosettes was generally northwest/southeast (see figure 16).

The rosettes were arranged so that one sensor in each (labeled sensor a) measured the stress towards a survey point on caisson 4. The average of these stresses has been plotted for comparison with the CRI sensor data. As each of these sensors faces approximately NW these can be used to estimate the average maximum stress (see

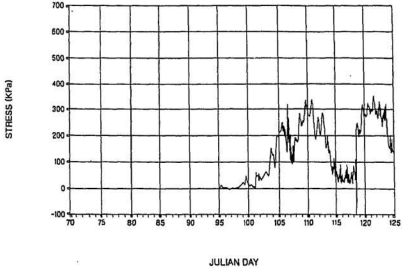

Figure 17: Stress towards the CRI, averaged from the three rosettes.

figure 17). This method is expected to be accurate to within 10 % and this approach is required because data loss from sensors in rosette 3 (other than sensor 3a) resulted in no principal maximum stresses being calculated for the last week of the field period.

From the pressure data it appears that there were two types of deformation of the sea ice as it moved past the grounded rubble (see figure 18). Short term fluctuations of up to 200 kPa (see day 106) are typical of a brittle type of failure mode, while slowly varying pressure (days 110 to 113) indicates a ductile (creep) type deformation.

On the last field visit the fresh ice deformation shown in figure 19 was observed about 100 m NE of the stress sensors. This appears to be a buckling type of failure and matches descriptions of similar features at Adams Island (Frederking et al., 1983). The above water portion of the ice sheet is visibly curved and as the finger like projections are not indicative of a fast fracture type failure it is hypothesised that the ride-up of this ice "tongue" occurred very slowly. Although the feature in figure 19 was localized it was one of at least five fresh vertical ice sheet movements on the southern edge of the rubble and it could account for the measured fluctuations in ice

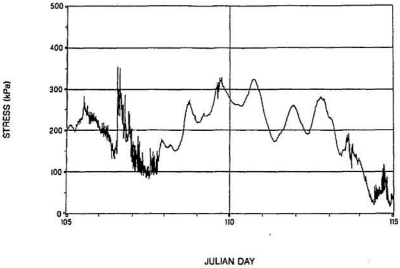

Figure 18: The expanded plot of stresses measured by stress sensor S1a clearly shows that periods of steady pressure were interrupted by rapidly fluctuating, apparently brittle, deformations. During the entire period the maximum principal stress did not reach 400 kPa.

pressure over the days preceding the photograph. The deformation required at least 3 m of ice movement and the sudden pressure fluctuations at average stresses below even 100 kPa indicates that such "failure" mechanisms have very low thresholds and may be important when considering limiting forces.

When ice is stressed it creeps, therefore the presence of sustained sea ice pressure of the order of hundreds of kPa means that the ice sheet was moving. Landfast ice is frozen to the shore and its ability to move and apply loads to fixed objects is therefore restricted. It is thus relevant to examine the source(s) of this movement relative to the measured pressures.

The magnitude of the loads may be limited in two ways:

1. The restriction on ice sheet movement may limit the force or,
2. The force applied may be limited by the driving force.

Figure 19: This photograph shows a fresh vertical deformation 100 m north east of the stress sensors. Note the polar bear tracks in the foreground.

Both of these will be examined, beginning with a model for landfast ice movement. In a manner similar to that used by Croasdale (1975) the landfast ice will be treated as a semi-infinite ice sheet, fixed at the shore, and unrestrained at the seaward edge (see figure 20).

Ice is a visco-elastic material and, during creep deformation, the pressure exerted by the ice sheet is proportional to the cube root of the indentation rate. During creep, the wider the structure the faster the ice must move in order to generate a given pressure (strain rate is a function of the ice speed and structure width). As the rubble field at Kaubvik was 0.8 km wide, significant movements are required to generate the measured pressures.

It is hypothesized that movement of the landfast ice was the result of thermal expansion, and wind and current stresses. Based on this hypothesis, work was done to quantify the contribution of each of these sources of movement and develop a model to predict the movement from measured data.

Calculations (see appendix B) show that stresses due to tidal currents are expected to be negligible, and as wind-induced currents are not expected in ice covered water, it was decided that currents would not be included in the analysis. Based on this, a computer program was written (also appendix B) which used the wind data from Tuktoyaktuk and sea ice temperature data to calculate the landfast ice sheet movement. The wind stresses produce elastic, delayed elastic, and creep deformations which were calculated based on the work done by Sinha (1983a). The wind stresses were calculated using a drag coefficient of .003 (Feldman et al, 1981), and the 30 km strip of ice between the CRI and shore was divided into 5 km wide strips for the creep calculations. The thermal expansion was calculated using a coefficient of expansion of 0.000051 m/m °C (Michel, 1978) and all the calculations were done without including any restraining influence of the CRI. As the mercury filled pressure sensors were

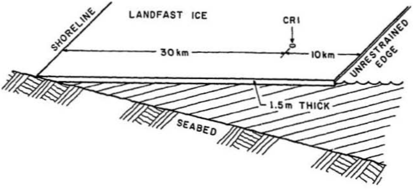

Figure 20: Showing the physical model of a landfast ice sheet used for the computer program.

located south of the rubble field, only the north-south component of the movement was studied. The wind data was averaged over 12 hr intervals and the temperature was taken every 12 hr. The movement rate at a point 30 km offshore was calculated (location of the CRI) and the results are shown in figure 22. When compared to the measured pressure data (fig 21) some similarity can be seen. The movement rate is small between days 114 and 118 which coincides with the low pressures measured at that time, the movement rate drops sharply on day 123 coinciding with the drop in pressure on that day, and the daily cycling of the movement curve is reflected in the pressure data.

The resultant pressures can be estimated using the reference stress method for creep indentation as presented by Sanderson (1984). Between days 105 and 125 the average maximum movement rate (five highest peaks) was 1.03 m/day. This translates into an indentation strain rate of $1.49 \cdot 10^{-8}$ /sec for an 800 m wide indenter (appendix C). From the results of Sanderson (1984) the average contact pressure is calculated to be between 535 kPa (granular sea ice) and 290 kPa (columnar sea ice). The maximum

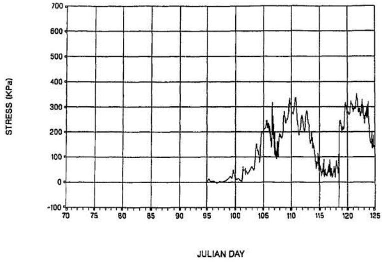

Figure 21: Plot of sea ice pressure averaged from mercury filled pressure sensors 1a, 2a, and 3a.

average pressure measured during the same period (five highest peaks) was 333 kPa, well within the predicted range.

The computer program also calculated the accumulated sea ice movement (see figure 23) and the shape of this curve is very similar to the temperature curve (fig 24). When the total movement rate is separated into wind and temperature driven components (figs 25 and 26) we see that the contribution of wind driven movement rate is very small in this model and does not appear to correlate with the pressure data. The maximum wind driven movement rate is 20 times less than the maximum rate of thermal expansion. Separation of the elastic, delayed elastic, and creep components of the wind movement also shows that elasticity and delayed elasticity are by far the major contributors to wind-driven movements.

Despite the apparently small movement contribution from the wind it would be premature to dismiss it as a source of ice movement in real life for two reasons. First, the model is only concerned with movements perpendicular to the shoreline, and

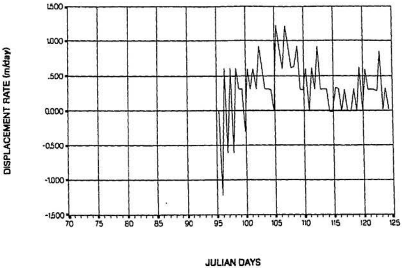

Figure 22: Plot of landfast ice movement rate at a point 30 km from shore, predicted from wind and temperature data.

second, flaws in the landfast ice may increase the mobility of the ice sheet.

Any movements parallel to the shoreline would not be expected to originate from thermal expansion. Wind travelling parallel to shore will deform the ice in shear, with the shear strain calculated as follows:

$$\text{Shear Strain} = \frac{\text{Length of movement parallel to shore}}{\text{Distance from shore}}$$

This is the same form as compressive strain but the modulus of rigidity (G) for an elastic solid in shear is much smaller than the modulus of elasticity (E) for compression. This can be seen from the following relation (Higdon et al, 1978).

$$G = \frac{E}{2(1 + \text{Poisson's Ratio})} = \frac{\text{Shear Stress}}{\text{Shear Strain}} \tag{5}$$

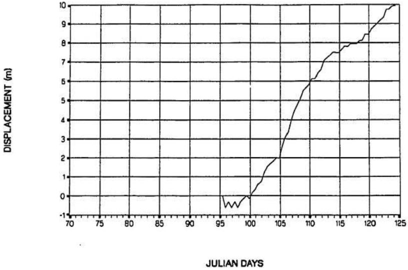

Figure 23: Plot of landfast sea ice movement versus time, predicted from wind and temperature data.

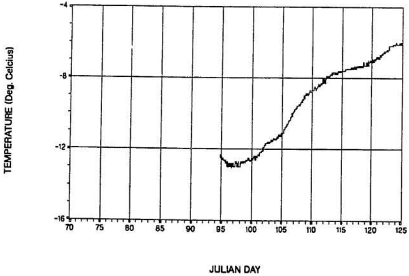

Figure 24: Plot of sea ice temperature versus time. Temperature was measured 0.6 m deep in the ice.

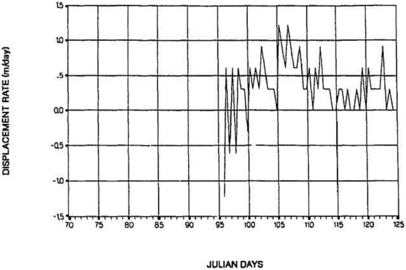

Figure 25: Component of landfast ice movement rate due to thermal expansion.

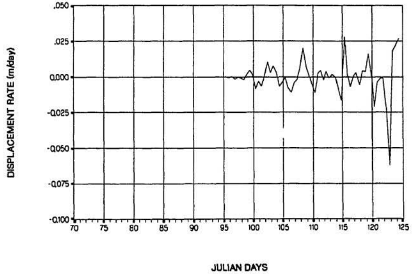

Figure 26: Plot of predicted landfast ice movement rate due to wind stress.

The theoretical limits for Poisson's Ratio are 0.0 and 0.5 and so, depending on the actual Poisson's ratio for sea ice, a given wind will produce 2 to 3 times the elastic movement if it blows parallel to shore as opposed to perpendicular to the shore.

Landfast ice is composed of separate ice sheets frozen together with ridges and other flaws throughout. These flaws may open under tensile stresses and increase the mobility of the ice sheet, perhaps to the point where driving force, and not mobility, dominates. The model does not account for this and, although the predicted movements are generally similar to the pressure data, the correlation is not ideal. For example on day 118 pressure sensors 1a, 2a, and 3a all measured a sharp increase in pressure that is inconsistent with the calculated movement rates. This might occur if a lead(s) opened up between the CRI and shore. In order for this to occur tensile stresses in the ice sheet are required. It so happens that the maximum tensile wind stress occurred at that time (see Jordaan et al, 1988) with a peak wind speed of 28 kmh and a northerly component of 18 kmh which is calculated to have produced a tensile stress of 4 kPa at the shore. If such tensile stresses are sufficient to open cracks and produce large offshore movements of the ice sheet, then the pressure on the rubble field may become dominated by the driving force. This can be approximated by assuming that a wedge of ice between the CRI and the shore transmits wind stress to the rubble field (see figure 27). With an apex angle of 80° the wedge would have an area of 775 km^2. On day 118, the average jump in the measured sea ice pressure was 150 kPa, implying a global load increase of 180 MN on the rubble field. The wind at that time is calculated to have applied a maximum wind stress of 118 MN on the wedge. This is not sufficient to produce the observed loading even if the wedge was only restrained by the CRI. As the ice at Kaubvik is historically within the landfast margin, it would be difficult to justify the assumption that the wedge was only restrained by the CRI. The magnitude of the pressure rise can thus not be

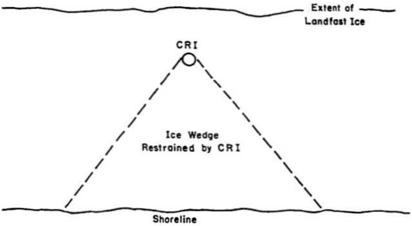

Figure 27: Showing the wind stressed wedge that is assumed to load the rubble field at Kaubvik.

easily explained but the timing does seem to coincide with the southerly wind.

In conclusion, we see that the general shape and magnitude of the computer predicted movement rate profile is in agreement with the measured pressure data. This supports the use of load calculation based on landfast ice movement rates with the modeled movement rate dominated by thermal expansion. The predicted wind movement rates are generally random with respect to the measured pressures but the timing of one major discrepancy between the predicted movement rate and the actual pressure seems to coincide with a wind event, enforcing the idea that wind stresses can be more significant than the model predicts. As an initial analysis of landfast ice movement the model presented provides useful insights into the phenomena of landfast ice movement but the influence of wind is not straightforward and future work should concentrate on the transmission of wind induced stresses to structures within the landfast ice.

5.3 Rubble Strains

A strain array was installed at a bearing of 140 T (true north) and a distance of 125 m from the centre of the CRI. The chosen site was a small flat ice surface in a valley between two rubble sails and near the outer edge of the rubble field. The flat surface was the result of sea water flooding and the array was thus located at water level. It was oriented so that LVDT (Linear Variable Differential Transformer) number 1 was along a line 12 degrees east of true north (see figure 28). The post holes were drilled using a template and fresh water from a vacuum flask was used to fill the holes and secure the posts. The LVDTs were wired to a multiplexer, which in turn was connected to a Campbell Scientific 21x micrologger. The strain array was designed to measure the two dimensional strain field at the surface of an ice sheet. It consisted of 6 Schaevitz 200 H.R. D.C series LVDTs which measured the relative displacement between four posts frozen into the ice surface. The output from any three LVDTs can be used to calculate the maximum and minimum principal strains, shear strain, and the principal strain angle.

The system was activated at 19:00 hours local time on Julian Day 70 and was designed to read and store the strains every hour, on the hour. For data processing purposes the air temperature inside the insulated box was also measured, along with the internal data logger and external battery voltage. The stored data was dumped to a cassette tape on subsequent field trips. By the time that the array was retrieved, the snow in the valley had accumulated to a depth of more than 0.5 m and completely buried the box which covered the strain array installation. The LVDT's were designed to operate at 24V DC excitation voltage, but in order to maintain a constant input voltage during the field period, the two external 12V batteries were regulated down to 20V. This successfully controlled the voltage to within ± 0.02 V. The entire system worked reliably for the 51 day field period, and more than 7300 strain

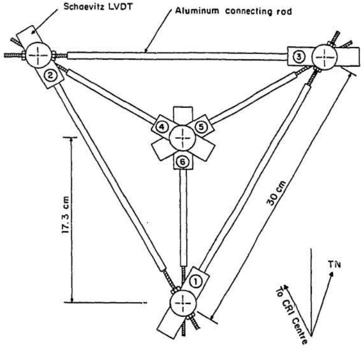

Figure 28: Strain array dimensions and orientation.

readings were obtained. The subsequent data processing included compensation for the reduced excitation voltage, as well as temperature effects on the LVDT's and the array linkages.

Although any three LVDTs can be used to calculate all the principal strains, the greatest accuracy is obtained from strains at widely spaced angles. The largest angle possible between three directions is 120 degrees, which is the separation angle for the three inner and three outer legs of the array. For this reason the array is treated as an inner rosette and an outer rosette. The principal strains and strain angles were calculated using standard equations for a delta rosette (see Vaughn, 1975).

The posts move relative to each other as the supporting ice surface deforms under the influence of stress or temperature change. Indicated strain is a usually a combination of thermal, elastic, delayed elastic, and creep deformation, making analysis somewhat complex. The accuracy of the outer rosette should be slightly better than

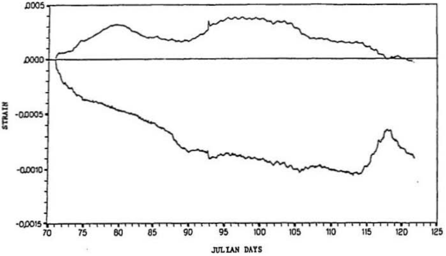

Figure 29: Maximum and minimum principle strains, inner rosette.

the inner rosette due to the greater distance between posts (gauge length) but practically speaking they measure strain at the same place and so both rosettes should give the same results. The actual results, however, gave differences between the inner and outer rosettes of approximately 50%. Upon closer examination it was realized that the deflections measured by LVDTs 3 (outer rosette) and 4 (inner rosette) were remarkably similar and were much larger then any of the others. The smaller inner gauge length (17.3 cm instead of 30 cm) means that equal deflections measured by inner and outer LVDTs will not give equal calculated strains. The measurement from these two LVDTs dominated the results and lead to speculation that processes other than direct strain were involved. For example a crack in the ice within the array could produce the observed results (see Jordaan et al, 1988).

The largest principal strains were tensile, and the smallest principal strains were compressive. Comparison with the pressure sensor data indicated that the large tensile strains correlated with sea ice pressure; during periods of high pressure, tensile strain increased, and during low sea ice pressure the accumulated tensile strain was reduced (compressive creep). This is opposite to what was expected. The maximum principal strain (maximum because of sign, not magnitude) correlated inversely with surface ice temperature. This indicates that this strain was related to the thermal expansion and contraction of the surface ice. Discussion of the strain results is limited here because of concerns about the significance of this data. The reader is referred to Jordaan et al, 1988 for a more detailed look at strain vs. stress and strain vs. temperature.

5.4 Rubble Profile

On the second field trip 8 holes were drilled along a 92 m survey line to profile the ice. The line extended from the floating ice onto the grounded rubble field. A 5 cm diameter auger was used to drill the holes and the hole depths were measured by keeping track of the number of 1 m auger flights used. Freeboard measurements were made and the number and estimated extent of any voids encountered was recorded. From these measurements it was determined that the area between the "undisturbed" sea ice and the tidal crack was filled with floating rubble which contained a thick refrozen layer. This disturbed region extended tens of metres out from the grounded rubble edge. In the floating ice zone the ratio of total freeboard to total ice drilled was 1:6.3 and the average ice thickness was 3.3 m. Buoyancy considerations allow average ice density to be calculated from this ratio (see appendix D), and a ratio of 1:6.3 indicates a density of 880 kg/m^3.

The grounded ice rubble contained few voids with soft, slushy ice encountered at the deeper depths indicating that the ice blocks were somewhat "rotten" after their long exposure to seawater. On the grounded rubble only one hole in a "valley" was drilled all the way to the seabed and in this hole rubble was present all the way to the bottom. This indicates that grounding occurred even between rubble sails.

5.5 Rubble Temperature Profiles

Two thermocouple arrays were installed on the first field trip. The long thermocouple array (12 m long) was installed in a rubble sail and the short thermocouple array (3 m long) was installed in the valley (see figure 30) near the strain array. A hole was drilled for each of the arrays using a gas powered 2 inch auger. The water level rose to within 3 cm of the top of the hole for the short array which was positioned so that the top thermocouple (0 m) was level with the ice surface. The long array was installed so that the top thermocouple (0 m) was approximately 4.5 m above the water line and protruded 0.5 m from the drilled hole. In order to hide the array from polar bears the protruding portion was cut off and in the process the 1 m depth thermocouple stopped functioning, leaving 15 of the original 17 thermocouples working. The clearance between the array and the hole was filled with snow and slush as much as possible. All the thermocouple leads were connected via multiplexers to a data logger which was shared between the thermocouple arrays and the strain array. The system was activated the day after the arrays were installed.

Once the system was activated no problems were encountered and over the following 51 days more then 33,000 temperature readings were successfully recorded.

There were a total of 27 thermocouples and the subsequent temperature profiles (see figure 31) allowed estimation of the refrozen layer thickness and growth rate. The interface between refrozen and un-refrozen rubble shows clearly as a sudden change in slope of the temperature versus depth profile at -2.75m. The temperature of the unfrozen rubble is a steady -1.7 deg celsius, indicating that the water in the keel is of normal salinity (brine build-up does not occur). The calculated refreezing rates are given in tables 3 and 4, and show that the rubble under the sail freezes quicker than rubble in the valley. This is despite the higher thermal gradient in the valley (see fig 32).

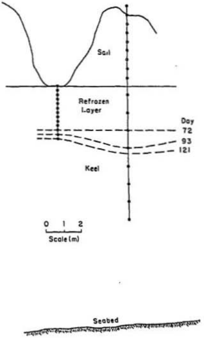

Figure 30: Diagram showing the installed positions of the thermocouple arrays and how the refrozen layer thickness increased during the field period.

It is expected that the weight of the sail reduces the size of the underlying void spaces and thus less cooling is required to freeze the compacted layer. In addition, horizontal heat flow will tend to even out the heat dissipation. The volume of the void spaces (water filled) can be determined from heat loss calculations combined with a value for the latent heat of freezing of sea water and the refrozen layer growth rate.

The following thermal constants for sea ice are given by Yen (1981).

Thermal Conductivity = 1.8 W/m K

Latent Heat of Freezing = 293 kJ/kg (at -2.0 °C)

Using these and the average thermal gradient of 4.3 °C/m (days 72 to 121) the heat loss was calculated to be 7.74 Watts (see appendix E). This implies that 2.28 kg

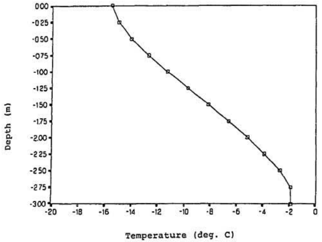

Figure 31: From the temperature profile the interface between refrozen and unfrozen rubble can clearly be distinguished. Profile taken from the short array, midnight day 84.

of water per m^2 freeze per day which is a thickness of only 0.25 cm. As the actual average refrozen layer growth rate is 2.2 cm/day, 88% of the keel must already be ice. The porosity is thus 12%.

A rubble packing factor of 88% is quite high because FCC (Face Centered Cubic) sphere packing is only 74%. It is expected that compaction from the overlying ice, the presence of slush and ice fragments between the blocks, and the initial freezing around the cold ice blocks, all contribute to the scarcity of water in the keel.

Table 3: Rates of refreezing for the short thermocouple array (sea level at 0.0 m depth).

Depth (m)	Freeze-in Date Julian Day	Refreezing Rate (cm/day)	Comments
2.50	71.7	1.2	Average vertical thermal gradient was 4.7 deg/m
2.75	92.8		
2.75	92.8	2.1	Average refreezing rate was 1.7 cm/day
3.00	121.8		

Table 4: Rates of refreezing for the long thermocouple array (sea level at 4.5 m depth).

Depth (m)	Freeze-in Date Julian Day	Refreezing Rate (cm/day)	Comments
7.0	72.0	4.8	Average vertical thermal gradient was 4.0 deg/m
8.0	92.8		
8.0	92.8	1.2	Average refreezing rate was 2.7 cm/day
† 8.35	121.8		

† Extrapolated from the temperature depth profile

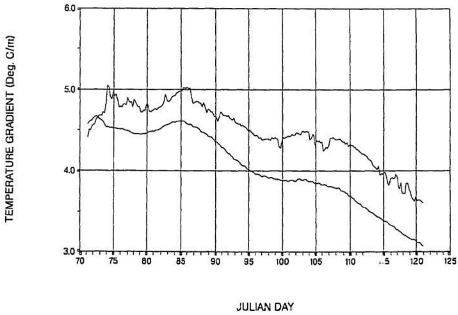

Figure 32: Plot of the average thermal gradient directly above the refrozen layer freezing front. The top curve is for the valley and the bottom curve is for the sail.

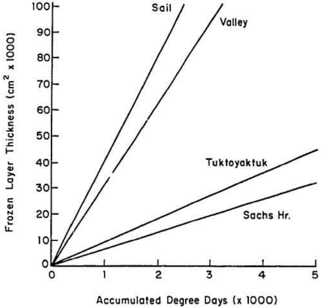

Figure 33: The graph above shows how dramatic the rate of refrozen layer growth differs from sea ice growth at two locations.

The calculations show that the refrozen layer grows more than 8 times as quickly as floating sea ice with the same thermal gradient. The thermal gradient is not constant, however, and will decrease as the frozen layer gets thicker. A better measure of ice growth rates is the comparison between accumulated degree days and the square of the ice thickness (Parker, 1987). This has been done by using Tuktoyaktuk temperature data for the winter of 1986/87 and by estimating the date of rubble formation to be Jan 1, 1987 (see Frederking et al, 1988). The resulting graph (see figure 33) shows how dramatic the difference is between the growth rate of the refrozen layer in comparison to sea ice growth.

The refrozen layer is expected to be continuous within the rubble field because no significant accumulations had formed since January and the thermocouple array data came from near the outer edge of the rubble field (thinnest layer expected there),

there were few visible cracks, all the cracks except one were less than 1 m wide and these are expected to have refrozen quickly (days) with extra cooling provided by the adjacent ice.

This all means that a substantial and rapidly formed refrozen layer exists in the ice rubble which should be taken into account in any ice rubble models. It is expected that this layer is even thicker next to the CRI because these rubble piles are the oldest.

5.6 Ice Properties

A 10 cm diameter ice corer was used to obtain ice samples from the sea ice and ice rubble. A thermocouple probe was used to measure the ice temperature profile of two of these cores.

For microstructure examination, the hotplate technique was used to make sixteen thin sections from various cores. These sections were placed between crossed polaroid filters and photographed. Crystallographic examination of the thin sections showed that the grains were small at the surface, approximately 50 per square cm in some cases, and got larger with increasing depth, up to 3 cm long and 1 cm wide at a depth of 145 cm. The average platelet spacing was 0.75 mm, similar to that illustrated in Weeks et al, 1969.

Twenty salinity measurements were made on two cores with an optical salinometer. The salinometer was calibrated with cold tap water and each test was done twice to increase the reliability of the results. The salinity tests yielded a maximum salinity of 7.5 ppt, an average salinity of 3.0 ppt, and a minimum salinity of 0.0 ppt. These salinities are slightly lower than normal for sea ice (Weeks et al, 1980) but the cores were taken from sail rubble blocks which meant that the samples were very well drained.

Nine uniaxial compression tests were done on samples from 4 cores. A 5 ton capacity soil test machine was used to compress the samples which typically had a

7cm x 7cm square cross section. Unfortunately the uniaxial compression data could not be analyzed because some of the test details were not recorded, however, nothing unusual was observed during the tests.

All these tests were done under "field" conditions and are thus not as accurate as more carefully controlled laboratory tests. The main object was to ensure that the ice at Kaubvik was not unusual in any way and as this appears to have been the case, more accurate laboratory results reported in the literature will be used for most of the subsequent theoretical work.

5.7 Instrumented Auger

An attempt was made to measure ice hardness versus depth with an instrumented auger. Unfortunately the drilling times were not recorded with the result that drilling energies could not be calculated. The torque measurements are presented in Jordaan et al, 1988.

6 PROPOSED LOAD TRANSMISSION MODEL

6.1 General

The simplest approach used to calculate load transmission treats the rubble field as a rigid body. The transmitted load is therefore equal to the total force minus the rubble sliding resistance. This theory is referred to in this text as the simple theory, and to its credit, the simple theory has been used for at least 10 years. The simple theory produces two results, depending on whether two-dimensional or three-dimensional analysis is used. The two-dimensional calculation always results in load reduction at the structure while the three-dimensional calculation can produce estimates of load concentration at the structure.

A review of the literature indicates that, in addition to the Kaubvik project, considerable time and money has been spent on field studies of ice rubble. From this work a variety of information has been collected such as landfast ice pressures, rubble sail heights, grounding depths, rubble field sizes and shapes, and refrozen layer characteristics. This is all necessary information for any load transmission model; however, if more physically correct models are to be used, material properties must be incorporated and in this respect there is still a large shortage of data. In particular, data on pressures within the rubble are scanty and sometimes conflicting, full scale properties of rubble elasticity, creep, delayed elasticity, and compaction are either unknown or can only be estimated within orders of magnitude. Even such basic information as rubble porosity has not been accurately obtained. The shape and behaviour under load of each structure may influence the field measurements so that some of the pre 1983 data from sand/gravel islands may also not be appropriate for caisson structure analysis.

The shortage of data makes it difficult to calibrate any theoretical models, and impossible to verify them; however, general understanding of material behaviour, combined with available field data do allow development of an improved load transmission model.

The field work at Kaubvik indicated that a substantial and rapidly formed refrozen layer existed within the rubble and so it was decided to concentrate on examining the role of the refrozen layer in load transmission.

Given the nature of the investigation it was desirable to use a model that was simple and flexible enough to handle a wide variety of material properties and rubble field geometries. A full blown finite element analysis does not meet these criteria so it was decided to represent the rubble as a system of springs and dampers.

6.2 Geometric Model

The first step was to specify a geometric rubble field model. For the purpose of this work, only horizontally uniform grounded rubble on a level seabed will be examined (see figure 34). Incorporation of seabed slope, variation of grounding pressure and refrozen layer thickness can be done in the future by varying the appropriate force, spring, and damper values.

6.3 Physical Model

It will be assumed that the sails provide weight only, so that the deformations of interest are those of the refrozen and un-refrozen rubble. Before the arrangement of springs and dampers shall be considered, it is important to identify the possible rubble deformations caused by horizontal loading of the refrozen layer. This is illustrated in figure 35.

The following deformations are thus considered important for modelling:

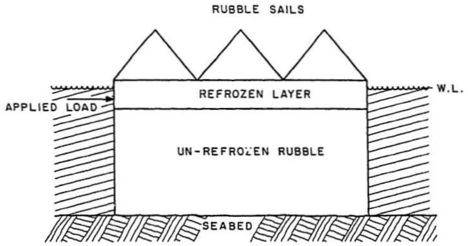

Figure 34: Two dimensional geometric model of an "aged" rubble field (ie has a refrozen layer).

Refrozen layer:	Compressive strains
	Sliding at the refrozen/un-refrozen interface
Un-refrozen rubble:	Shear strains
	Compaction (compressive) strains
	Sliding at the rubble/seabed interface

Deformation in ice is usually divided into four components; elastic, delayed elastic, secondary creep and tertiary creep strains. Ice rubble is assumed to have a similar behaviour, with additional deformation possible as a result of compaction.

Rheologic modelling of deformation under load can thus be done using a system of springs and dampers connected in series and parallel. Tertiary creep only occurs after relatively large accumulation of strain, of the order of 1% (Mellor, 1979) and for the purposes of this study shall be neglected. Although compaction is not strictly an elastic process (very little recovery), it does have an effective stiffness which can be modelled using a spring, provided that the load is not subsequently removed. A spring damper system to model elastic, delayed elastic and secondary creep is a

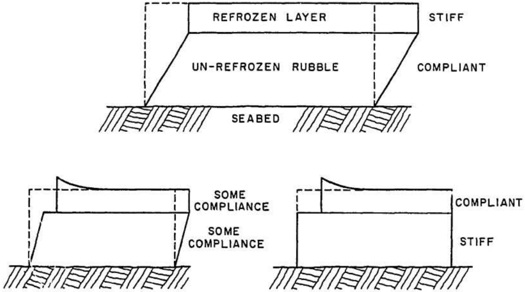

Figure 35: Diagrams showing how relative stiffness of the refrozen in comparison to un-refrozen rubble is expected to affect the deformation of a grounded ice rubble field.

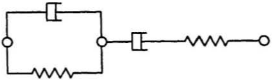

Figure 36: The spring-damper system commonly used to rheologically model ice compliance. This arrangement is known as a Burger's Body.

parallel spring and damper, in series with a spring and a damper. This is a common rheological model for ice and is called a Burger's Body (see figure 36).

The Burger's Body can be used (with various spring and damper coefficients) to model the compressive deformations in refrozen rubble, and the compaction and shear deformations in the un-refrozen rubble. Sliding at interfaces, such as the rubble/seabed and un-refrozen/refrozen rubble interfaces, is assumed to be a frictional process and can thus be represented by coulomb dampers.

A complete spring-damper system to represent a segment of grounded rubble field is shown in figure 37.

Although this is a rather complex system, there are certain simplifications that will be made for this study. these are:

1. Auger profiles of "grounded " rubble have almost universally shown that the rubble was incompletely grounded. It is thus reasonable to assume that compaction pressures in the lower portion ᶜ the rubble are not transmitted over long distances. This allows the removal of the entire lower rubble compaction element.
2. Delayed elastic properties for un-refrozen rubble are not known. This is an important restriction on the accuracy of this and other material property based

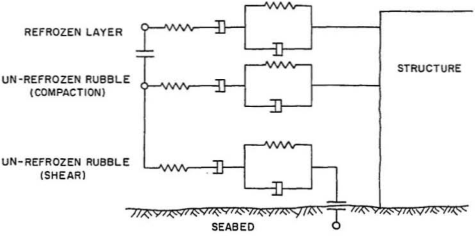

Figure 37: Diagram showing a spring-damper system to model deformations in grounded ice rubble. An entire rubble field is composed of a series of these "units" connected together.

> models. However, even without any delayed elasticity the initial (time = 0) and final (time = ∞) reaction forces can be calculated because they are independent of the delayed elastic characteristics of the ice.

For the purposes of this study, the lower compaction element will be removed, and the effects of delayed elasticity will not be examined. The simplified system is shown in figure 38 and the entire rubble field is modelled as a repeating series of this basic unit.

Other important simplifications include the assumption that the refrozen layer was continous and that the material properties could be apprximated by average values, even though the actually vary both horizontally and vertically.

Having established the arrangement of springs and dampers, the next step is to calculate the spring and damper coefficients.

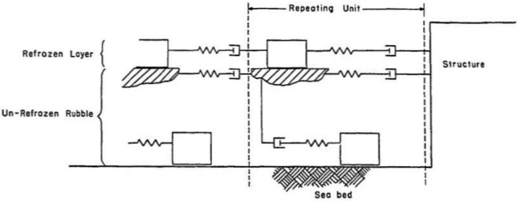

Figure 38: Simplified spring-damper system used in this study.

6.4 Element Coefficients

In order to have identical repeating units, a rubble field is most conveniently divided into sail width segments. Each repeating unit has eight elements; three springs, three viscous dampers, and two sliding elements (coulomb dampers). The coefficient for each element is calculated from ice and rubble material properties, as well as the particular rubble field geometry.

The element coefficient calculations are made with the following assumptions:

- The rubble field sail heights and widths are uniform.
- The water depth is constant.
- The space between the refrozen layer and the seabed is entirely filled with rubble.
- The refrozen layer has uniform thickness.

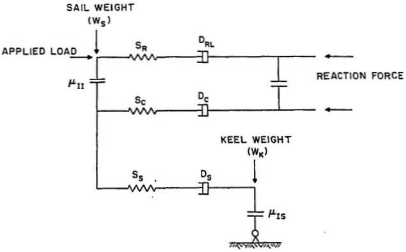

Figure 39: Single unit with eight elements.

6.4.1 Sliding Elements

In order to specify each coulomb damper, the normal force and friction coefficient must be known. For the refrozen/un-refrozen rubble the friction coefficient is obtained from the literature and the normal force W_s is calculated.

$$W_s = \left(\frac{H_s \cdot 0.5 \cdot E_{xt} \cdot \rho_i \cdot \frac{(1-P)}{100}}{N_s} - \frac{E_{xt} \cdot (\rho_w - \rho_i) \cdot T_{RL}}{N_s} \right) \cdot g \qquad (6)$$

where:
$E_{xt} =$ Rubble field extent (m)
$T_{RL} =$ Refrozen layer thickness (m)

For the un-refrozen rubble/seabed contact, the coefficient of friction is also taken from the literature and the normal force W_g is calculated as follows:

$$W_g = W_s - \left(\frac{(\rho_w - \rho_i)\frac{(1-P)}{100}(H_w - T_{RL}) \cdot E_{xt}}{N_s} \right) \cdot g \qquad (7)$$

where:

$H_w =$ Water depth (m)

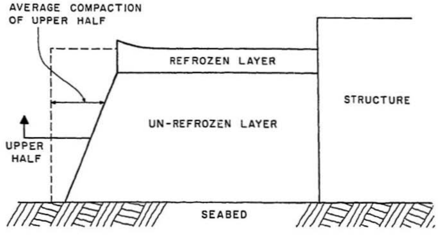

Figure 40: Figure showing how average compaction of the upper portion of un-refrozen rubble is related to refrozen layer deformation and bottom sliding (linear assumption).

6.4.2 Spring Elements

The equivalent spring stiffness for the refrozen layer element is calculated as follows:

$$S_{RL} = \frac{E_i \cdot T_{RL} \cdot N_e}{E_{xt}} \tag{8}$$

where:
$S_{RL} =$ Refrozen layer spring constant (N/m)
$E_i =$ Young's Modulus for ice (saline) (Pa)

The compaction stiffness is not so straight forward, because the compaction forces are assumed to be transmitted for long distances only in the upper un-refrozen rubble, and compaction is not, strictly speaking, an elastic process. It will, however, be treated as a spring because compaction force increases with displacement, and this analysis is principally concerned with behaviour during load application, not removal.

It will be shown later that refrozen/un-refrozen rubble sliding is not expected to take place and so we can see from figure 40 that the average compaction deflection of the load carrying layer depends only on compression of the refrozen layer and on whether bottom sliding takes place. The compaction distance thus falls between the following limits:

$$0.75\delta_{RL} \leq \delta_{Avg} \leq 1.0\delta_{RL}$$

where:
$\delta_{RL} =$ Displacement of refrozen layer (m)
$\delta_{Avg} =$ Average displacement (m)

This is not a wide range and so for simplicity an average value will be used:

$$\delta_{Avg} = 0.87\delta_{RL}$$

The compaction spring constant S_C can now be calculated as follows:

$$S_C = 0.87 \cdot \left(\frac{0.5 \cdot (H_w - T_{RL}) \cdot E_C \cdot N_s}{E_{xt}} \right) \tag{9}$$

where:
$E_C =$ Un-refrozen rubble compaction mo
0.5 is used because only the upper half is considered

Finally, shear strain is horizontal deformation at the top surface, divided by the vertical height. The shear spring stiffness S_S is:

$$S_S = \frac{E_{xt} \cdot G_r}{N_s \cdot (H_w - T_{RL})} \tag{10}$$

where:

$G_r =$ Un-refrozen rubble shear modulus (N/m^2)

6.4.3 Damper Elements

The viscous damper for the refrozen layer (D_{RL}) is non-linear as it is based on power law flow (secondary creep) with n=3 (Sinha 1983a). It is calculated as follows:

$$D_{RL} = \frac{T_{RL}^3 \cdot N_s}{C_{RL} \cdot E_{xt}} \tag{11}$$

where:

C_{RL} = Refrozen layer creep modulus (m^3/s N)

For un-refrozen rubble compaction creep there is very little information, however, settlement data from Kaubvik (Frederking et al, 1988) indicates a linear relation between settlement rate and local grounding pressure (see figure 41). Therefore the un-refrozen rubble compaction creep damper (D_C) will be assumed to provide linear damping. The damper coefficient is calculated as follows:

$$D_C = 0.87 \cdot \left(\frac{.5 \cdot (H_w - T_{RL}) \cdot N_s}{C_C \cdot E_{xt}} \right) \tag{12}$$

where:

C_C = Un-refrozen rubble creep modulus (m^2/s N)

It is assumed that un-refrozen rubble is a cohesive but porous material that behaves in many ways like solid ice. Creep in shear is therefore modelled as a power law flow process with n = 3, the same as for solid ice (see Sinha, 1983a). The shear creep damper coefficient is calculated as follows:

$$D_S = \frac{{E_{xt}}^3}{{N_s}^3 \cdot C_S \cdot (H_w - T_{RL})} \tag{13}$$

where:

C_S = Un-refrozen rubble shear creep modulus (m^3/s N^3)

Having established theoretical relationships between rubble properties and associated spring and damper element coefficients, the various ice, rubble, and friction properties have to be determined. Most of these have to be determined from data reported in the literature, rather then from measurements at Kaubvik, and in some cases only small scale test data is available.

7 ICE AND RUBBLE PROPERTIES

In order to use the theoretical model for quantitative predictions, various properties of water, sea ice, and rubble are required. Some of the properties can be obtained from published literature and where ever possible this will be supplemented with interpretations from the Kaubvik field data. As the output from this model is so strongly dependent on the assumed ice properties, a considerable effort has been made to determine reasonable values for these. Unfortunately no full scale measurements of natural rubble mechanical properties are reported in the literature. In order to overcome this, ranges of values will be estimated. A submerged block of ice rubble, with an initial temperature below freezing, will bond to other blocks at the contact points (Pilkington et al, 1982). In the extreme, inter-block bonding may produce a material with properties similar to sea ice. Calculations based on the properties of sea ice at melting should thus give a reasonable upper bound value for un-refrozen rubble properties. The presence of pores will, however, reduce the strength and stiffness of the ice and so the approach presented by Pounder (1965), will be used to adjust the properties by multiplying by 0.85 (1 - porosity/100).

The lower bound values will be calculated from model tests or fragmented ice reported in the literature. Some of the properties have ranges covering orders of magnitude and in order to give a feel for this, table 5 lists material stiffnesses covering more than five orders of magnitude (Juvinall, 1983; Avallone et al, 1987).

In cases where only a single value can be estimated a range of half an order of magnitude above and below the single value will be used as the range.

In order to make reasonable conclusions, the sensitivity of the model will be examined over the full range of all the assumed values.

Table 5: List of material elastic stiffnesses covering more than five orders of magnitude.

Material	Elastic Modulus (MPa)
Steel	207,
Aluminum	72,000
Marble	56,000
Wood	10,000
ABS Plastic	1,700
Low Density Polyethylene	170
Vulcanized Rubber	1.4

7.1 Seawater Density

Sea water density, for our purposes, does not vary significantly (¡ 1%) and is the most accurately known parameter. A typical value for arctic sea water (30 ppt, -1° C) is (Pickard et al, 1982)

$$\rho_w = 1024 \text{ kg/m}^3$$

7.2 Sea-Ice Density

The theoretical density of freshwater ice is 917 kg/m^3 (Michel, 1978). When saline water freezes, almost all the salt is rejected and the resultant ice contains air bubbles, brine pockets, and brine drainage channels. Measurements of sea ice density produce variable results, depending mainly on the brine drainage and bubble content of the sample. Values reported in the literature vary between 400 - 1190 kg/m^3 (Pounder et al, 1959; Sun Oil, 1974; Irwin, 1975; Sinha, 1983b, 1984; Gow et al, 1987) with the average between 850 - 900 kg/m^3. The higher densities appear to occur when brine drainage is minimized, thus a value of

$$\rho_i = 900 \text{ kg/m}^3$$

will be used. This may cause slight overestimation of the sail weight but some of the drained brine may remain in the sail.

7.3 Rubble Porosity

The theoretical porosity for uniform spheres arranged in a face centered cubic (FCC) arrangement is 26%. The scant data in the literature gives variable values for rubble porosity. Rigby et al (1976) estimated ridge porosity from voids encountered during drilling. This is a rough estimate as small voids and porous ice are not detected, with a resulting porosity estimate of 5 - 10% . Using the same approach the Kaubvik data gives a porosity of 2.5% in the un-refrozen rubble. On the other hand, Keinonen (1977) cut trenches through two ridge sails and mapped the cross sections. Using only the main rubble blocks, porosities of 36% and 43% were estimated.

Model (small scale) tests on ice rubble have been carried out and in these cases the porosity measurements are much easier to make. Values between 32% - 51% are reported for uncompacted model rubble (Keinonen, 1978; Wong et al, 1988; Gale et al, 1986, 1988; Prodanovic, 1979; Sayed, 1987) and this can be reduced to 21% by compaction, with further reduction occurring during shearing (Gale et al, 1987). Porosity values assumed in the literature vary from 20 - 40% (Kovacs et al, 1980; Allyn et al, 1979; Sayed et al, 1984; Allen, 1970; Parmerter et al, 1972, 1973).

Analysis of the Kaubvik thermocouple data gives an average keel porosity below the refrozen layer of 12%. It is felt that this provides the most accurate full scale measure of keel rubble water content (porosity). Adjusting this slightly upwards to account for higher porosity in the deeper rubble, an average value of

$$P = 15\ \%$$

will be used. Ice formation in the keel during warming of the submerged rubble will initially have decreased the keel porosity but snow accumulation in the sail will have a similar effect. For this reason the same porosity value will be used for the keel and sail.

7.4 Friction Coefficients

Ice is usually considered to be one of the lowest frictional materials on earth (Tusima, 1977). Small scale laboratory measurements on cold freshwater ice support this idea, often producing friction coefficients well below 0.1 (Oksanen, 1983). This philosophy has prompted some theorists to neglect friction in rafting and ridge building force calculations (Parmerter, 1975; Parmerter et al, 1972, 1973). However, experience on a larger scale seems to indicate that ice may have substantial friction. Friction coefficients are required in order to predict sliding failure at the refrozen/un-refrozen rubble interface, and at the seabed. For simplicity the friction coefficients in the theoretical model are not separated into static and dynamic components. The values for the assumed friction coefficients will thus be a compromise between the static (maximum) and kinetic (minimum) values.

7.4.1 Refrozen/Un-Refrozen Rubble Sliding

The refrozen layer grows down from sea level, incorporating the upper rubble blocks. Sliding failure below the freezing front is thus governed by the internal shear strength of the un-refrozen rubble. This is a function of the contact friction, "grain" interlocking, and intergranular cohesion. In the theoretical model this sliding resistance is treated as a "friction coefficient". No full scale measurements are reported in the literature so they will have to be estimated from four sources. These are; 1) ice/ice friction data 2) ridge geometry 3) model (small scale) ice rubble shear tests and 4) solid ice shear strength. The first three sources provide lower bound estimates, while the last source provides a value for cohesive rubble.

Table 6: Measured ice/ice friction coefficients.

Experiment	μ			Source
	Max	Min	Avg	
Decaying sea-ice block pulled over ice floe. Static/kinetic not specified	3.66	1.69	2.67	Irwin 1975
Saline model ice. Top - Top Bottom - Bottom Kinetic values approx. 30% smaller	- -	- -	0.23 0.46	Prodanovic 1979
Freshwater ice blocks approx 1/2 m^3 Static friction	2.0	-	0.6	Marshall 1989

1. Ice/Ice Friction

   Laboratory measurements by Tusima (1977) indicate that friction increases as ice softens near melting and field experiments with deteriorating sea ice have yielded friction coefficients in excess of 3.0 (Irwin, 1975). In order to further investigate natural ice/ice friction, a series of measurements were carried out on lake ice (Marshall, 1989). These yielded static friction coefficients up to 2.0 and kinetic coefficients up to 1.2. From this we see that natural ice tends to have more friction than smooth, hard lab ice (μ_{ii} ¡ 0.1) and the range of friction coefficients covers orders of magnitude. For modelling purposes only friction data appropriate to conditions at Kaubvik will be used (see table 6).

   From this an average ice/ice friction coefficient is assumed to be,

$$\mu_{ii} = 1.2$$

2. Ridge Geometry

Table 7: First year ridge sail and keel slope angles from direct measurements.

Sail			Keel			Source
Max	Min	Avg	Max	Min	Avg	
51.8	8.8	26.1	-	-	-	Tucker et al 1981
60	10	25	-	-	34	Wright et al 1978
-	-	24	-	-	33	Weeks et al 1971

Depending on the mechanics of ridge formation the maximum ridge slope angles may reach the angle of repose of fresh rubble which is the minimum angle of internal friction (Bowles, 1984). Table 7 summarizes data from the literature.

Lower sail and keel angles have been reported from analysis of straight line sonar and laser ice profiles (Lowery et al, 1979; Weeks et al, 1971), but such profiles traverse the ridges at random angles and overlapping of keels may create features that are wide and shallow. For these reasons such data is not included here. As table 7 shows, the average keel slope angle is 33.5° ($\tan 33.5^\circ = 0.66$)which is steeper than average sail slopes, and sail slopes can reach 60° ($\tan 60^\circ = 1.73$).

3. Model (Small Scale) Shear Tests

Small scale, fragmented ice, shear box tests have been carried out by various people, with the results summarized in table 8.

4. Solid Ice Shear Strength

The following equation for failure (maximum) stress in shear has been fitted to data from direct shear tests with varied normal forces (Roggensack, 1975);

$$\tau_f = 74.6 + 0.47\sigma_n$$

Table 8: Internal angle of friction from shear box tests on fragmented ice.

Experiment	Friction Angle		Source
	Max	Min	
Saline model ice, scale 1:50	47	-	Keinonen et al 1978
Freshwater ice, samples with random and uniform grains (respectivly).	45	36	Gale et al 1986
Saline model ice, scale 1:50. Larger and smaller peices respectively.	53	47	Prodanovic 1979
Constant shear area.	34	11	Weiss et al 1981

where:

τ_f = Failure stress (kPa)

σ_n = Normal stress (kPa)

These tests were carried out on columnar freshwater ice at -2.5 °C, with normal pressures between 33 and 136 kPa and give a shear stress equivalent to static friction.

In conclusion, the first three "lower bound" sources indicate an internal friction coefficient μ_{RR} between 0.20 (Weiss et al, 1981) and 3.0 (Irwin, 1975) and for our purposes a middle value of 1.2 will be used (tan50 = 1.2) as a lower limit.

For an upper bound estimate* Roggensack's equation will be modified by accounting for the rubble porosity. This gives;

$$\tau_f = (0.85 \cdot 74.6) + .47\sigma_n$$

Table 9: Experimentally measured ice/soil friction coefficients

Experiment	μ_k			μ_s			Source
	Max	Min	Avg	Max	Min	Avg	
Sea-ice blocks towed over beach gravel	0.58	0.32	0.39	0.79	0.42	0.50	Shapiro et al 1987
Sea-ice blocks pulled over beach gravel (assumed static)	-	-	-	1.0	0.47	0.73	Irwin 1975
Model ice, scale 1:20 - 1:40, pulled over sand	-	-	-	-	-	0.75	Abdelnour et al 1982
Saline ice pulled over soils	-	-	-	1.47	0.85	1.06	Utt et al 1980

$$\mu_{RR} = \frac{63400}{\sigma_n} + 0.47$$

* This actually becomes the minimum value when the contact pressure exceeds 120 kPa.

Refrozen/un-refrozen rubble sliding is thus modelled as a frictional process with the friction coefficient expected to fall within the following range;

$$1.2 \leq \mu_{RR} \leq \frac{63400}{\sigma_n} + 0.47$$

7.4.2 Ice/Seabed Friction

Table 9 summarizes the available data for ice/soil friction coefficients.

The estimated lower bound for the internal angle of friction of the sand berm at Kaubvik is 34° (Shinde, 1988) which implies a friction coefficient of 0.67. For ice/soil contact the average measured static friction coefficient is 0.66, with the associated kinetic friction coefficient expected to be less. For the purposes of calculation, the average coefficient of friction is expected to fall within the following range:

$$0.50 \leq \mu_{is} \leq 1.0$$

7.5 Elastic Shear Stiffness

In the ice literature, shear stiffness G is almost never measured directly, however, for an elastic material the shear stiffness is related to the Modulus of Elasticity by the following equation:

$$G = \frac{E}{2(1+\nu)}$$

where:

E = Modulus of Elasticity (N/m^2)

ν = Poisson's Ratio (N/m^2)

The theoretical limits of poisson's ratio are 0.0 - 0.5. As no values are reported in the literature for ice rubble, the following value will be assumed to be approximate.

$$\nu = 0.25$$

Appropriate maximum and minimum values for the Elastic Modulus are thus required.

Maximum Stiffness:

From Weeks et al (1984) we see that the elastic modulus is inversely proportional to ice temperature and porosity. From the literature (Weeks et al, 1984; Saeki et al, 1981; Frederking et al, 1981) we find that reported values for E fall into the following range:

$$0.4 \cdot 10^9 \leq E \leq 60.0 \cdot 10^9$$

The four values above 10 GPa are thought to be erroneous (Frederking et al, 1981) and the low values were obtained with slow loading rates and are therefore influenced by creep effects. Eliminating the inappropriate values we find that the "true" elastic modulus for sea ice at melting with a loading rate of 1 MPa/sec is approximately $4 \cdot 10^9$ (Pa).

The stiffness of porous ice will be somewhat less and, to adjust the value, it will be multiplied by 0.85 (1 - porosity/100), yielding a final value;

$$E = 3.4 \cdot 10^9$$

Minimum Stiffness:

Minimum stiffness is expected to occur before consolidation and the formation of interblock bonds. This can be estimated from small scale tests on fragmented ice. Triaxial tests on such material were carried out by Gale et al (1988) and biaxially confined tests were carried out by Sayed (1987). Gale et al, obtained a pre "breakover" stiffness of 0.1 GPa, where breakover was the point at which internal shearing (yield) began. M. Sayed conducted tests at constant strain rates, with output of displacement versus normal pressure. The normal pressure fluctuated, as failure planes formed and "healed". After a slip plane healed, the normal pressure rose rapidly because the rubble was effectively precompacted. The slope of the stress strain curve at that point gives a "precompacted" ice rubble stiffness. Measurements from the graphs indicate that this stiffness was approximately;

$$E = 0.009 \cdot 10^9$$

This yields the minimum value for Young's Modulus.

It is hypothesised that the important differences between the two experiments were precompaction and the test speed. The tests by M. Sayed were relatively fast and did not start with significant precompaction, while the tests by Gale et al were slower with initial isotropic compression (pre-compaction). Using the results from M. Sayed as the minimum, the elastic modulus falls within a range covering almost two and a half orders of magnitude.

The following range for the Shear Modulus of ice rubble is thus considered appropriate;

$$1.4 \cdot 10^9 \leq G_r \leq 0.0036 \cdot 10^9$$

7.6 Elastic Compaction Stiffness

Compaction is a material densification process achieved by the reduction of porosity of a granular material. Pressure and/or vibration pack the grains, reducing the overall volume and porosity. Although this is not an elastic (recoverable) process, there is an associated stiffness which can be calculated from the following:

$$E_C = \frac{\text{Pressure}}{\text{Unit volume change}}$$

As this is a non-recoverable process, any previous compaction will stiffen the material. Previously un-compacted fragmented saline ice, compressed in a box was found to have a compaction stiffness E_C of (Keinonen et al, 1978);

$$E_C = 57 \cdot 10^3$$

Volumetric strain and deviatoric stress measurements from triaxial tests on fragmented ice (Gale et al, 1987) indicate that prior to failure, precompressed rubble has a compaction stiffness of:

$$E_C = 160,000 \cdot 10^3$$

This gives a range for compaction stiffness of;

$$57 \cdot 10^3 \leq E_C \leq 160,000 \cdot 10^3$$

7.7 Shear Creep

There is no creep data for ice rubble in shear reported in the literature and thus, shear creep can only be inferred from data on solid ice. The following generalized equation for power law creep (Karr et al, 1989) allows calculation of creep in shear, from uniaxial data.

$$\dot{\epsilon}_{ij} = \frac{3}{2}K\left(\frac{3}{2}S_{ij} \cdot S_{ij}\right)^{\frac{n-1}{2}} \cdot S_{ij} \tag{14}$$

where:

S_{ij} = stress vector

$\dot{\epsilon}_{ij}$ = Strain rate vector

n = Power law flow exponent

For viscous creep in pure shear this yields:

$$\dot{\gamma} = 9 \cdot K \cdot \tau^3$$

where:

$\dot{\gamma}$ = Shear strain rate (/s)

τ = Shear stress (N/m^2)

K = Constant

where K is determined from Sinha's equation for the uniaxial case (see section 7.9). For ice at melting this yields:

$$\dot{\gamma} = 48.8 \cdot 10^{-25} \cdot \tau^3$$

This is further reduced by porosity which increases the stress in the ice. As the creep rate is a function of the stress cubed, porosity has a large effect on the creep rate.

$$\dot{\gamma} = 48.8 \cdot 10^{-25} \cdot \left(\frac{\tau}{(1-0.15)}\right)^3 = 8 \cdot 10^{-24} \cdot \tau^3$$

As this is the only estimate obtainable, the range will be assumed to cover one order of magnitude, with;

$$2.5 \cdot 10^{-24} \leq C_S \leq 2.5 \cdot 10^{-23}$$

where:

$C_S = \frac{\dot{\gamma}}{\tau^3}$

7.8 Compaction Creep

Solid ice is not subject to compaction creep and in the literature there are no reported small scale tests on compaction creep of fragmented ice. However, if extrusion of un-refrozen rubble at the edges of the rubble field is assumed to be negligible, rubble field settlement data from Kaubvik can be used to calculate compaction strain rate versus pressure. At 15 points on the rubble field, initial height, position, and settlement over a 95 day period were recorded (Frederking et al, 1988). By plotting each point on a bathymetric chart the water depth at each location was also determined. It was then assumed that all the settlement occurred in the below water un-refrozen rubble. The thickness of this layer was calculated by subtracting an average refrozen layer thickness of 1.5 m from the water depth. The weight of the overlying ice, combined with the buoyancy of the submerged ice was then used to calculate the average pressure in the un-refrozen rubble layer. The resulting data are plotted in figure 41. Only 12 points are used because buoyancy calculations indicated that there was no contact with the seabed at three locations.

A straight line starting at the origin which passes through the data has the following equation:

$$\dot{\epsilon} = 10^{-13}\sigma$$

and although most ice creep is non-linear, the linear assumption fits the data and will thus be used.

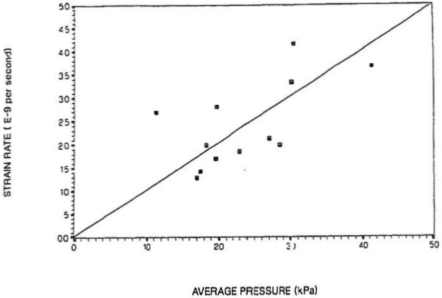

Figure 41: Graph of average consolidation pressure within the un-refrozen rubble versus settlement strain rate.

Medium scale model basin tests by K.R. Croasdale and Associates (1986) indicate an average compaction (settlement) creep rate of $3 \cdot 10^{-7}$ /sec for a pressure of 30 kPa, over a period of 9 days. Again using a linear assumption, this gives a compaction creep coefficient of $1 \cdot 10^{-11}$ /sec. These tests were done during a period of rapid deterioration of the rubble (thawing) and are thus expected to give a lower bound (least stiff) value. The compaction creep coefficient is thus expected to fall within the range;

$$1 \cdot 10^{-13} \leq C_C \leq 1 \cdot 10^{-11}$$

7.9 Refrozen Layer Mechanical Properties

Extensive theoretical and experimental work by N.K. Sinha (1978a, 1978b, 1981, 1983a, 1983b, 1984) has yielded the following equation which predicts the deformation of columnar freshwater ice under load;

$$\text{Total Strain} = \epsilon_t = \epsilon_e + \epsilon_d + \epsilon_v$$

where

ϵ_e = Elastic strain = $\frac{\sigma}{E}$

ϵ_d = Delayed elastic strain = $\frac{C_1 \cdot d_1 \cdot \sigma}{d \cdot E}(1 - exp(-(a_T \cdot t)^b))$

ϵ_v = Viscous strain = $\dot{\epsilon}_{v1} \cdot t \cdot \left(\frac{\sigma}{\sigma^1}\right)^n$

E = 9.5 GPa

$C = 9$

d = Grain diameter (mm)

d_1 = 1 mm

σ = Applied stress (N/m^2)

σ^1 = Reference stress (1 MPa)

a_T = 0.00025 /sec (at T = 263 K)

t = Time (sec)

$b = 0.34$

$\dot{\epsilon}_{v1}(at\ T_1) = \frac{\dot{\epsilon}_{v1}\ (at\ T_2)}{S_{1,2}}$

$S_{1,2} = exp\left(\frac{Q}{R}\left(\frac{1}{T_1} - \frac{1}{T_2}\right)\right)$

Q = Activation energy = 67,000 J/mole

R = Universal gas constant = 8.316 J/mole K

T_1 and T_2 are temperatures in K

$\dot{\epsilon}_{v1} = 1.76 \cdot 10^{-7}$ /sec (263 K and 1 MPa)

$n = 3$

Sinha's equation has also been applied to columnar sea ice with good results (Frederking et al, 1981; Sinha, 1984) provided that the grain diameter term d represents the platelet spacing, rather than the entire grain width. This equation will thus be used to calculate the refrozen layer deformation.

This equation includes both elastic and creep terms and thus fully describes deformation versus time for primary and secondary creep. Tertiary creep only starts after significant deformation has taken place, so for the purpose of this model, tertiary creep will not be included.

The two variables required are the platelet spacing and the ice temperature. The Kaubvik data indicates an average platelet spacing of 0.75 mm and an average refrozen layer temperature of - 7.5° C. For this specific case, Sinha's equation reduces to;

$$\epsilon_e = \frac{\sigma}{9.5 \cdot 10^9}$$

$$\epsilon_d = 1.26 \cdot 10^{-9} \cdot \sigma \cdot (1 - exp(-.000334 \cdot t)^{.34})$$

$$\epsilon_v = 2.35 \cdot 10^{-25} \cdot \sigma^3 \cdot t$$

NOTE: At time = infinity delayed Elastic Strain = $1.26 \cdot 10^{-9} \cdot \sigma$

The average material moduli are thus

$$E = \frac{\sigma}{\epsilon} = 9.5 \cdot 10^9$$

$$C_{RL} = \frac{\dot{\epsilon}_v}{\sigma^3} = 2.35 \cdot 10^{-25}$$

7.10 Summary Of Ranges And Averages

Having established the ranges in which each property is expected to fall, it is useful to calculate average values. A stiffness range of $10 \leq E \leq 1000$ covers a span of two orders of magnitude and has a mean average of 505. This is still of the order of 1000,

Table 10: Summary of the property values and ranges used in the theoretical model.

PROPERTY	MAX	AVG	MIN
Sea water density (ρ_i)	-	1024 kg/m^3	-
Ice density (ρ_w)	-	900 kg/m^3	-
Rubble porosity (P)	-	15 %	-
Refrozen/un-refrozen rubble friction (μ_{RR})	$\frac{63400}{\sigma_n+.47}$	-	1.2
Rubble/seabed friction (μ_{is})	1.0	0.71	0.5
Refrozen layer elastic modulus (E_i)	3.0 GPa	9.5 GPa	30.0 GPa
Un-refrozen rubble elastic shear modulus (G_r)	1.4 GPa	0.07 GPa	0.0036 GPa
Un-refrozen rubble “elastic” compaction modulus (E_C)	160,000 kPa	3000 kPa	57 kPa
Refrozen layer creep modulus (C_{RL})	$7.4 \cdot 10^{-26}$	$2.35 \cdot 10^{-25}$	$7.4 \cdot 10^{-25}$
Un-refrozen rubble shear creep modulus (C_S)	$2.5 \cdot 10^{-24}$	$8 \cdot 10^{-23}$	$2.5 \cdot 10^{-23}$
Un-refrozen rubble compaction creep modulus (C_C)	$1 \cdot 10^{-11}$	$1 \cdot 10^{-12}$	$1 \cdot 10^{-13}$

and so a straight mean is not appropriate. Therefore a log mean is used to calculate the average value.

$$Avg = 10^{0.5(logMax+logMin)}$$

This yields an average of 100, one order of magnitude above and below the extreme values. Table 10 summarizes the values that are used.

8 MODEL RESULTS AND DISCUSSION

Despite the conceptual simplicity of the model, actual calculation of load transmission through a series of repeating units is a very cumbersome process. In order to produce numerical results it was thus necessary to use a computer. First a fortran program was written (see appendix F) to calculate the spring and damper coefficients, given a rubble field geometry. The output from this program was used as input to a commercial finite element package called ABAQUS. ABAQUS was used to simplify the programming, and the spring/damper model eliminated the need for a full finite element mesh (see appendix F). The resulting program was short, easily modified, and used to calculate the load distributions for more than 70 different rubble field cases. Although the spring/damper model can be used for 3D calculations, as will be demonstrated, it is basically two-dimensional and the present work is primarily a 2D analysis.

Before any actual calculations are carried out it is useful to make some observations and predictions concerning the expected results. It is apparent that;

1. Regardless of the assumptions, the 2D analysis will always indicate that grounded rubble reduces loads transmitted to the structure.
2. Load transmission to the seabed is enhanced by increasing the total rubble/seabed sliding resistance, the rubble field extent and the un-refrozen rubble shear stiffness. It is also enhanced by decreasing the refrozen layer stiffness and the compaction stiffness.
3. For the 3D case, assuming no global sliding, the load on the structure depends initially on the elastic deflection, and finally on the creep velocity of the rubble in the region of the structure. Both these vary with position within the rubble

field, increasing as one moves towards the loaded edge.

4. In the 3D case, the structure is surrounded by refrozen and un-refrozen rubble many times thicker than the surrounding sea ice. The rubble is thus physically capable of applying much greater loads to the structure than the thinner sea ice.

5. Relative movement (sliding) at the rubble/seabed interface will begin before global sliding, and will start at the loaded edge.

6. Because delayed elasticity effects are not included, only the initial and final load distributions have any real significance. The initial distribution is independent of the damper viscosities and the final distribution is independent of the spring stiffnesses.

It was decided to use the field data from Kaubvik to specify a realistic rubble/structure scenario. The spring/damper model would then be used to investigate the sensitivity of the load distribution to changes in the base case parameters. To this end the rubble field and loading measured on Julian Day 118 (April 29th) was chosen. At that time the conditions shown in table 11 applied.

The step load is calculated from the change in average sea ice pressure towards the CRI. On day 118 the pressure increased from zero to 250 kPa in a relatively short period of time. Using the assumption that the load is mainly carried by the upper 2/3 of the ice sheet, it is calculated that a 1.6 m thick ice sheet applying a pressure of 250 kPa produces a force of 267 kN/m along the waterline. Because delayed elasticity was not considered, the theoretical modelling concentrated on examining the load distributions at the moment of application of the load (time=0), and at the end condition (time=∞). The initial elastic distribution was calculated statically

Table 11: Input values for the baseline rubble field.

Avg. sail height	4 m
Avg. Water depth	10.5 m
† Rubble extent	75 m
† Number of sails	5
Total rubble field width	400 m
Refrozen layer thickness	3 m
Sea Ice thickness	1.6 m
Step loading	267 kN/m

† Between the tidal crack and structure, to the south.

which means that the dampers were not considered by ABAQUS. The final creep conditions were calculated dynamically but with stiffer springs to reduce the time required to reach steady state. As with the finite element analyses done by Evgin et al (1984) and Canadian Marine Engineering Ltd. (1988), some difficulties were encountered with the slider elements. It appears that, during the dynamic runs, many coulomb dampers underwent sliding, causing the internal ABAQUS matrices to become unstable, leading to small time steps and sometimes premature termination the program. However, the program used in this work was simpler than a complete finite element program and so this problem was overcome by removing the coulomb dampers which immediately (time = 0) started sliding, and replacing them with horizontal loads equal to the sliding resistance. This did not alter the load distribution but reduced the complexity of the calculations, allowing the time varying loads to be calculated. All the desired data was thus generated and the use of the spring/damper model simplified the process.

For comparison, the ABAQUS results in the following discussion will be contrasted with predictions based on simple theory (rigid body) calculations. Figure 42 shows the simple theory applied to the baseline case.

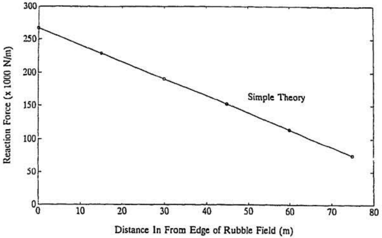

Figure 42: Simple theory prediction of reaction force versus horizontal position in the rubble field for the baseline case. Reaction force is the applied force minus the load transmitted to the seabed.

8.1 2D Hand Calculations

Although a computer is required to calculate the load distribution through several repeating spring/damper units, hand calculations with only one unit can provide useful information. In particular, such calculations give the maximum force that can be transmitted without global sliding, the minimum force required to cause refrozen/unrefrozen rubble sliding, and an approximation of the initial rate of change of loading due to creep effects.

8.1.1 Max. Transmitted Force Without Complete Sliding

At time = 0 (elastic conditions) the maximum reaction force seen by the structure without complete rubble sliding is calculated as follows;

$$F_s = W_g \cdot \mu_{is} \left(\frac{S_{RL} + S_C}{S_S} \right) \tag{15}$$

At higher loads than this, the spring-damper results match those from the simple theory predictions because all the rubble is sliding. For average baseline conditions, the maximum reaction force without global sliding is 513 kN/m .

At time = ∞ (final steady state creep) the maximum reaction force at the structure before global sliding occurs is calculated as follows;

$$F_s = W_g \cdot \mu_{is} \left(\frac{D_{RL}}{D_S} \right)^{0.33} \tag{16}$$

So for average conditions the maximum reaction force before global rubble sliding starts is 20 kN/m. This clearly shows that, under average conditions, the simple theory predictions are closest to the spring/damper model predictions during steady state creep .

8.1.2 Refrozen/Un-Refrozen Rubble Sliding

The externally applied load F_a at which refrozen/un-refrozen rubble sliding begins to take place, for the elastic case, is calculated from the following equation;

$$F_a = \frac{((\mu_{ii} \cdot W_s) - (\mu_{is} \cdot W_g)) \cdot (S_C + S_{RL})}{S_C} + (\mu_{is} \cdot W_g) \tag{17}$$

For average conditions, sliding begins to occur when the applied force reaches 1.2 GN/m, and for the spring stiffness combination enabling easiest sliding, 2.8 MN/m is still required. At final steady state conditions, the following equation is appropriate;

$$F_a = \left(\frac{D_{RL} \cdot [(W_s \cdot \mu_{ii}) - (W_g \cdot \mu_{is})]}{D_C} \right)^{0} .33 + (W_s \cdot \mu_{ii}) \tag{18}$$

In this case, under average conditions, F_a must exceed 2.9 MN/m and with damper stiffnesses chosen for easiest sliding, it must exceed 756 kN/m. Although this calculation is only for one unit rigidly supported by a structure, the addition of more units will only decrease the potential for refrozen/un-refrozen rubble sliding. Therefore refrozen/un-refrozen rubble sliding is thus not expected to occur and the spring damper model can be simplified by removing the upper coulomb dampers. This was done for all the ABAQUS calculations.

8.1.3 Rate Of Change Of Reaction Force

Following the initial elastic deformation, the reaction forces will gradually change as the dampers flow. Calculations based on one unit will give an order of magnitude approximation of the rate at which this occurs. The following equation has been simplified by leaving out the effect of the compaction elements, as later calculations will show that they carry very little load.

$$\dot{F}_s = \left(\frac{1}{D_S}\left(\frac{S_S \cdot F_s}{S_{RL}}\right)^3 - \frac{F_s^3}{D_{RL}}\right) \cdot S_S \cdot S_{RL} \cdot \left(\frac{1}{S_S + S_{RL}}\right) \qquad (19)$$

Under average conditions, with an initial reaction force at the structure of 100 kN/m the rate of load redistribution predicted by this equation is 0.002 N/sec, and for the most rapid rate this increases to 0.8 N/sec. In either case the rate of load redistribution is very slow.

8.2 2D ABAQUS Results

8.2.1 Elastic Results

Figure 43 shows the results of spring/damper model calculations for baseline case geometry but with material stiffnesses (not coulomb dampers) chosen to allow maximum, minimum, and average load transmission to the structure.

Maximum load transmission is achieved by assuming the maximum refrozen layer and compaction stiffnesses, and the minimum un-refrozen rubble shear stiffness. Minimum load transfer is accomplished by the reverse, and average values are used for the average conditions. It is apparent from the results that great deviation from the simple theory prediction is possible, and the uncertainty approaches the maximum

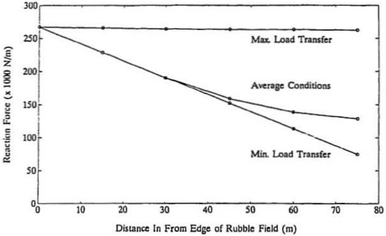

Figure 43: Average and extreme load distributions obtained by varying the spring stiffnesses in the spring/damper model.

theoretical error. Thus no reliable magnitudes of transmitted load can be predicted from these calculations. The same is presumably true for all other models, unless other authors have more accurate values for the material properties. Having established that the percent of load transmitted is sensitive to the initial assumptions it is important to examine the influence that each input parameter has on the output. The parameters can be divided into three categories; material properties, geometry, and loading. Beginning with the material properties, figure 44 gives an indication of the model sensitivity to compaction stiffness.

The results show that, even though the assumed range of values for compaction stiffness covers more than three orders of magnitude, it has a negligible effect on the resulting load distribution. This is because, relative to the refrozen layer, the compaction stiffness is very small and therefore the compaction spring element does not carry a significant portion of the load. Unless future measurements indicate that compaction stiffness is greater than assumed here it may be neglected without

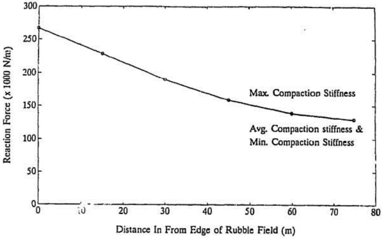

Figure 44: Spring/damper results for baseline case with variation of compaction stiffness to give maximum, minimum, and average load transmission.

significantly affecting future model results.

Variation of refrozen layer stiffness gives the results shown in figure 45. From this it is aparent that the assumed range of values for the refrozen layer stiffness has a significant effect on the output. However, the elastic stiffness of ice is the best measured mechanical property and the order of magnitude range used could probably be safely narrowed at the present level of knowledge. In this case reduction at the top end (stiffest) of the range would most likely take place. Thus top priority for further experimental work on the elastic modulus of solid ice is not warranted.

Variation of un-refrozen rubble shear stiffness gives the results shown in figure 46, and this clearly shows that the output is very strongly influenced by the uncertainty in un-refrozen rubble shear stiffness. The assumed range of values covers more than two and a half orders of magnitude and is one of the least well measured properties. The results of all future theoretical work on load transmission through grounded rubble depend very strongly on the reliability of the assumed shear stiffness values

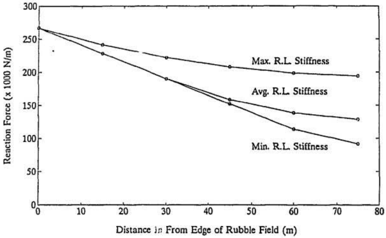

Figure 45: Spring/damper model results with variation of the refrozen layer stiffness only, to produce the maximum range of transmitted loads.

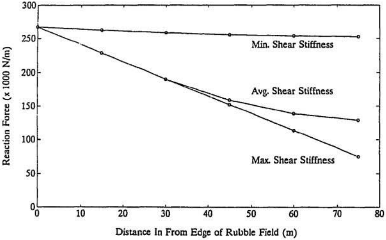

Figure 46: Spring/damper model output for baseline case and variation of un-refrozen rubble shear stiffness only, to give maximum range of transmitted loads.

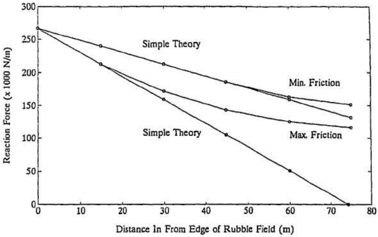

Figure 47: Simple theory versus spring/damper model predictions for the baseline case, using maximum and minimum ice/soil friction.

and experimental measurements of this should have a high priority.

The final property required for the elastic analysis is ice/seabed friction. Figure 47 shows the sensitivity of the output to this parameter. In this case the variation of assumed friction coefficient changes the simple theory predictions, as well as the spring/damper model output. Along the coincident portions of the curves, both theories predict sliding. The region in which the proposed model deviates from the simple theory prediction is the area where no sliding is predicted by the proposed model. It is apparent from figure 47 that the higher the friction coefficient, the greater the deviation of the simple theory from the proposed model; however, the variation of friction coefficients has only a moderate effect on the spring/damper model output. In fact the simple theory is more sensitive to friction than the proposed model.

Small scale friction measurements are relatively easy to make and some more data would be useful; however, as with the refrozen layer elastic stiffness, the range assumed here is conservative and could fairly easily be reduced with the present level

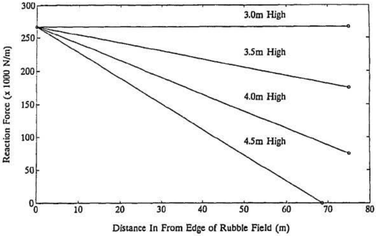

Figure 48: Simple theory predictions of reaction force versus sail height.

of knowledge. The most questionable values are felt to be at the top end of the range. One of the short commings of the spring/damper model presented here, is the use of single friction coefficients. As a first approximation the static and kinetic friction coefficients were combined but in future models consideration should be given to incorporating separate static and kinetic friction coefficients.

Now to examine the effects of rubble field geometry, beginning with water depth and sail height.

For the proposed model, variation of sail height would have exactly the same effect as variation of friction coefficient which has just been discussed. For this reason figure 48 shows the effect on the simple theory only. It is clear that the model is quite sensitive to sail height, as a 1 m reduction in average sail height would reduce sliding resistance to zero.

Variation of water depth will similarly affect sliding resistance, but it will also change the compaction and shear stiffnesses. Because of this, the spring/damper results will not deviate so greatly from simple theory predictions in shallower water.

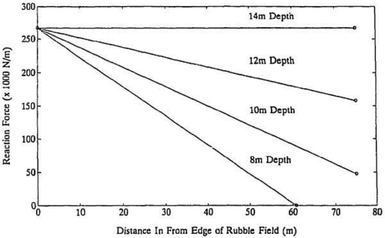

Figure 49: Simple theory predictions of reaction force versus water depth.

Relative to the assumed property range; however, this is small. As figure 49 shows, an increase in water depth of 3.5 m is required to reduce sliding resistance to zero. Therefore, relative to measurement accuracy, the model is more sensitive to sail height than water depth.

Fig 50 shows variation of transmitted force versus refrozen layer thickness. The difference in initial slope is due to changes in grounding pressure which changes because refrozen layer buoyancy varies. As expected, the stiffer (thicker) refrozen layer transmits more force; however, the results are only moderately sensitive to this parameter.

Fig 51 shows how load on the structure varies with the extent of protective rubble. This graph is not quite the same as the previous graphs as it required 12 ABAQUS runs to generate one curve. The points on the curve give the reaction force at the structure only, pressures within the rubble field cannot be read from the graph.

As expected, the graph indicates that the wider the rubble accumulation, the greater the protection. It is also apparent that the greatest difference between the

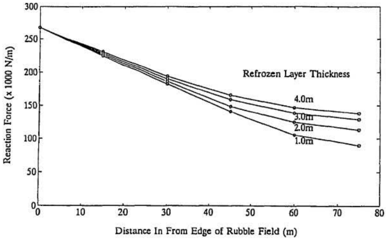

Figure 50: Influence of refrozen layer thickness on load distribution.

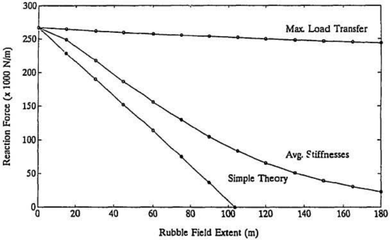

Figure 51: Reaction force at the structure (only) versus rubble field extent for simple theory and the spring/damper model.

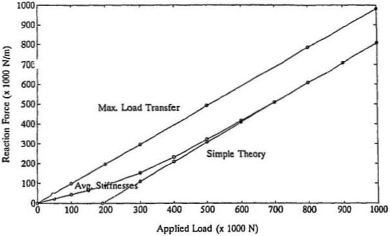

Figure 52: Applied load vs reaction force at the structure (only), for the baseline case. Simple theory and spring/damper model predictions.

simple theory and the spring/damper model occurs at the point when the simple theory first indicates complete protection. The simple theory prediction at this loading will not coincide with the spring/damper model prediction, except at the no rubble condition, and so regardless of the rubble field width, the structure should always see some load.

Figure 52 shows the variation of reaction force at the structure as applied load is varied. The results indicate that for a given rubble field, the simple theory and spring/damper model predictions will coincide, provide that a sufficient loading is applied. This happens when all the units begin to slide. It is also apparent that, as in figure 51, the greatest error occurs when the applied load just equals the total rubble field sliding resistance.

It has thus been established that the deviation of the spring/damper model predictions from the simple theory is strongly dependant on the input values, within the assumed ranges. The sensitivity of the output to each of the inputs has also been

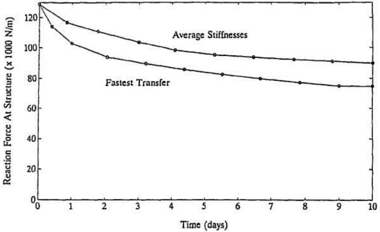

Figure 53: Reaction force versus time for average spring and slider stiffnesses with dampers chosen to give average and fastest rates of load redistribution.

examined, showing that the most critical input parameter is the un-refrozen rubble shear stiffness. It is now necessary to examine the final, long term viscous response.

8.2.2 Viscous Results

Under load, solid polycrystalline ice initially deforms elastically, followed by a combination of decaying delayed elastic strain rate, and steady viscous creep. Once all the delayed elasticity has been accumulated, the minimum, or secondary, creep rate is reached. The following predictions are based on the final steady state creep rate. Without including the effects of delayed elasticity, accurate determination of the time required to reach steady state cannot be made. However, it is still interesting to look at the reaction force versus time prediction in order to get an "order of magnitude feel" for the times involved.

From figure 53 we can see that the time required for load redistribution is of the order of hours or days, rather than seconds or minutes. This is important because the largest (design) loads, such as impact with a multiyear floe or landfast ice break-up,

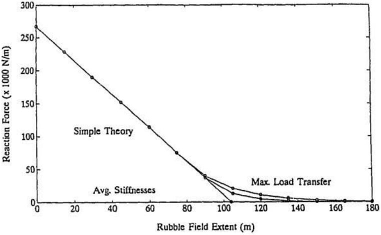

Figure 54: Spring/damper model and simple theory predictions for steady state (time=∞) reaction force at the structure versus extent of the rubble field.

are likely to be transitory. The fact that load redistribution due to creep is expected to occur slowly means that it is not so important for design considerations.

Having established that steady state conditions are not reached quickly the expected steady state load distributions will be examined.

Figures 54 and 55 show that, in the long term, the rubble is very effective at transmitting loads to the seabed, regardless of the assumed inputs, and thus the results are very close to the simple theory predictions. At steady state the spring/damper model is thus not sensitive to the input values within the assumed ranges of properties. This is surprising at first because both the shear stiffness and refrozen layer compressive stiffness ranges cover an order of magnitude, and the compaction stiffness range covers two orders of magnitude but there appear to be two main reasons for this.

1. The shortage of information on shear creep of rubble resulted in a relatively small assumed range, based only on estimates for porous ice.

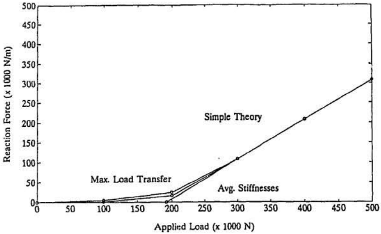

Figure 55: Spring/damper model and simple theory predictions for reaction force at the structure versus applied load.

2. The power law flow of ice with n = 3 means that differences in stress between the refrozen and un-refrozen rubble has a very strong effect on the creep rate.

For the baseline case, the compressive stress in the refrozen layer is carried by a three metre thickness, while the shear stress is limited by ice/seabed friction, and carried over a 75 metre width. Initially, average compressive stress is 66 kPa, while the average shear stress is only 1.8 kPa. The gauge length in compression (75 m) is also much longer than for shear (10.5 m), and so for the average deformation rates to be approximately equal, the shear stiffness constant C_S must be 150,000 times "softer" than the compression stiffness constant. With the assumed ranges, the softest un-refrozen rubble in shear is only 340 times softer than the hardest refrozen layer ice in compression. These results are independent of the initial assumed elastic properties. Thus, for the 2D case, the spring-damper model indicates that steady state conditions are less important than initial conditions and can reasonably be approximated by the simple theory. Changes in geometry and ice/seabed friction will

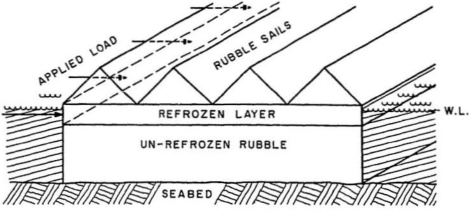

Figure 56: Semi-infinite, unrestrained, three dimensional rubble field represented by the spring-damper model without a structure.

alter the steady state load distribution in the same way as the simple theory which has been discussed earlier.

8.3 3D ABAQUS Results

It is beyond the scope of this work to carry out a full three dimensional analysis; however, it is appropriate to explain how this can be done with the proposed spring-damper model. For the 2D analysis, one side of the rubble field was assumed to be fixed, ie., resting against a rigid, immovable, structure. If this boundary condition is removed, the spring-damper system represents an unrestrained (except sliding), semi-infinite rubble field (see figure 56).

The spring damper model can now be used to predict elastic and viscous response of such a rubble field to external loadings. As an example, this has been done for a 450 m wide rubble field, with average baseline properties, subjected to a 1 MN/m horizontal external force. The results are plotted in figures 57 to 60.

The rubble field is well grounded enough to resist global sliding; however, the

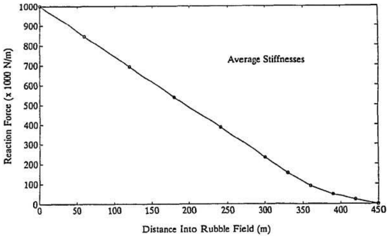

Figure 57: Transmitted force versus position in the rubble field for initial elastic conditions.

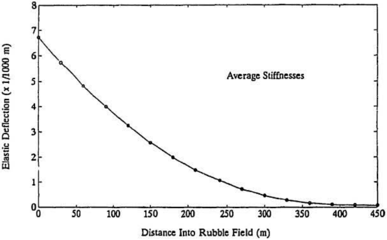

Figure 58: Initial refrozen layer elastic deflection versus position for average conditions.

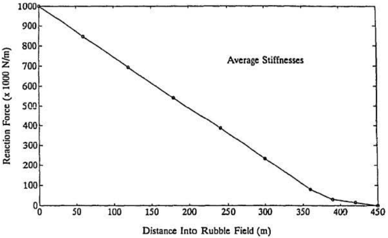

Figure 59: Transmitted force versus position in the rubble field for final steady state (creep) conditions.

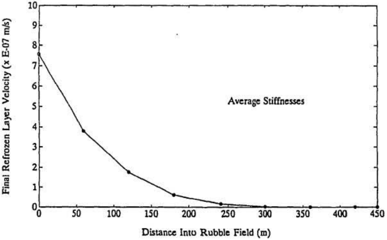

Figure 60: Refrozen layer velocity versus position in the rubble field for final steady state (creep) conditions.

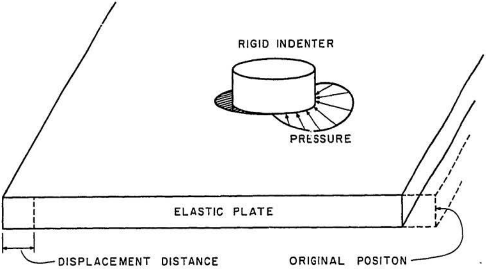

Figure 61: Representing the ice structure interaction problem as an elastic plate of thickness t pushed a distance C past a fixed, rigid peg of diameter D.

spring-damper model allows calculation of deformations within the rubble. If a structure was embedded in such a rubble field, it would have to resist these deformations, and the loads on the structure would presumeably depend on the magnitude of the movements. As the results show, the scale of the movement is very dependent on position within the rubble. If it is assumed that the presence of a structure does not greatly influence the movement of the semi-infinite rubble field, and that load on the structure is basically applied by the refrozen layer, the loads can be calculated using the following approaches.

8.3.1 Elastic Calculation

The refrozen layer is treated as an elastic plate with a rigid, fixed structure, protruding through it (see figure 61).

Unfortunately, a classical solution for this problem does not seem to have been worked out in any text on elasticity theory. It would be possible to assume a pressure distribution and frictionless contact, and derive the solution from the general case for pressure against the edge of a hole in a semi-infinite plate (Sokolnikoff, 1956; Muskhelishvili, 1975). This; however, requires the use of complex calculus and series expansion, and considering all the uncertainty inherent in the loading calculations, it is deemed more appropriate to use simpler, semi-infinite plate edge loading calculations such as those presented by Timoshenko et al, (1970). In order to approximate infinite plate results from semi-infinite plate equations the calculated loads will be doubled. This is required because the ice sheet all around the structure is stressed as a result of the movement and therefore the refrozen layer in "front" and "behind" the structure all contribute to the loading. This is not an exact method, but it should give answers of the correct order. For a frictionless indenter of width D, applying uniform pressure at the edge of a semi-infinite plate, the equation for the deformation at the centre is (Timoshenko et al, 1970);

$$\delta_c = \frac{2 \cdot F}{\pi \cdot E_i \cdot t_i} log\left(\frac{D}{2}\right) \tag{20}$$

where

$\delta_c =$ deformation at the centre of the indenter

$t_i =$ ice thickness

For the rubble field, the deformation is determined from the spring-damper model and the total force can then be calculated from equation 20. This is rewritten as (multiplied by 2);

$$F = \frac{\delta_c \cdot \pi \cdot E_i \cdot t_i}{log(\frac{D}{2})} \tag{21}$$

If it is assumed that the addition of rubble to the right hand side of the rubble field in does not provide any additional significant restraint, then the results from figures 57 and 58 can be used to calculate the baseline case in three dimensions. Figure 57 shows that a force of 267 kN/m is felt in the rubble 286 m from the 1 MN/m loaded edge. This is equivalent to the loaded edge in the baseline case. For the baseline case the structure was 75 m into the rubble field, putting it 361 m into the field in both figures. From figure 58 we see that the elastic deformation of the refrozen layer at that point is $1.6 \cdot 10^{-4}$ m and from equation 21 it is calculated that a load of 8.2 MN is required for a 100 m diameter structure to resist the deformation. This is less than the load predicted by the 2D analysis (13 MN) and because the rigid structure is a stress concentrator, this value should be larger. Never-the-less it is larger than the zero value predicted by the simple theorey (rubble field does not slide) and the the result is affected by the simplifications. including the assumption that compaction of the unrefrozen rubble against the structure could be ignored. Thus some refinement is required, but it is assumed that the basic approach is correct.

8.3.2 Viscous Calculation

Using assumptions similar to those for the elastic case, the steady state creep load can be calculated. This has been done by various authors for ice loads on structures (Bruen et al, 1984; Ponter et al, 1983; Hamza, 1985; and Sanderson, 1984). The most detailed analysis is presented by Sanderson, who used the reference stress method and plastic limit analysis for three different assumed ice types. The maximum and minimum values were always obtained with the reference stress method, by assuming purely granular or purely columnar ice types. The loads for edge loading of a semi-infinite plate were calculated using the following equation (see appendix C for details);

$$F = 1.15 \cdot D \cdot t_i \cdot F_\sigma(\dot{\epsilon}) \tag{22}$$

where:

F = Total load (MN)

t_i = Ice thickness (m)

$F_\sigma(\dot{\epsilon})$ = stress at corresponding strain rate $\dot{\epsilon}$.

If, as with the 3D elastic case, we assume that the addition of rubble to the right hand side of the rubble field does not significantly alter the given velocity profile, then figures 59 and 60 can be used to calculate the baseline case in three dimensions. At the structure location the unrestrained refrozen layer velocity is $1.2 \cdot 10^{-11}$ m/s and using the method illustrated in appendix C, the calculated load on a 100 m wide structure is

$$2.5\ MN \leq F \leq 2.1\ MN$$

given

Refrozen layer thickness = 3 m

Average refrozen layer temperature = 265.5 K

Again these values are smaller than the 2D results, only giving forces of the order of 23 kN/m, but it is clear from figure 60 that the loads (velocity) increase dramatically towards the loaded edge. The rigid structure is obviously a stress concentrator, rather than a stress reliever and so the calculated values should be larger than the 2D results. This is assumed to be because the ice properties used by Sanderson are different than those used in the velocity calculation (softer). As with the 3D elastic calculation the results are greater then the zero value predicted by the simple theory, but refinement of the calculation is still required.

8.4 Comparison With Field Data

As noted in the M.U.N. field data report (Jordaan et al, 1988), vertical cracks were observed in the rubble and one of these radiated from a corner of the CRI. This implies that the CRI induced stresses within the rubble, leading to partial failure of the rubble field. As some cracks were up to 1 m wide, this also shows that large masses of rubble can move somewhat independently.

The NRC rubble movement data from Kaubvik indicates an average rubble field movement of the order of 0.25 m over a three month period. This is equivalent to an average velocity of $3 \cdot 10^{-8}$ m/s which is an order of magnitude greater than that predicted by the 3D analysis for average properties. This implies that the viscosities used in the spring-damper model are too high but the field measurements are complicated by tilting of the rubble sails, crack formation, and downslope movement. For these reasons the error should not be considered excessive.

On day 118 measurements indicated that the average sea ice pressure rapidly increased by 250 kPa, leading to a calculated force of 267 kN/m, and this was taken as the baseline case for the model. For that day, ESSO collected data from 6 micro cell pressure sensors on the three southern caissons (numbers 4, 5, and 6)(see appendix A). Although the accuracy of these sensors is ± 340 kPa, four of these sensors indicated changes in pressure within the resolution of the data ($\approx$ 60 kPa). Two of these sensors indicated compressive stress and two of the sensors indicated tensile stress, although tensile stress would not be predicted. In contrast, the shearbar panel mounted on caisson 7 (west side) indicated an increase in tensile stress up to 70 kPa. The resolution of the shearbar data is almost an order of magnitude better than the microcell data. For these pressures the shearbar data is expected to be more reliable and the indicated tensile stress is compatible with the expected WNW rubble field deformation. There were also two microcells on caisson 7 and one indicated no change in pressure, while the other indicated a small increase in compressive stress. The only conclusions that can be made from this are that pressures were small, tended to be variable, and that the accuracy and resolution of the microcells was insufficient for analysis of these loads. It must be remembered that the refrozen layer at the structure was expected to be about 4 m thick at that time, so that a pressure of only 50 kPa in the upper 2/3 of the refrozen layer is equivalent to a load of 133 kN/m, or a total load of 16 MN. This is small (3.5 %) compared to the design load but it is well within the range predicted by the spring-damper model. The lack of shearbars on the southern caissons and questionable accuracy of the microcells when subjected to small loads means that the results from proposed spring-damper model cannot be verified with the Kaubvik field data. Although this is somewhat disappointing, at least the measured pressures do not conflict with the theoretical predictions.

In general, the CRI data from Kaubvik shows that peak sensor pressures occurred before rubble accumulation, but average sensor pressure often reached or exceed previous values after the formation of stable rubble. This indicates that the largest global forces (not pressures) occurred after rubble formation. The possibility that large loads can occur in rubble is indicated by measurements from CRI sensors on Jan 30th, and April 15th (see appendix A) when pressures of 1.5 MPa and 1 MPa were recorded respectively. Sea ice pressure data is not available for these events but it is assumed that these pressures would not be predicted by the simple theory, thus demonstrating the need for more sophisticated modelling.

9 CONCLUSIONS

Despite the many simplifying assumptions required and shortage of data on rubble properties, several important conclusions can be made.

1. Published data of pressures against structures embedded in rubble show that the pressures are almost always small but this, as well as the Kaubvik data, show that loads can be transmitted through grounded ice rubble before global rubble field sliding occurs.

2. A substantial and rapidly formed refrozen layer was detected during the field program. This is expected to be able to carry higher loads than the surrounding sea ice and is therefore physically capable of applying large loads to a structure. To date there is no proof that such loadings occur but it is a possibility that requires careful examination. One refrozen layer property that should be more thoroughly examined in future studies is the size and frequency of refrozen layer discontinuities and their effect on load transmission.

3. The ABAQUS results show that when rubble deformations are included in transmitted load calculations, the results can vary significantly from those obtained using the simple theory (rigid body assumption).

4. It cannot be concluded from the theoretical work by itself that grounded rubble fields always reduce loads on structures and as no field data is presented in the literature, of loads experienced during major events such as global sliding, there is no firm basis for assuming that grounded rubble is always beneficial. One possible benifit that rubble accumulations may have, however, is that they may reduce the design sea ice pressure by influncing the ice failure mode. Although this was not examined in this thesis it is expected to be an important part of future load transmission models.

5. The 3D method presented appears to be a reasonable first approach for using the 2D spring/damper model for 3D load calculations. Additional assumptions were required, however, and so furthur refinement is needed before reliable results can be obtained.

6. Ice rubble properties are not well documented, leading to a wide range of predicted loads. From this study it was concluded that the most important properties requiring experimental verification are the shear and delayed elastic properties of un-refrozen ice rubble.

7. The field results do not significantly conflict with the theoretical results but there are not enough data in the literature, or from the Kaubvik field program, to verify the model.

8. Unless experimental work indicates that the assumed range of properties for compaction stiffness and compaction creep are wrong, they can be neglected in future theoretical models without introducing serious error.

9. Possible future improvements to the ABAQUS model include the incorporation of; seabed slope, non-rigid seabed behaviour, refrozen layer discontinuities, sea-ice/rubble failure, vertical and horizontal variation of ice properties, non-rigid behaviour of the structure, kinetic and static friction values (rather than an average) and water, rubble and structure masses.

10 REFERENCES

Abdelnour, R. and Sayed, M. (1982) "Ice Ride-Up On A Man-Made Island", *Offshore Technology Conference*, paper 4313, Houston, Texas

Agerton, D.J. and Kreider, J.R., (1979) "Correlation Of Storms And Major Ice Movements In The Nearshore Alaskan Beaufort Sea", *conference on Polar and Ocean Engineering Under Arctic Conditions* (POAC), Vol. I, Trondheim, Norway

Albery Pullerits Dickson & Associates Ltd (1984) "Caisson-Retained Island For ESSO Wins Top Honour", *Canadian Consulting Engineer*, October

Allen, J.L. (1970) "Analysis Of Forces In A Pile-Up Of Ice", *NRC Conference on Ice Engineering and Avalanche Forecasting and Control*, Calgary (1969), Technical Memorandum No. 98, Ottawa

Allyn, N.F.B. and Charpentier, K. (1982) "Modelling Ice Rubble Fields Around Arctic Offshore Structures", paper 4422, *Offshore Technology Conference* (OTC), Houston

Allyn, N. and Wasilewski, B.R. (1979) "Some Influences Of Ice Rubble Field Formations Around Artificial Islands In Deep Water", *conference on Polar and Ocean Engineering Under Arctic Conditions* (POAC), Vol. I, Trondheim, Norway

Avallone, E.A. and Baumeister III, T. (1987) " *Marks' Standard Handbook For Mechanical Engineers*", McGraw-Hill Book Co., Toronto

Bercha, F.G. and Ghoneim, G.A.M. (1982) "Evaluation Of Pile-Up Formation And Structure Interaction Forces", *NRC Workshop on Sea Ice Ridging and Pile-Up*, Calgary (1980), Technical Memorandum No. 134

Bercha, F.G., Potter, R.E., Goss, R.D. and Ghoneim, G.A. (1980) "Effect Of Pile-Ups And Rubble Fields On Ice-Structure Interaction Forces", paper 3884, *Offshore Technology Conference* (OTC), Houston

Bowles, J.E. (1984) " *Physical And Geotechnical Properties Of Soils*", 2nd edition, McGraw-Hill Book Co.

Brown, C.B. (1976) "Interaction Of Pack Ice With Structures And Associated Ice Mechanics", *AIDJEX Bulletin*, No. 34, Seattle

Bruen, F.J. and Vivatrat, V. (1984) "Ice Force Prediction Based On Strain Rate Field", *3rd Int. conference on Offshore Mechanics and Arctic Engineering* (OMAE), Vol. III, New Orleans

Canadian Marine Engineering Ltd. (1988) "Analytical Models For Broken Ice Zones", *contract report for AES/SAG*, No. 1-2:88-10, prepared for Public Works Canada

Croasdale, K.R. (1975) "Ice Forces On Marine Structures", *International Association for Hydraulic Research symposium* (IAHR), Hanover, New Hampshire

Croasdale, K.R., Der, C.Y. and Shinde, S.B. (1988) "Ice Forces And Geotechnical Response Of The ESSO CRI 1986/87), *report to Natural Sciences and Engineering Council*, report No. ERCL.RS.05

Cox, G.F.N., Johnson, J.B., Bosworth, H.W. and Vincent, T.J. (1988) "Mukluk Ice Stress Measurement Program", *conference on Polar and Ocean Engineering Under Arctic Conditions* (POAC '87), Alaska, Vol. II

Danielewicz, B.W. (1983) "On Estimating Large Scale Ice Forces From Deceleration Of Ice Floes", *conference on Polar and Ocean Engineering Under Arctic Conditions* (POAC), Helsinki, Vol. IV

Danielewicz, B. and Blanchet, D. (1988) "Measurements Of Multi-Year Ice Loads On Hans Island During 1980 And 1981", *conference on Polar and Ocean Engineering Under Arctic Conditions* (POAC), Alaska, Vol. I

Danielewicz, B.W. and Metge, M. (1982) "Ice Forces On Hans Island 1981", *APOA Project 181*, Candian Marine Drilling Ltd. report APOA-181-1

Danielewicz, B.W. and Metge, M. (1981) "Ice Forces On Hans Island 1981", *APOA Project 181*, Canadian Marine Drilling Ltd., Report No. APOA 181-1

De Paoli, S. and Pilkington, G.R. (1983) "Field Observations Around Tarsuit Island", *conference on Polar and Ocean Engineering Under Arctic Conditions* (POAC), vol III, Helsinki

Duckworth, R. and Westermann, P.H. (1988) "Stress And Strain Measurements In Ice. Field Techniques", *Polar Instrumentation Workshop*, Monterey

Evgin, E. and Morgenstern, N.R. (1984) "Unified Analysis Of Offshore Structures", *contract report prepared for the National Research Council Of Canada*, No. osu83-00111

Favrat, D. (1982) "Ice Conditions Around Artificial Islands 1976-77", *APOA Project 122*, Report IPRT.ME.78.33, ESSO Resources Canada Ltd, Calgary

Feldman, U., Howarth, P.J. and Davies, J.A, (1981) "Estimating Surface Wind Direction Over Drifting Open Pack Ice", *Journal of Geophysical Research*, Vol 86, No. C9

Fenco Consultants Ltd. (1981) "Pack Ice/Rubble Field Interaction Study Issungnak 1980", *APOA Project 171*, Contract Report for Gulf Canada Resources Inc., Report APOA 171-1

Frederking, R. and Sayed, M. (1988) "Measurements Of Ice Load Transmission Through Grounded Ice Rubble Kaubvik I-43, 1987", *NRC contract report for Canadian Oil and Gas Lands Administration*, No. CR-5420.1

Frederking, R., Wessels, E., Maxwell, J.B., Prinsenberg, S. and Sayed, M. (1986) "Ice Interaction With Adams Island, Winter 1984-85", *International Association for Hydraulic Research* (IAHR) symposium, Iowa, Vol. III

Frederking, R., Wessels, E., Maxwell, J.B., Prinsenberg, S. and Sayed, M. (1986) "Ice Pressures And Behaviour At Adams Island, Winter 1983/84", *Canadian Journal Of Civil Engineering*, Vol. 13 No 2

Frederking, R., Maxwell, J.B. and Prinsenberg, S. (1986) "Overview Of Project To Measure Ice Forces At Adams Island", *Canadian East Coast Workshop on Sea Ice*, Dartmouth, Nova Scotia

Frederking, R.M.W., Sayed, M., Wessels, E., Child, A.J. and Bradford, D. (1984) "Ice Interaction With Adams Island, Winter 1982-83", *International Association for Hydraulic Research* (IAHR) symposium, Vol. III, Hamburg

Frederking, R., Sanderson, T., Wessels, E. and Inoue, M. (1983) "Ice Behaviour Around A Small Arctic Island", *conference on Polar and Ocean Engineering Under Arctic Conditions* (POAC), Helsinki, Vol. II

Frederking, R.M.W. and Wright, B., (1982) "Characteristics And Stability Of An Ice Rubble Field Issungak, February-March 1980", *Workshop on Sea Ice Ridging and Pile-Up* (1980), NRC Technical Memorandum No. 134, Calgary

Frederking, R.M.W., Sinha, N.K. and Gold, L.W. (1981) "Mechanical Properties Of Sea Ice", *Proceedings of the 8th Canadian Congress of Applied Mechanics*, Moncton, New Brunswick

Gale, A.D., Sego, D.C. and Morgenstern, N.R. (1986) "Behaviour Of Cohesionless Broken Ice", *3rd Canadian Conference on Marine Geotechnical Engineering*, St. John's

Gale, A.D., Wong, T.T., Sego, D.C. and Morgenstern, N.R. (1988) "Stress-Strain Behaviour Of Cohesionless Broken Ice", *conference on Polar And Ocean Engineering* (POAC '87), Vol. III, Alaska, (preprint)

Gow, A.J., Arcone, S.S. and McGrew, S.G. (1987) "Microwave And Structural Properties Of Saline Ice", *CRREL Report*, No. 87-2

Hamza, H. (1985) "Winter Ice Forces On Large Offshore Structures" *4th Int. conference on Offshore Mechanics and Arctic Engineering* (OMAE), Vol. II, Dallas

Hawkins, J.R., James, D.A. and Der, C.Y. (1983) "Design, Construction And Installation Of A System To Measure Environmental Forces On A Caisson Retained Island", *conference on Polar and Ocean Engineering Under Arctic Conditions* (POAC), Vol. IV, Helsinki

Higdon, A., Ohlsen, E.H., Stiles, W.B., Weese, J.A. and Riley, W.F., (1978) " *Mechanics Of Materials*", John Wiley & Sons, Toronto

Irwin, G.J. (1975) "Ice Pressures At The Shore Of Lincon Bay", *Canadian Defense Research Establishment*, DREO Report No. 729, Ottawa

Johnson, J.B., Cox, G.F.N. and Tucker, W.B. (1985) "Kadluk Ice Stress Measurement Program", *conference on Polar and Ocean Engineering Under Arctic Conditions* (POAC), Greenland, Vol. I

Jordaan, I.J., Marshall, A.R. and Nadreau, J.P. (1988) "Full Scale Field Measurement Program Kaubvik Caisson Retained Island", *Ocean Engineering Research Group Data Report*, Memorial University of Nfld., St. John's

Juvinall, R.C. (1983) " *Fundamentals Of Machine Component Design*", John Wiley & Sons, Toronto

K.R. Croasdale and Associates Ltd. (1986) "Measurements Of The Properties Of Broken Ice Zones And Ice Rubble", *Contract report for Public Works Canada*

K.R. Croasdale and Associates Ltd. (1985) "Ice Investigations At A Beaufort Sea Caisson 1985", *Contract report for National Research Council of Canada and U.S. Dept of the Interior*

Karr, D.G. and Choi, K. (1989) "A Three Dimensional Constitutive Damage Model For Polycrystaline Ice", *Mechanics of Materials*, Vol. 8

Keinonen, A. (1977) "Measurements Of Physical Characteristics Of Ridges On April 14 and 15, 1977", *Winter Navigation Research Board*, report No. 22, Finland

Keinonen, A. and Nyman, T. (1978) "An Experimental Model-Scale Study On The Compressive, Frictional, And Cohesive Behaviour Of Broken Ice Mass", *International Association for Hydraulic Research* (IAHR) symposium, Vol. II, Lulea, Sweden

Kovacs, A. and Sodhi, D.S. (1981) "Sea Ice Piling At Fairway Rock, Bering Strait, Alaska: Observations And Theoretical Analyses", *conference on Polar and Ocean Engineering Under Arctic Conditions* (POAC), Quebec, Vol. II

Kovacs, A. and Sodhi, D.S. (1980) "Shore Ice Ride-Up And Pile-Up: Field Observations, Models, Theoretical Analyses", *Cold Regions Science and Technology*, Vol. 2, April

Kry, P.R. (1980) "Implications Of Structure Width For Design Ice Forces", *Physics and Mechanics of Ice*, Springer-Verlag, New York

Kry, P.R. (1977) "Ice Rubble Fields In The Vicinity Of Artificial Islands", *conference on Polar and Ocean Engineering Under Arctic Conditions* (POAC), Vol. I, St. John's

Lowry, R.T. and Wadhams, P. (1979) "On The Statistical Distribution Of Pressure Ridges In Sea Ice", *Journal of Geophysical Research*, Vol 84, No. C5, May

Maattanen, M. (1983) "Design Of Navigational Structures For Ice Forces", *Design for Ice Forces*, American Society of Civil Engineers (ASCE)

Marshall, A.R., Croasdale, K.R., Frederking, R.M., Sayed, M., Jordaan, I.J. and Nadreau, J.P. (1989) "Measurements Of Load Transmission Through Grounded Ice Rubble", *conference on Polar and Ocean Engineering Under Arctic Conditions* (POAC), Lulea, Sweden

Marshall, A.R. (1989) "Field Measurements Of Ice/Ice Friction", *Unpublished*

McGonigal, D. (1981) "Ice Stress Panel Results Issungnak 1980", *APOA Project 171*, Gulf Canada Resources Inc., Report No. APOA 171-1, Vol. V, Calgary

McGonigal, D., Wright, B.D. and Foo, P.M. (1986) "Natural Shoal Rubble Pile Study Beaufort Sea March-April 1979", *APOA Project 170*, Gulf Canada Resources Ltd., Report No. 170-2, Calgary

McKenna, R.F., Marshall, A.R. and Jordaan, I.J., (1988) "The Application Of AES Environmental Data To Ice Interaction Modelling", Ian Jordaan and Associates Inc. *Draft Final Report to Canadian Climate Centre*, Atmospheric Environment Service, Environment Canada, 1988

Mellor, M. (1979) "Mechanical Properties of Polycrystaline Ice", *preprint prepared for IUTAM symposium on the Physics and Mechanics of Ice*, Denmark

Metge, M. (1976) "Ice Conditions And Defence At Netserk B-44 and Adgo P-25 During The Winter Of 1974-75", *APOA Project 104*, Report IPRT-6ME.-76, Imperial Oil, Calgary

Metge, M., Danielewicz, B. and Hoare, R. (1981) "On Measuring Large Scale Ice Forces; Hans Island 1980", *conference on Polar and Ocean Engineering Under Arctic Conditions* (POAC), Quebec, Vol. II

Michel, B. (1978) " *Ice Mechanics*", Les Presses De L'Universite Laval, Quebec

Muskhelishvili, N.I. (1975) " *Some Basic Problems Of The Mathematical Theory Of Elasticity*", 2nd edition (English translation), Noordhoff International Publishing, Netherlands

Nelson, R.D. and Sackinger, W.M. (1976) "Ice Stress Measurements At ADGO and Netserk Islands, 1974-1975", *APOA Project 104*, Report ASTIS-G- 70289, Geophysical Institute, University of Alaska

Nelson, R.D. and Sackinger, W.M. (1974) "Ice Stress Measurement At Adgo Island" *APOA Project 104*, Report ASTIS-G-70270, Imperial Oil Ltd., Calgary

Oksanen, P. (1983) "Friction And Adhesion Of Ice", *Ph.D (Eng) thesis*, Technical Research Centre of Finland , Finland

Parker, M.N. (1987) "Ice Thickness Climatology For Northern Canada", *Scientific Services Report*, Atmospheric Environment Service

Parmerter, R.R. (1975) "A Model Of Simple Rafting In Sea Ice", *Journal Of Geophysical Research*, Vol 80, No. 15, May

Parmerter, R.R and Coon, M.D. (1973) "On The Mechanics Of Pressure Ridge Formation In Sea Ice", *Offshore Technology Conference* (OTC), No. 1810, Dallas

Parmerter, R.R. and Coon, M.D. (1972) "Model Of Pressure Ridge Formation In Sea Ice", *Journal of Geophysical Research*, Vol. 77, No. 33

Pickard, G.L. and Emery, J.W. (1982) " *Descriptive Physical Oceanography*", 4th edition, Pergamon Press, Oxford

Pilkington, G.R. (1983) "The Physical Environment Of The Beaufort Sea and Its Impact On Operations And Structures", *conference on Canadian Offshore Drilling & Downhole Technology* (CODD), Edmonton

Pilkington, R., Blanchet, D. and Metge, M. (1983) "Full Scale Field Measurements Of Ice Forces On An Artificial Island", *conference on Polar and Ocean Engineering Under Arctic Conditions* (POAC), vol. IV, Helsinki

Pilkington, G.R., O'Rourke, J.C., Steen, J.W. and Banke, E.G. (1982) "Ridge Keel Observations", *1980 NRC Workshop on Sea Ice Ridging and Pile-Up*, Calgary, Technical Memorandum No. 134

Ponter, A.R.S., Palmer, A.C., Goodman, D.J., Ashby, M.F., Evans, A.G. and Hutchinson, J.W. (1983) "The Force Exerted By A Moving Ice Sheet On An Offshore Structure Part 1. The Creep Mode", *Cold Regions Science and Technology*, 8

Pounder, E.R. (1965) " *The Physics Of Ice*", Pergamon Press, Oxford

Pounder, E.R. and Little, E.M. (1959) "Some Physical Properties Of Sea Ice I", *Canadian Journal of Physics*, Vol. 37

Prodanovic, A. (1979) "Model Tests Of Ice Rubble Strength", *conference on Polar and Ocean Engineering Under Arctic Conditions* (POAC), Vol. I, Trondheim, Norway

Rigby, F.A. and Hanson, A. (1976) "Evolution Of A Large Arctic Pressure Ridge", *AIDJEX Bulletin*, No. 34, Dec.

Roggensack, W.D. (1975) "Large Scale Laboratory Direct Shear Tests On Ice", *NRC Canadian Geotechnical Journal*, Vol. 12, No. 2

Saeki, H., Ozaki, A. and Kubo, Y. (1981) "Experimental Study On Flexural Strength And Elastic Modulus Of Sea Ice", *conference on Polar and Ocean Engineering Under Arctic Conditions* (POAC), Laval, Quebec, Vol I.

Sanderson, T.J.O. (1984) "Theoretical And Measured Ice Forces On Wide Structures", *International Association for Hydraulic Research* (IAHR) State-Of-The-Art Report On Ice Forces

Sayed, M. (1989) (geotechnical engineer at NRC) *personal communication*

Sayed, M., Frederking, R.M.W. and Wessels, E. (1988) "Field Measurements Of Stress And Deformations In A First Year Ice Cover Adjacent To A Wide Offshore Structure", *Canadian Geotechnical Journal*, Vol. 25 No 4

Sayed, M. (1987) "Mechanical Properties Of Model Ice Rubble", *Materials and Member Behaviour*, Structural Congress, Orlando, Florida, p 647-659

Sayed, M., Frederking, R.M.W. and Bradford, D. (1986a) "Ice Cover Deformations At Adams Island, Winter 1982-83", *Canadian Geotechnical Journal*, Vol. 23, No 3

Sayed, M. and Croasdale, K.R. (1986b) "Ice Stress Measurements In A Rubble Field Surrounding A Caisson Retained Island", *Ice Technology Conference*, Cambridge Mass.

Sayed, M. and Frederking, R.M.W. (1984) "Grounded Rubble Fields Adjacent To Offshore Structures", *Cold Regions Science and Technology*, No. 10

Semeniuk, A. (1977) "Ice Pressure Measurements At Arnak L-30 And Kannerk G-42", *APOA Project 122*, Report IPRT-15ME-77, Imperial Oil, Calgary

Shapiro, L.H and Metzner, R.C. (1987) "Coefficients Of Friction Of Sea Ice On Beach Gravel", *Journal Of Offshore Mechanics and Arctic Engineering*, vol 109

Shinde, S.B., (1988),(geotechnical engineer at ESSO), *personal communication*

Shinde, S. (1982) "Ice Conditions At Issungnak 1978-1979", *APOA Project 170*, ESSO Resources Canada Ltd., Report No. APOA 170-1, Calgary

Shinde, S.B. (1981) "Ice Conditions Around Issungnak 1979/80", *APOA Project 171*, ESSO Resources Canada Ltd., Report No. 171-1, Vol. III, Calgary

Sinha, N.K. (1978a) "Short-Term Rheology Of Polycrystaline Ice", *Journal of Glaciology*, Vol. 21, No. 85

Sinha, N.K. (1978b) "Rheology of Columnar-Grained Ice", *Experimental Mechanics*, Vol. 18, No. 12

Sinha, N.K. (1981) "Constant Stress Rate Deformation Modulus Of Ice", *conference on Polar and Ocean Engineering Under Arctic Conditions* (POAC), Vol. I, Quebec City

Sinha, N.K. (1983a) "Creep Model Of Ice For Monotonically Increasing Stress", *Cold Regions Science and Technology*, Vol. 8

Sinha, N.K. (1983b) "Field Test 1 Of Compressive Strength Of First-Year Sea Ice", *Annals of Glaciology*, Vol. 4

Sinha, N.K. (1984) "Uniaxial Compressive Strength Of First-Year and Multi-Year Sea Ice", *Canadian Journal of Civil Engineering*, Vol. II

Sokolnikoff, I.S. (1956) " *Mathematical Theory Of Elasticity*", 2nd edition, McGraw-Hill Book Co., New York

Spedding, L.G., (1979) "Landfast Ice Motion Observed In The MacKenzie Delta Region Of The Southern Beaufort Sea In The 1972/73 Winter", *conference on Polar and Ocean Engineering Under Arctic Conditions* (POAC), Vol. I, Trondheim

Stander, E. (1985) "The Measurement And Analysis Of Strainmeter Data From Adams Island, November 1982 To June 1983", *C-CORE Report*, No. 85-1, St. John's

Strilchuk, A.R. (1977) "Ice Pressure Measurements Netserk F-40 1975-76", *APOA Project 105*, Report No. APOA 105

Sun Oil Company (1974) "Static Loading Tests Resolute Bay-Winter 1973/74", *APOA Project 64*, Report No. 745B-74-14,

Templeton III, J.S. (1979) "Island Defense And Monitoring", *Technical Seminar on Alaskan Beaufort Sea Gravel Island Design*, Exxon Company, U.S.A.

Timoshenko, S.P. and Goodier, J.N. (1970) " *Theory Of Elasticity*", 3rd edition, McGraw-Hill Kogakusha Ltd., Tokyo

Tucker, W.B. and Govoni, J.W. (1981) "Morphological Investigations Of First-Year Sea Ice Pressure Ridge Sails", *Cold Regions Science and Technology*, vol. V, No. 12

Tusima, K. (1977) "Friction Of A Steel Ball On A Single Crystal Of Ice", *Journal of Glaciology*, Vol. 19, No. 81

Utt, M.E. and Clarke, R.A. (1980) "Coefficient Of Friction Between Submerged Ice And Soil", *ASME Energy Technology Conference*, No. 80-Pet-41, New Orleans

Vaudrey, K.D. (1980) "Issungnak Rubble Pile-Field Installation Of Stress Panels-Interim Report", APOA Project 171, *Gulf Research and Development Co.*, Technical Memorandum No. 446 TK 019, Calgary

Vaughn, J. (1975) " *Strain Measurements*", Published by Bruel & Kjaer

Weeks, W.F. and Mellor, M. (1984) "Mechanical Properties Of Ice In The Arctic Seas", *Arctic Technology and Policy*, McGraw-Hill International Book Co.

Weeks, W.F. and Ackley, S.F. (1980) "The Growth, Structure And Properties Of Sea Ice", *The Geophysics of Sea Ice*, Plenum Press, London

Weeks, W.F., Kovacs, A. and Hibler III, W.D. (1971) "Pressure Ridge Characteristics In The Arctic Coastal Environment", *conference on Polar and Ocean Engineering Under Arctic Conditions* (POAC), vol. I, Norway

Weeks, W.F. and Assur, A. (1969) "Fracture Of Lake And Sea Ice", *CRREL Report*, No. 269, Hanover, New Hampshire

Weiss, R.T., Prodanovic, A. and Wood, K.N. (1981) "Determination Of Ice Rubble Shear Properties", *International Association for Hydraulic Research* (IAHR) symposium, Vol. II, Quebec City

Williams, J.R., Mustoe, G.G.W. and Worgan, K. (1986) "Force Transfer And Behaviour Of Rubble Piles", *International Association for Hydraulic Research* (IAHR) symposium, Vol. I

Wong, T.T, Gale, A.D., Sego, D.C. and Morgenstern, N.R. (1988) "Shear Box Tests On Broken Ice", *conference on Polar and Ocean Engineering Under Arctic Conditions* (POAC '87), Vol. III, (preprint)

Wright, B., Pilkington, G.R., Woolner, K.S. and Wright, W.H. (1986) "Winter Ice Interactions With An Arctic Offshore Structure", *International Association for Hydraulic Research symposium* (IAHR), vol. III, Iowa

Wright, B.D., Hnatiuk, J. and Kovacs, A. (1978) "Sea Ice Pressure Ridges In The Beaufort Sea", *International Association for Hydraulic Research* (IAHR) symposium, Vol. I, Lulea, Sweden

Yen, Y-C, (1981) "Review Of Thermal Properties Of Snow, Ice And Sea Ice", *CRREL Report*, No. 81-10, Hanover, New Hampshire

APPENDIX A

Late Winter ESSO Data (Pressures at CRI)

From The Southern Caissons (numbers 4, 5 & 6)

Sensor identification tags.

Format is XX YZ W, where

XX = Sensor type
Y = Caisson number (1-8)
Z = Relative position on caisson
W = Relative position in cluster

Sensor types are: MR = Micro cell
SB = Shearbar

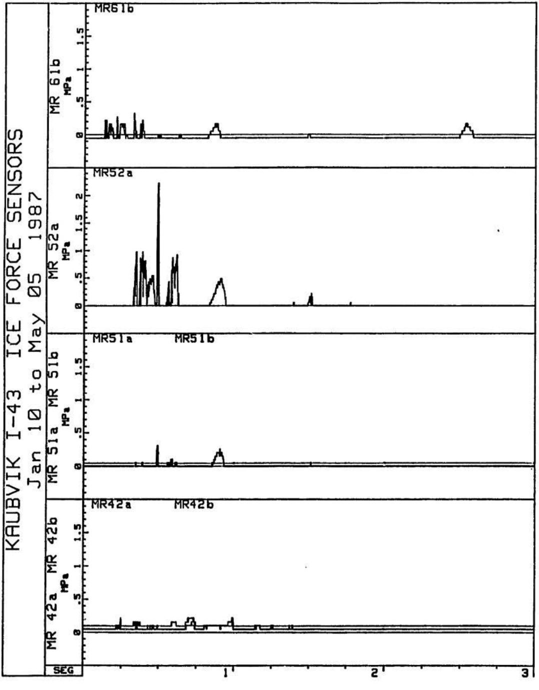
KAUBVIK I-43 ICE FORCE SENSORS
Jan 10 to May 05 1987
MR 61b
MPa
MR61b
0
.5
1
1.5
MR 52a
MPa
MR52a
0
.5
1
1.5
2
MR 51a MR 51b
MPa
MR51a
MR51b
0
.5
1
1.5
MR 42a MR 42b
MPa
MR42a
MR42b
0
.5
1
1.5
SEG
1
2
3

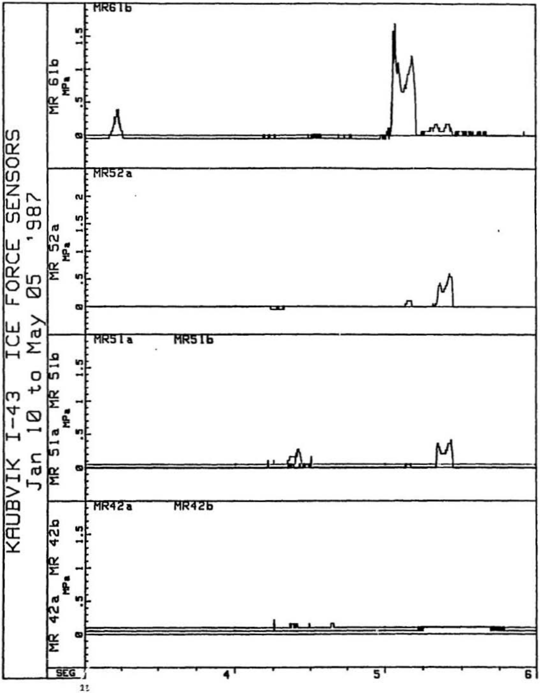
KAUBVIK I-43 ICE FORCE SENSORS
Jan 10 to May 05 '987
MR61b
MR 61b
MPa
MR52a
MR 52a
MPa
MR51a
MR51b
MR 51a MR 51b
MPa
MR42a
MR42b
MR 42a MR 42b
MPa
0
.5
1
1.5
2
SEG
4
5
6
11

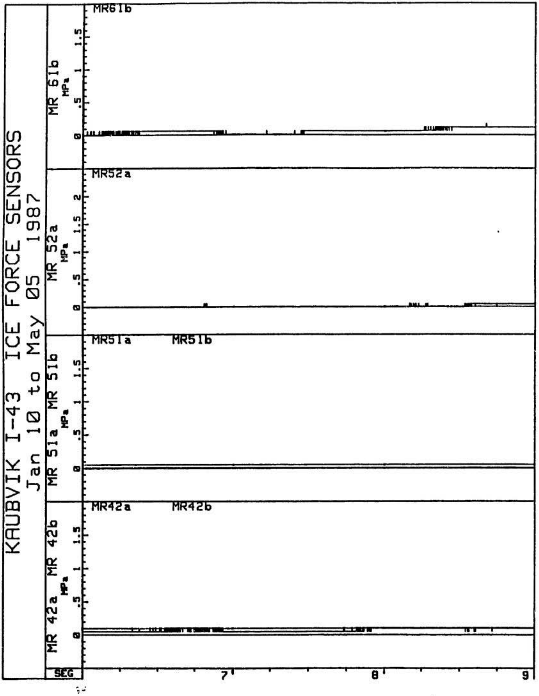
KAUBVIK I-43 ICE FORCE SENSORS
Jan 10 to May 05 1987
MR 61b
MPa
MR61b
0
.5
1
1.5
MR 52a
MPa
MR52a
0
.5
1
1.5
2
MR 51a MR 51b
MPa
MR51a
MR51b
0
.5
1
1.5
MR 42a MR 42b
MPa
MR42a
MR42b
0
.5
1
1.5
SEG
7
8
9

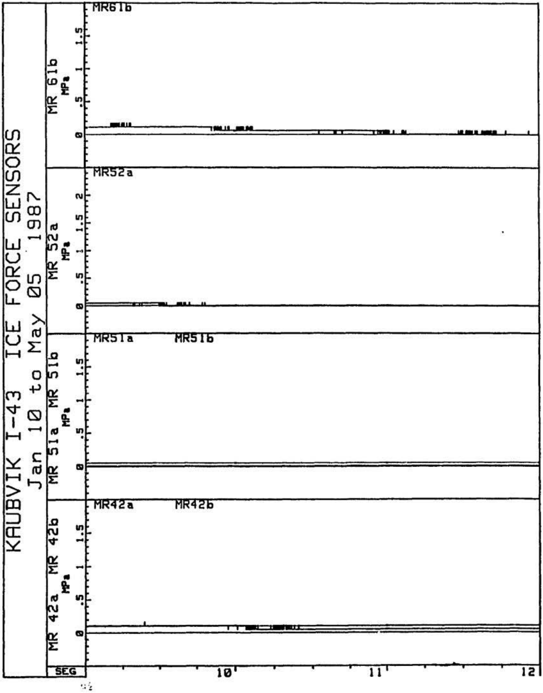
KAUBVIK I-43 ICE FORCE SENSORS
Jan 10 to May 05 1987
MR 61b
MPa
MR61b
MR 52a
MPa
MR52a
MR 51a MR 51b
MPa
MR51a
MR51b
MR 42a MR 42b
MPa
MR42a
MR42b
0
.5
1
1.5
2
SEG
10
11
12

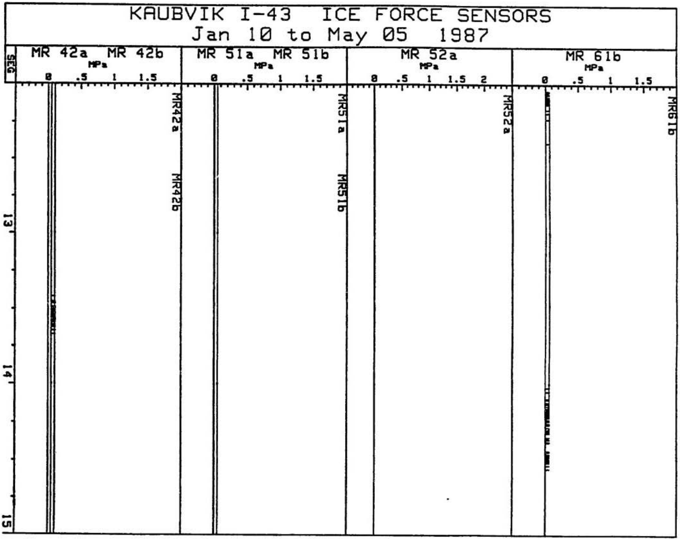

KAUBVIK I-43 ICE FORCE SENSORS
Jan 10 to May 05 1987

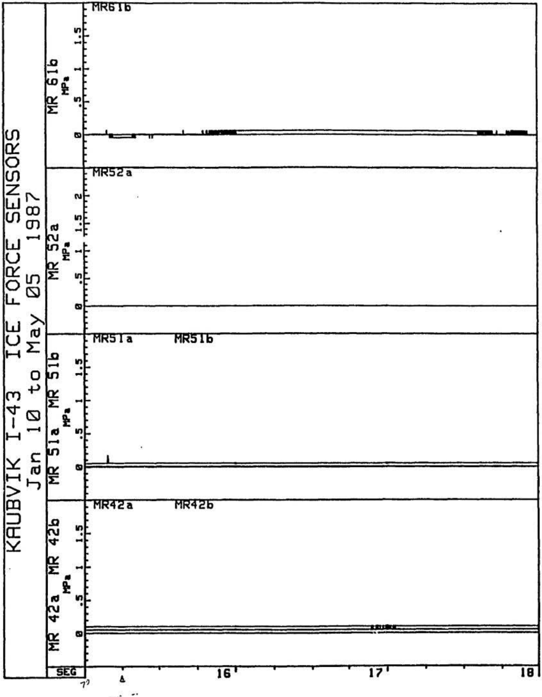
KAUBVIK I-43 ICE FORCE SENSORS
Jan 10 to May 05 1987
MR 61b
MPa
MR61b
MR 52a
MPa
MR52a
MR 51a MR 51b
MPa
MR51a
MR51b
MR 42a MR 42b
MPa
MR42a
MR42b
0
.5
1
1.5
2
SEG
4
16
17
18

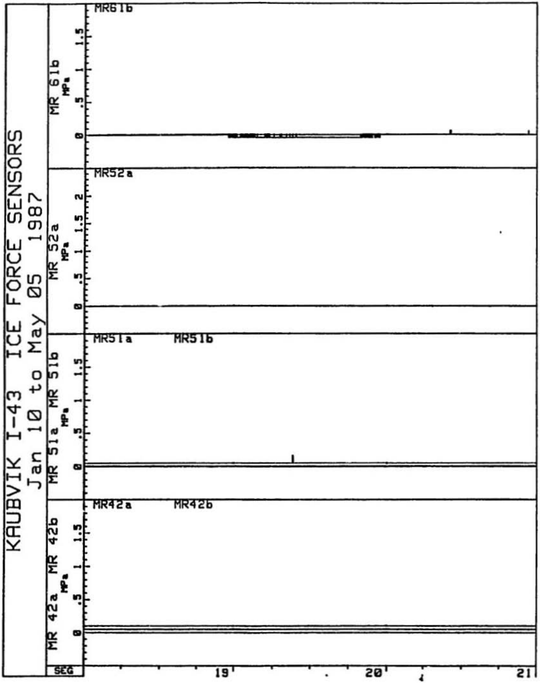

KAUBVIK I-43 ICE FORCE SENSORS
Jan 10 to May 05 1987

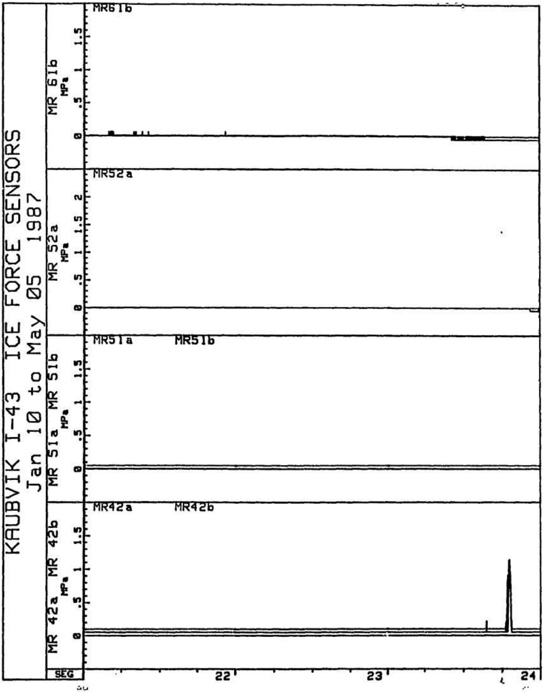
KAUBVIK I-43 ICE FORCE SENSORS
Jan 10 to May 05 1987
MR 61b
MPa
MR61b
MR 52a
MPa
MR52a
MR 51a MR 51b
MPa
MR51a
MR51b
MR 42a MR 42b
MPa
MR42a
MR42b
0
.5
1
1.5
2
SEG
22
23
24

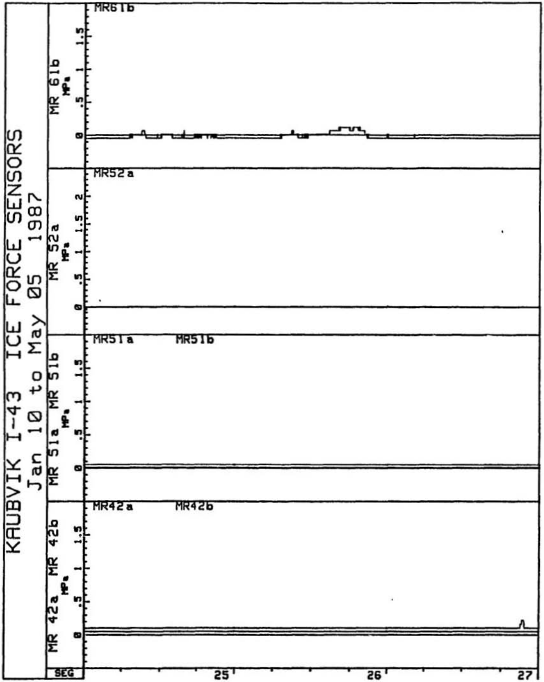
KAUBVIK I-43 ICE FORCE SENSORS
Jan 10 to May 05 1987
MR 61b
MPa
MR61b
MR 52a
MR52a
MR 51a MR 51b
MR51a
MR51b
MR 42a MR 42b
MR42a
MR42b
0
.5
1
1.5
2
SEG
25
26
27

10'5

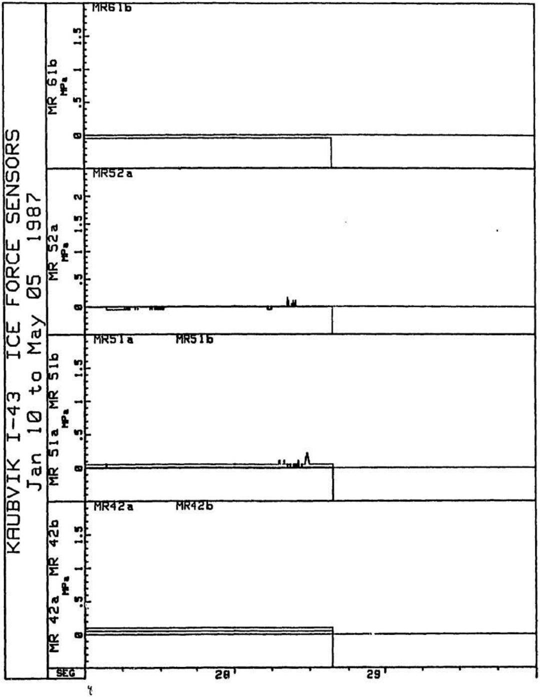
KAUBVIK I-43 ICE FORCE SENSORS
Jan 10 to May 05 1987
MR 61b
MPa
MR61b
0
.5
1
1.5
MR 52a
MPa
MR52a
0
.5
1
1.5
2
MR 51a MR 51b
MPa
MR51a
MR51b
0
.5
1
1.5
MR 42a MR 42b
MPa
MR42a
MR42b
0
.5
1
1.5
SEG
28
29

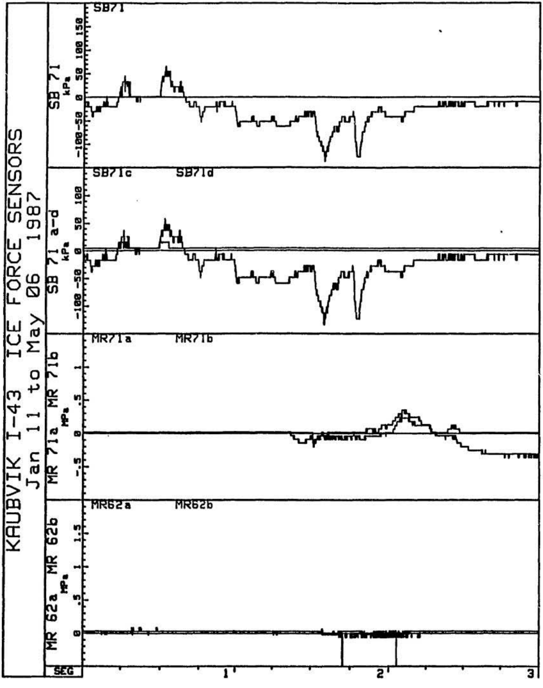
KAUBVIK I-43 ICE FORCE SENSORS
Jan 11 to May 06 1987
SB71
SB 71 kPa
150
100
50
0
-50
-100
SB71c
SB71d
SB 71 a-d kPa
100
50
0
-50
-100
MR71a
MR71b
MR 71a MR 71b MPa
1
.5
0
-.5
MR62a
MR62b
MR 62a MR 62b MPa
1.5
1
.5
0
SEG
1
2
3

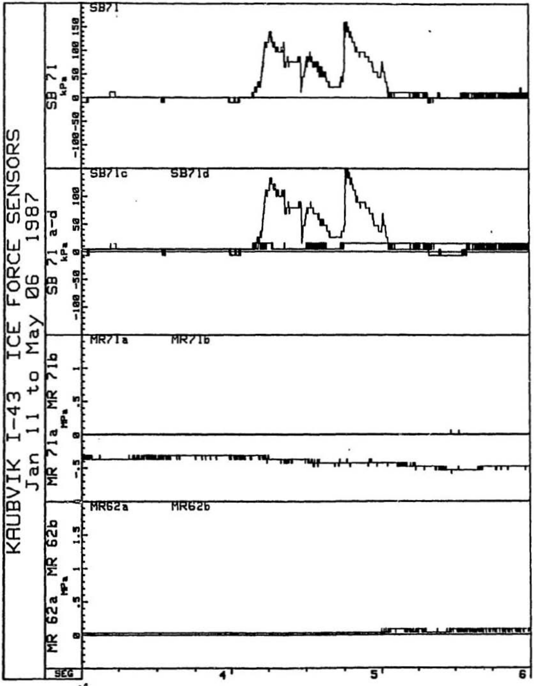
KAUBVIK I-43 ICE FORCE SENSORS
Jan 11 to May 06 1987
SB71
SB 71 kPa
150
100
50
0
-50
-100
SB71c
SB71d
SB 71 a-d kPa
100
50
0
-50
-100
MR71a
MR71b
MR 71a MR 71b MPa
1
.5
0
-.5
MR62a
MR62b
MR 62a MR 62b MPa
1.5
1
.5
0
SEG
4
5
6

23

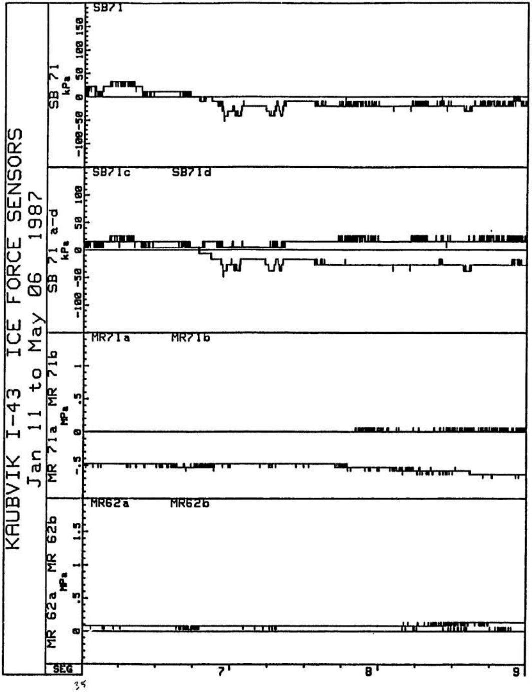
KAUBVIK I-43 ICE FORCE SENSORS
Jan 11 to May 06 1987
SB71
SB 71
kPa
150
100
50
0
-50
-100
SB71c
SB71d
SB 71 a-d
kPa
100
50
0
-50
-100
MR71a
MR71b
MR 71a MR 71b
MPa
1
.5
0
-.5
MR62a
MR62b
MR 62a MR 62b
MPa
1.5
1
.5
0
SEG
7
8
9

35

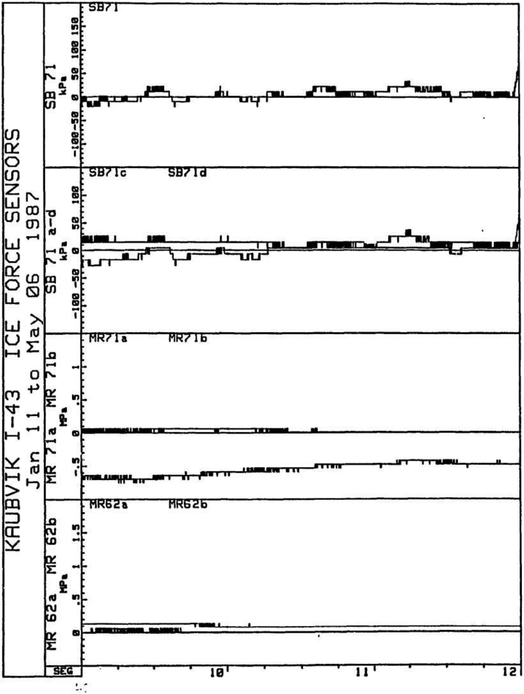
KAUBVIK I-43 ICE FORCE SENSORS
Jan 11 to May 06 1987
SB 71
kPa
-100
-50
0
50
100
150
SB71
SB 71 a-d
kPa
-100
-50
0
50
100
SB71c
SB71d
MR 71a MR 71b
MPa
-.5
0
.5
1
MR71a
MR71b
MR 62a MR 62b
MPa
0
.5
1
1.5
MR62a
MR62b
SEG
10
11
12

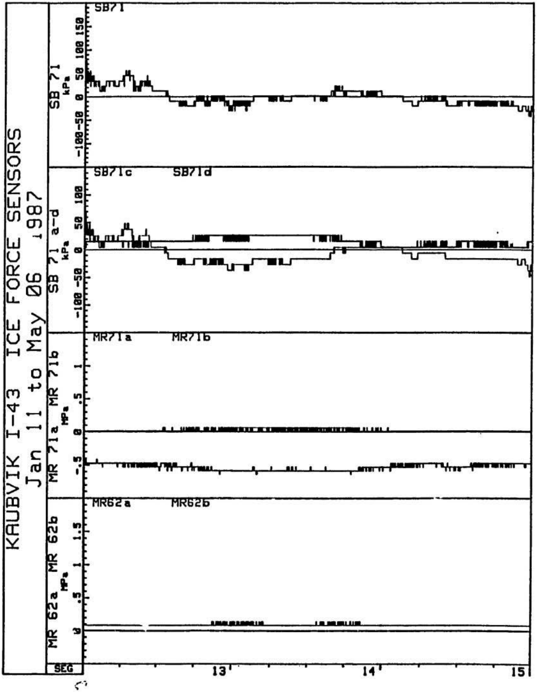
KAUBVIK I-43 ICE FORCE SENSORS
Jan 11 to May 06 1987
SB71
SB 71
kPa
150
100
50
0
-50
-100
SB71c
SB71d
SB 71 a-d
kPa
100
50
0
-50
-100
MR71a
MR71b
MR 71a MR 71b
MPa
1
.5
0
-.5
MR62a
MR62b
MR 62a MR 62b
MPa
1.5
1
.5
0
SEG
13
14
15

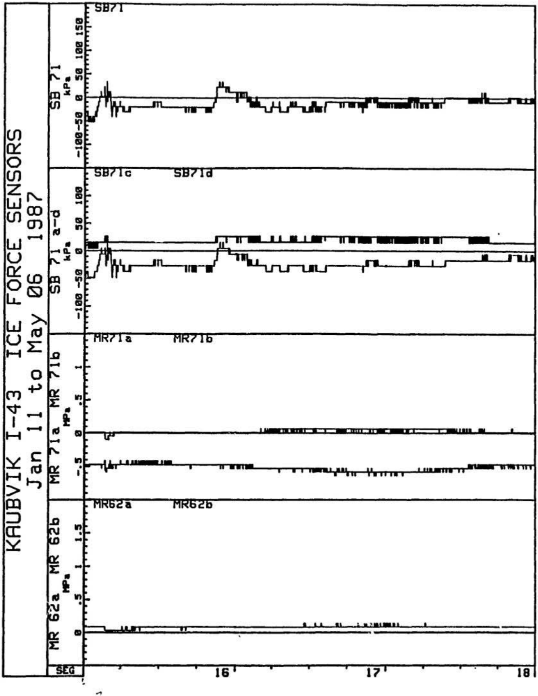
KAUBVIK I-43 ICE FORCE SENSORS
Jan 11 to May 06 1987
SB71
SB 71
kPa
-100
-50
0
50
100
150
SB71c
SB71d
SB 71 a-d
kPa
-100
-50
0
50
100
MR71a
MR71b
MR 71a MR 71b
MPa
-.5
0
.5
1
MR62a
MR62b
MR 62a MR 62b
MPa
0
.5
1
1.5
SEG
16
17
18

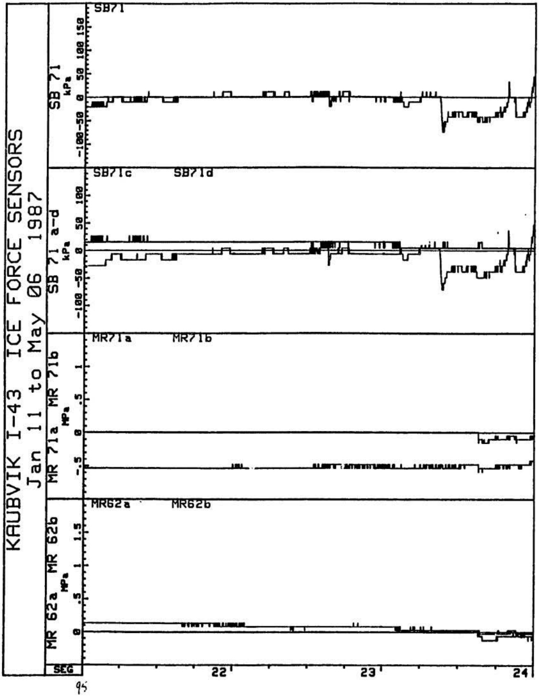
KAUBVIK I-43 ICE FORCE SENSORS
Jan 11 to May 06 1987
SB71
SB 71
kPa
-100 -50 0 50 100 150
SB71c
SB71d
SB 71 a-d
kPa
-100 -50 0 50 100
MR71a
MR71b
MR 71a MR 71b
MPa
-.5 0 .5 1
MR62a
MR62b
MR 62a MR 62b
MPa
0 .5 1 1.5
SEG
22
23
24

95

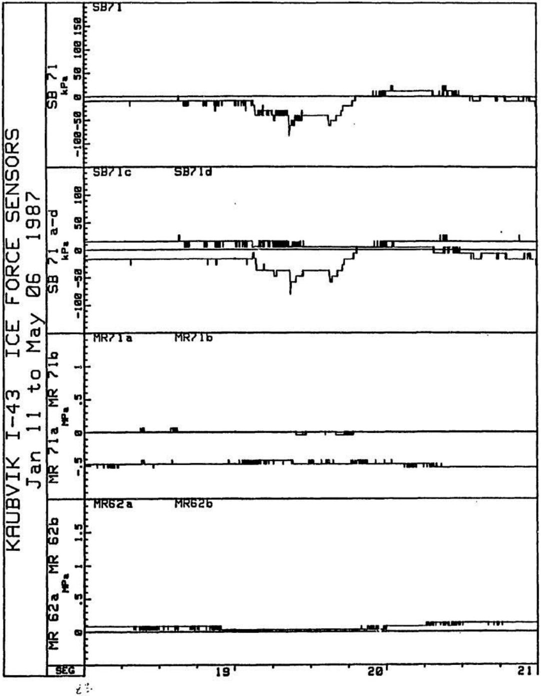
KAUBVIK I-43 ICE FORCE SENSORS
Jan 11 to May 06 1987
SB71
SB 71
kPa
150
100
50
0
-50
-100
SB71c
SB71d
SB 71 a-d
kPa
100
50
0
-50
-100
MR71a
MR71b
MR 71a MR 71b
MPa
1
.5
0
-.5
MR62a
MR62b
MR 62a MR 62b
MPa
1.5
1
.5
0
SEG
19
20
21

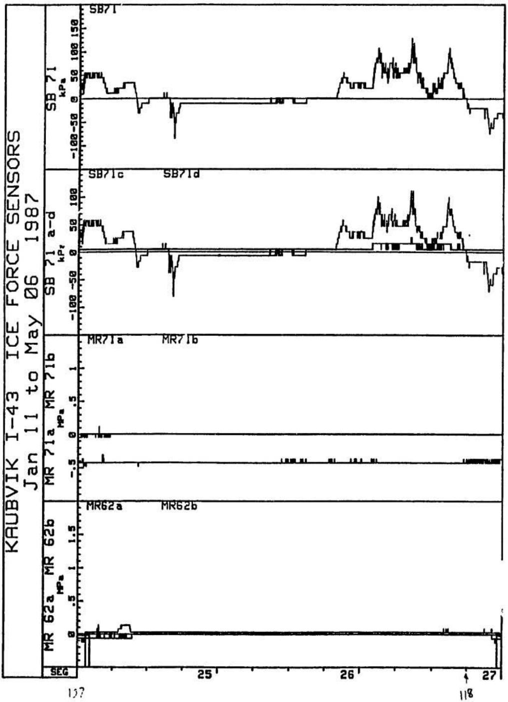
KAUBVIK I-43 ICE FORCE SENSORS
Jan 11 to May 06 1987
SB71
SB 71 kPa
150
100
50
0
-50
-100
SB71c
SB71d
SB 71 a-d kPa
100
50
0
-50
-100
MR71a
MR71b
MR 71a MR 71b MPa
1
.5
0
-.5
MR62a
MR62b
MR 62a MR 62b MPa
1.5
1
.5
0
SEG
25
26
27
117
118

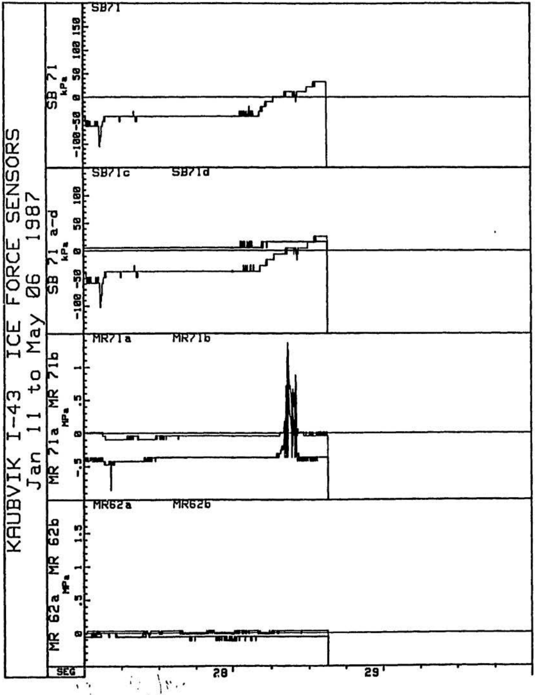
KAUBVIK I-43 ICE FORCE SENSORS
Jan 11 to May 06 1987
SB71
SB 71
kPa
-100 -50 0 50 100 150
SB71c
SB71d
SB 71 a-d
kPa
-100 -50 0 50 100
MR71a
MR71b
MR 71a MR 71b
MPa
-.5 0 .5 1
MR62a
MR62b
MR 62a MR 62b
MPa
0 .5 1 1.5
SEG
28
29

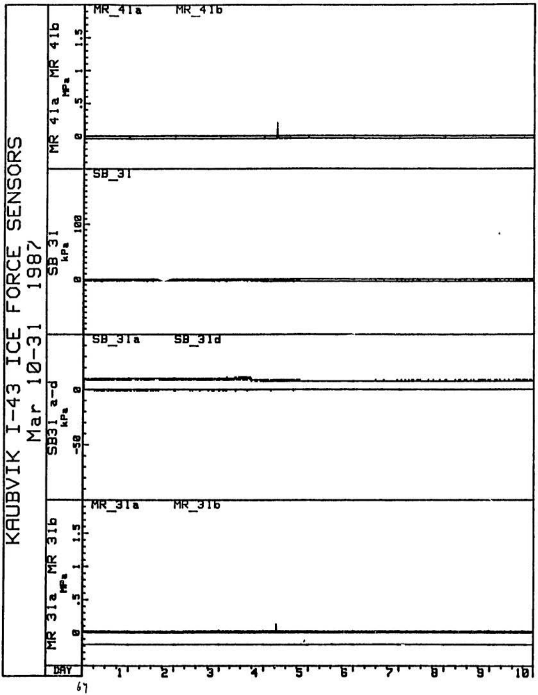
KAUBVIK I-43 ICE FORCE SENSORS
Mar 10-31 1987
MR 41a MR 41b MPa
MR_41a MR_41b
1.5
1
.5
0
SB 31 kPa
SB_31
100
0
SB31 a-d kPa
SB_31a SB_31d
0
-50
MR 31a MR 31b MPa
MR_31a MR_31b
1.5
1
.5
0
DAY
1
2
3
4
5
6
7
8
9
10

67

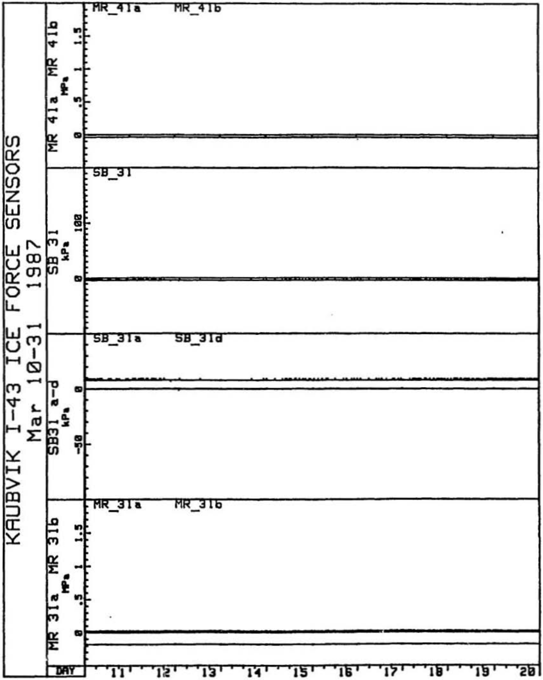
KAUBVIK I-43 ICE FORCE SENSORS
Mar 10-31 1987
MR 41a MR 41b
MPa
0
.5
1
1.5
MR_41a
MR_41b
SB 31
kPa
0
100
SB_31
SB31 a-d
kPa
-50
0
SB_31a
SB_31d
MR 31a MR 31b
MPa
0
.5
1
1.5
MR_31a
MR_31b
DAY
11
12
13
14
15
16
17
18
19
20

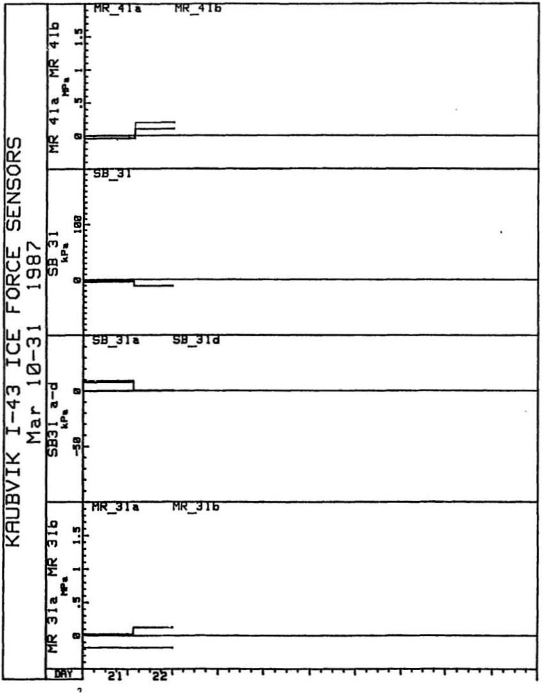
KAUBVIK I-43 ICE FORCE SENSORS
Mar 10-31 1987
MR 41a MR 41b
MPa
1.5
1
.5
0
MR_41a
MR_41b
SB 31
kPa
100
0
SB_31
SB31 a-d
kPa
0
-50
SB_31a
SB_31d
MR 31a MR 31b
MPa
1.5
1
.5
0
MR_31a
MR_31b
DAY
21
22

APPENDIX B

Map Of MacKenzie Bay

Tidal Current Calculation

Fortran Program To Calculate Landfast Ice Movements

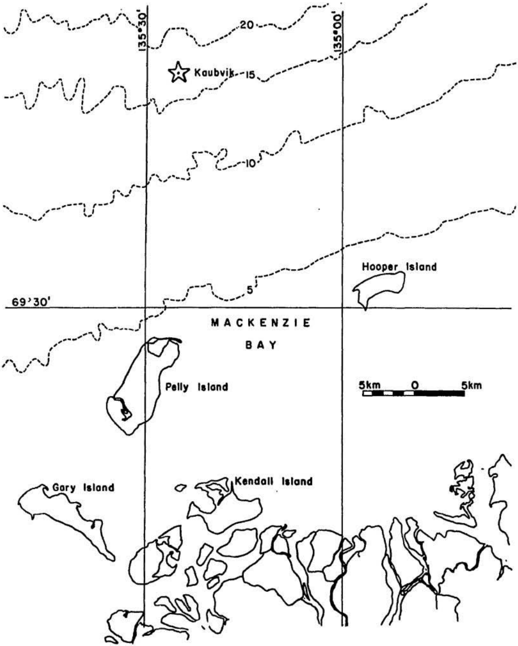
135°30'
135°00'
20
Kaubvik
15
10
5
Hooper Island
69°30'
MACKENZIE
BAY
Pelly Island
5km
0
5km
Gary Island
Kendall Island

TIDAL CURRENT CALCULATION

Tidal current velocities have been estimated using the following approach. Tidal fluctuations in the Southern Beaufort Sea are generally small and average 15 cm (Pilkington, 1983). As tides occur twice daily it takes 6 hours for the water level to go from low tide to high tide. Kaubvik is about 30 km offshore at a water depth of about 20 m. Using a 2D approximation, a water level rise of 15 cm over an area of 30,000 m^2 (30 km x 1 m) requires a volume of 4500 m^3 of water. This is assumed to flow through a 20 m^2 cross section over a period of 6 hours. The average flow rate is thus 0.0104 m/s.

The drag that such a current imposes on an ice sheet can be calculated from the following (Maattanen, 1983):

$$Drag = \frac{1}{2} \cdot C_d \cdot v^2 \cdot \rho_w$$

where

C_d = Drag coefficient (0.04)

$Drag$ = Shear stress (N/m^2)

ρ_w = Sea water density (1024 kg/m^3)

v = Water velocity (m/s)

The current drag is thus .0022 N/m^2 which is the same as that produced by a 2.7 kmh wind, and 1% of that produced by a 27 kmh wind. This indicates that tidal currents produce negligible drag and this assumption is reinforced by the sea ice pressure sensor data (no diurnal pressure fluctuations).

```
c234567890
c   **********************************
c   *    This program was written by    *
c   *                                   *
c   *         ALFRED MARSHALL            *
c   *                                   *
c   *  on Sept 30, 1988.  The program   *
c   *  is designed to calculate the     *
c   *  wind and temperature induced     *
c   *  movement of landfast sea ice     *
c   *  at a piont within the landfast   *
c   *  ice margin (a potential island   *
c   *  site).  Various input parameters*
c   *  are required at the appropriate *
c   *  prompts.                         *
c   **********************************
c
        integer NUMI,i
        real L,W,THICK,DIAM,START,FINISH,Cd,MXSTRESS,DATE,TEMP
        real EELASTIC,EDELAYED,INITIAL,DATE1,STRESS1,ECREEP,CREEP
        real TEMP1,MOVEMENT1,DATE2,STRESS2,ETEMP,MOVEMENT,REAL
        real NUMR,COUNT,AVGSTRESS,KELVIN
        real SMAX1,SMAX2,SMIN1,SMIN2,SAVG1,SAVG2,TAS,TCF,ST,WIND
        character*10 IFILE,OFILE
        write(*,'(a)')' Enter the input (wind & temp) datafile nam
        read(*,'(a)') IFILE
        write(*,'(a)')' Enter the output datafile name:'
        read(*,'(a)') OFILE
        write(*,'(a)')' Enter the distance of the point from shore
        read(*,*) L
        write(*,'(a)')' Enter the desired number of divisions of L
        read(*,*) NUMI
        write(*,'(a)')' Enter the width of landfast ice margin (km
        read(*,*) W
        write(*,'(a)')' Enter the ice thickness (m):'
        read(*,*) THICK
        write(*,'(a)')' Enter average sea ice grain diameter (mm):
        read(*,*) DIAM
        write(*,'(a)')' Enter the wind stress drag coeff. (Cd/2):'
        read(*,*) Cd
        write(*,'(a)')' Enter start date in julian days:'
        read(*,*) START
        write(*,'(a)')' Enter the finish date:'
        read(*,*) FINISH
        open(1,file=IFILE, status='old')
        open(2,file=OFILE, status='new')
c   Before starting into the main loop we find the start,
c   and then read and calculate the start conditions.
  100   read(1,*)DATE,WIND,TEMP
        if (DATE .lt. START) goto 100
        call maxstress(WIND,W,Cd,THICK,MXSTRESS)
        call elastic(MXSTRESS,L,W,EELASTIC)
        call delayed(EELASTIC,DIAM,EDELAYED)
c   initial is the initial recoverable deformation in the ice she
```

```
      INITIAL = EDELAYED+EELASTIC
      ST = 0.0
      write(2,*)DATE,INITIAL,ST
      DATE1 = DATE
      STRESS1 = MXSTRESS
      TEMP1 = TEMP
      MOVEMENT1 = INITIAL
c   Having established the initial conditions
c   we can now start the main loop
  200 read(1,*)DATE,WIND,TEMP
      if (DATE .gt. FINISH) goto 500
      call maxstress(WIND,W,Cd,THICK,MXSTRESS)
      call elastic(MXSTRESS,L,W,EELASTIC)
      call delayed(EELASTIC,DIAM,EDELAYED)
      DATE2 = DATE
      STRESS2 = MXSTRESS
      call viscous(DATE1,DATE2,STRESS1,STRESS2,L,NUMI,W,CREEP,
     + TEMP1,TEMP)
      ECREEP = ECREEP+CREEP
      STRESS1 = STRESS2
      call thermal(TEMP1,TEMP,L,ETEMP)
c
c   Now adding all four contributors to ice movement
      MOVEMENT = EELASTIC+EDELAYED+ECREEP+ETEMP
c
c   Now calculating movement rate
      RATE = (MOVEMENT-MOVEMENT1)/(DATE2-DATE1)
c
      MOVEMENT1 = MOVEMENT
      DATE1 = DATE2
      write(2,*)DATE,MOVEMENT,RATE
      TEMP1 = TEMP
      goto 200
  500 close(1)
      close(2)
      end



      subroutine maxstress(WIND,W,Cd,THICK,MXSTRESS)
c   This subroutine calculates the ice stress at the shoreline
c   Note: WIND is actually the north/south component of the
c   squared wind vector. Thus WIND does not have to be squared
c   in the drag equation.
c
      real WIND,W,Cd,THICK,MXSTRESS
      WIND = WIND/(3.6**2)
      MXSTRESS = (Cd*WIND*W*1000.0*1.3)/THICK
      return
      end
```

```
      subroutine elastic(MXSTRESS,L,W,EELASTIC)
c    This subroutine calculates the elastic deformation
c
      real MXSTRESS,L,W,EELASTIC,AVGSTRESS
      AVGSTRESS = ((1.0 - L/W)*MXSTRESS + MXSTRESS)/2.0
      EELASTIC = (AVGSTRESS*1000.0*L)/9.5E9
      return
      end


      subroutine delayed(EELASTIC,DIAM,EDELAYED)
c    This subroutine calculates the approx stored delayed elastici
c    Note long time intervals (3 hr plus) are assumed.
c
      real EELASTIC,DIAM,EDELAYED
      EDELAYED = (9.0/DIAM)*EELASTIC
      return
      end



      subroutine viscous(DATE1,DATE2,STRESS1,STRESS2,L,NUMI,W,
     + CREEP,TEMP1,TEMP)
c    This calculates the creep accumulated between shore and the i
c
      real DATE1,DATE2,STRESS1,STRESS2,L,W,CREEP,TEMP1,TEMP
     + SMAX1,SMAX2,T,AVGTEMP,TCF,TAS,SMIN1,SMIN2,SAVG1,SAVG2,
     + COUNT,NUMR,KELVIN
      integer NUMI,i
      CREEP = 0.0
      SMAX1 = STRESS1
      SMAX2 = STRESS2
c    Time = T
      T = (DATE2 - DATE1)*3600.0*24.0
      AVGTEMP = (TEMP1 + TEMP)/2.0
      KELVIN = 273.0 + AVGTEMP
C    Temperature Correction Factor = TCF
      TCF = 2.7183**((67000.0/8.32)*(1.0/263.0 - 1.0/KELVIN))
      DO 50 i=1,NUMI
      NUMR = NUMI
      COUNT = i
      SMIN1 = ((W-(COUNT*L)/NUMR)/W)*STRESS1
      SAVG1 = (SMAX1 + SMIN1)/2.0
      SMIN2 = ((W-(COUNT*L)/NUMR)/W)*STRESS2
      SAVG2 = (SMAX2 + SMIN2)/2.0
c    Total Average Stress = TAS
      TAS = (SAVG1 + SAVG2)/2.0
      CREEP=CREEP+1000.0*(L/NUMR)*(1.76E-7 * TCF)*((TAS/1E6)**3)
      SMAX1 = SMIN1
      SMAX2 = SMIN2
  50  continue
```

```
      return
      end



      subroutine thermal(TEMP1,TEMP,L,ETEMP)
c   This calculates the thermal expansion since time=0
c
      real TEMP1,TEMP,L,ETEMP
      ETEMP = ETEMP + (TEMP-TEMP1)*L*1000.0*5.1E-5
      return
      end
```

APPENDIX C

Reference Stress Calculation

REFERENCE STRESS CALCULATION

The following method is taken from Sanderson (1984) and is done using the two extreme assumptions; 1) that the ice sheet is composed entirely of granular ice, and 2) that the ice sheet is composed entirely of columnar ice. As presented in section 8.3.2, the equation for creep load is;

$$F = 1.15 \cdot D \cdot t_i \cdot F_\sigma(\dot{\epsilon})$$

where:

F = Total load (MN)

t_i = Ice thickness (m)

$F_\sigma(\dot{\epsilon})$ = stress at corresponding strain rate $\dot{\epsilon}$.

$$\dot{\epsilon} = \frac{U}{0.44 \cdot D} = A \cdot exp\left(\frac{-Q}{R \cdot T_1}\right) \cdot \left(\frac{\sigma}{1 - \frac{v}{v_o}}\right)^3$$

σ = Stress (MPa)

A = Constant depending on crystal type

U = global ice sheet velocity (m/s)

v = Brine volume = $.001 \cdot S\ (0.53 - \frac{49.2}{C})$

v_o = Reference brine volume

S = Salinity (ppt)

C = Temperature (°C)

The specific values for columnar and granular ice, as specified by Sanderson (1984), are:

Columnar Ice

$A = 3.5 \cdot 10^6$ /MPa^3 s

Q = 65,000 J/mol

$v_o = 0.16$

Granular Ice	273 - 265 K	265 - 0 K	
A	$7.8 \cdot 10^{16}$ /MPa^3 s	$4.1 \cdot 10^{8}$ /MPa^3 s	
Q	120,000 J/mol	78,000 J/mol	given

$v_o = 0.10$

C = -7.5 °C

$D = 100$ m

$R = 8.316$ J/mol K

$T_1 = 265.5$ K (avg)

$t_i = 3$ m

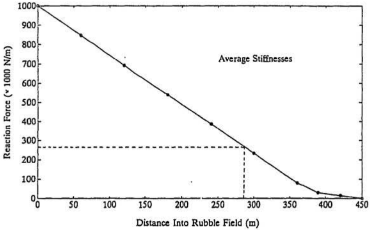

Figure A1: Transmitted force versus position in the rubble field for final steady state (creep) conditions.

If it is assumed that increasing the width of the rubble field does not significantly change the deformations in the first 450 m, then figure A1 can be applied to the baseline case. From figure A1, the position in the rubble field where a reaction force of 267 kN/m occurs, can be determined. This is at a horizontal distance into the rubble of 286 m and this position is therefore equivalent to the outer edge of the baseline case rubble field. The structure is located a furthur 75 m into the rubble, putting it at 361 m on the X axis of figure A1. In theory, figure A2 shows the refrozen layer velocity at a position of 361 m, however, the curve is too close to the x-axis in this case and so the velocity must be obtained from the raw ABAQUS output.

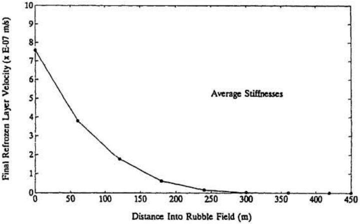

Figure A2: Refrozen layer velocity versus position in the rubble field for final steady state (creep) conditions.

The ice sheet velocity U at the structure was determined to be;

$$U = 1.22 \cdot 10^{-11}\ m/s$$

Continuing with the calculation, and using the values for granular ice at 265.5 K the effective strain rate is;

$$\dot{\epsilon} = \frac{1.22 \cdot 10^{-11}}{0.44 \cdot 100} = 2.77 \cdot 10^{-13}$$

therefore

$$A \cdot exp\left(\frac{-Q}{R \cdot T_1}\right) \cdot \left(\frac{\sigma}{1 - \frac{v}{v_o}}\right)^3 = 2.77 \cdot 10^{-13}$$

$$\sigma = \left(\frac{2.77 \cdot 10^{-13}}{A \cdot exp(\frac{-Q}{R \cdot T_1})} \cdot (1 - \frac{v}{v_o})^3\right)^{0.333}$$

where

$$v = 0.001 \cdot 5.0(0.53 - \frac{49.2}{-7.5})$$

$$v = 0.03545$$

Note: $S = 5.0$ (Sanderson, 1984) is used even though the measured average was 3.0, because many of the samples taken at Kaubvik were from the well drained sail rubble and therefore are expected to underestimate the salinity of the refrozen layer.

$$\sigma = \left(\frac{2.77 \cdot 10^{-13}}{7.8 \cdot 10^{16} \cdot exp(\frac{-120{,}000}{8.316 \cdot 265.5})} \cdot (1 - \frac{0.035}{0.1})^3\right)^{0.333}$$

$$\sigma = 7.26 \cdot 10^{-3}\, MPa$$

Therfore

$$F = 1.15 \cdot 100 \cdot 3 \cdot 7.26 \cdot 10^{-3}$$

$$F = 2.5\, MN$$

Similarly, with the assumption that the columnar ice assumption;

$$F = 2.1\, MN$$

APPENDIX D

Ice Density Calculation

CALCULATION OF ICE DENSITY

From ice profiling in the "disturbed" region adjacent to the grounded rubble, it was determined that the average freeboard to thickness ratio was 1:6.3. The disturbed region was ungrounded and therefore in isostatic equilibrium. For a given thickness of floating material, the freeboard height is inversly proportional to the material density and can be used to calculate the density. This is done as follows;

given that

$$\frac{t_i}{T_f} = 6.3$$

$$\rho_i = \frac{(\frac{t_i}{T_f} - 1) \cdot \rho_w}{\frac{t_i}{T_f}}$$

where

ρ_i = Sea ice density (kg/m^3)

t_i = Ice thickness (m)

T_f = Freeboard thickness (m)

ρ_w = Water density (1024 kg/m^3)

APPENDIX E

Porosity Calculation

ICE POROSITY CALCULATION

The following inputs are required for this calculation;

ρ_i = Sea ice density = 900 kg/m^3

λ = Thermal conductivity of sea ice = 1.8 W/m k

q_l = Latent heat of freezing of sea water = 293 kJ/kg

ΔT_g = Average thermal gradient above freezing front = 4.3 °C/m

Average refrozen layer growth rate = 0.022 m/day

Heat flow rate per square meter (q) from the un-refrozen rubble is calculated as follows;

$$q = \lambda \cdot \Delta T_g = 7.74\ W/m^2$$

If we assume that the specific heat capacity of the ice is negligible in comparison to the latent heat of freezing of the water, then this cooling all goes into freezing of sea water. The mass frozen per day is;

$$Mass = \frac{q}{q_l} \cdot 864000 = 2.28\ kg/day$$

Converting to volume, this becomes;

$$Vol = \frac{Mass}{\rho_i} = 0.00253\ m^3/day$$

This is equivalent to a growth rate of 2.53 mm/day. The actual growth rate is 22 mm/day, thus the porosity P is;

$$P = \frac{2.53}{22} \cdot 100\% = 12\%$$

APPENDIX F

Fortran Program To Calculate Element Values

ABAQUS Program For 2D Baseline Case

```
c     ************************************
c     *                                  *
c     *   This program was written by    *
c     *                                  *
c     *         ALFRED MARSHALL          *
c     *                                  *
c     *  on July 4, 1989 in order to     *
c     *  calculate the spring and        *
c     *  damper proerties which are      *
c     *  required for an abaqus simula-  *
c     *  tion of an ice rubblefield.     *
c     *                                  *
c     ************************************
c
c234567
       real EXTENT, HEIGHT, RLT, DEPTH, DENSITYI, DENSITYW, PORE,
       real CS(2), URRSS(2), LENGTH, PRESS, IFRICMAX, IFRICMIN, S
       real SFRICMIN, WS, WK, SRLMAX(2), SRLMIN(2), SCMAX, SCMIN,
       real SSMIN, VC(2), CC(2), SCC(2), DE(2), SRL(2), IFRIC, SF
       real SC, SS, DRLMAX, DRLMIN, DRL, DCMAX, DCMIN, DC, DSMAX,
       real SAILS
       character*10 OFILE
       write(*,'(A)')' Enter the name of the output file'
       read(*,'(A)') OFILE
       open(1,file=ofile, status='new')
c
c    The following parameters can be varied in order to investiga
c    the protective or other nature of various sizes of rubble
c    accumulation.
c
       write(*,'(A)')' Enter the rubblefield extent in metres'
       read(*,*) EXTENT
       write(*,'(A)')' Enter the number of sails'
       read(*,*) SAILS
       write(*,'(A)')' Enter the sail height in metres'
       read(*,*) HEIGHT
       write(*,'(A)')' Enter the refrozen layer thickness in metr
       read(*,*) RLT
       write(*,'(A)')' Enter the water depth in metres'
       read(*,*) DEPTH
c
c
c
c    The following are the physical property values for sea ice
c    and sea water.
c
c    Ice density (kg/cu. m)
       DENSITYI = 900
c    Water density (kg/cu. m)
       DENSITYW = 1024
c    Rubble porosity
       PORE = 0.15
c
c
```

```
c
c     Now calculating some constants
c
c     The unit length is (m):
        LENGTH = EXTENT/SAILS
c     The average RL/URR (Refrozen Layer/Un-Refrozen Rubble)
c     contact pressure is (Pa):
        PRESS = 9.81 *((HEIGHT * 0.5 * DENSITYI * (1-PORE)) -
     c ((DENSITYW - DENSITYI) * RLT))
c
c
c
c     The following ice property values have been determined from
c     the literature, Kaubvik data, and other sources
c
c     The refrozen layer youngs modulus is 9.5 E09, varying up and
c     down by a half an order of magnitude we get a range of (Pa)
         E(1) = 3.0 E10
         E(2) = 3.0 E09
c    The following is commented out as it is not applicable for mo
c    calculations.
cccccccccccccccccccccccc( :ccccccccccccccccccccccccccccccccccccc
c  c     The refrozen layer delayed elastic coefficient at time =
c  c     is 1.26 E-09, the range is
c            DE(1) = 3.98 E-09
c            DE(2) = 3.98 E-10
cccccccccccccccccccccccccccccccccccccccccccccccccccccccccccccc
c     Un-Refrozen Rubble compaction stiffness (Pa)
         CS(1) = 1.6 E08
         CS(2) = 5.7 E04
c     URR shear stiffness (Pa)
         URRSS(1) = 1.4 E09
         URRSS(2) = 3.6 E06
c     The viscous creep coefficient is 2.35 E-25, the range is
         VC(1) = 7.43 E-25
         VC(2) = 7.43 E-26
c     The compaction creep coefficiect range is
         CC(1) = 1. E-11
         CC(2) = 1. E-13
c     The shear creep coefficient is 8.0 E-24, the range is
         SCC(1) = 2.53 E-23
         SCC(2) = 2.53 E-24

c
c
c
c     Now we can show the maximum and minimum values for the RL
c     and URR physical properties.  These ranges are assumed to
c     be large enough to contain the actual values.
c
c     The RL/URR friction coefficient
         IFRICMAX = 63400/PRESS + 0.47
         IFRICMIN = 1.2
         IFRIC = 10**((log10(IFRICMAX) + log10(IFRICMIN))/2.0)
```

```
c    The soil friction range is:
        SFRICMAX = 1.0
        SFRICMIN = 0.50
        SFRIC = 10**((log10(SFRICMAX) + log10(SFRICMIN))/2.0)
c    The weight of the sail (at the bottom of the RL).
        WS = PRESS * LENGTH
c    The weight of the keel (at the seabed).
        WK = WS - ((DENSITYW - DENSITYI) * (1 - PORE) *
     c  (DEPTH - RLT) * LENGTH) * 9.81
c    The RL spring constant is:
c               At time = 0
        SRLMAX(1) = E(1) * RLT/LENGTH
        SRLMIN(1) = E(2) * RLT/LENGTH
        SRL(1) = 10**((log10(SRLMAX(1)) + log10(SRLMIN(1)))/2.0)
cccccccccccccccccccccccccccccccccccccccccccccccccccccccccccccc
c  c            At time = infinity
c          SRLMAX(2) = 1.0/(1.0/E(1) + DE(2)) * RLT/LENGTH
c          SRLMIN(2) = 1.0/(1.0/E(2) + DE(1)) * RLT/LENGTH
c          SRL(2) = 10**((log10(SRLMAX(2)) + log10(SRLMIN(2)))/2.
cccccccccccccccccccccccccccccccccccccccccccccccccccccccccccccc
c    The compaction spring stiffness is:
        SCMAX = 0.87 * ((DEPTH - RLT)/2.0 * CS(1)/LENGTH)
        SCMIN = 0.87 * ((DEPTH - RLT)/2.0 * CS(2)/LENGTH)
        SC = 10**((log10(SCMAX) + log10(SCMIN))/2.0)
c    The URR shear stiffness spring constant is:
        SSMAX = URRSS(1) * LENGTH/(DEPTH - RLT)
        SSMIN = URRSS(2) * LENGTH/(DEPTH - RLT)
        SS = 10**((log10(SSMAX) + log10(SSMIN))/2.0)
c    The RL damper coefficient is;
        DRLMAX = (RLT**3)/(VC(2) * LENGTH)
        DRLMIN = (RLT**3)/(VC(1) * LENGTH)
        DRL = 10**((log10(DRLMAX) + log10(DRLMIN))/2.0)
c    The compaction creep coefficient is;
        DCMAX = 0.87 * ((DEPTH - RLT)/(2.0 * LENGTH * CC(2)))
        DCMIN = 0.87 * ((DEPTH - RLT)/(2.0 * LENGTH * CC(1)))
        DC = 10**((log10(DCMAX) + log10(DCMIN))/2.0)
c    The shear creep coefficient is;
        DSMAX = (LENGTH**3)/(SCC(2) * (DEPTH - RLT))
        DSMIN = (LENGTH**3)/(SCC(1) * (DEPTH - RLT))
        DS = 10**((log10(DSMAX) + log10(DSMIN))/2.0)
c
c
c
c    Now to arrange the output
       write(1,'(A)')' This was run using the following input val
       write(1,'(A)')'  '
       write(1,*)' Rubble field extent          ',EXTENT
       write(1,*)' Number of sails              ',SAILS
       write(1,*)' Sail height is               ',HEIGHT
       write(1,*)' Refrozen layer thickness     ',RLT
       write(1,*)' Water depth                  ',DEPTH
       write(1,'(A)')'  '
c
c
```

```
c    The following are the calculated values
       write(1,*)'   Coefficient               Max        Avg
       write(1,*)' -----------------------------------------------
       write(1,*)'  Sail Weight (N)               -    ',WS,'
       write(1,*)'  Keel Weight (N)               -    ',WK,'
       write(1,*)'  Ice/Ice Friction      ',IFRICMAX,IFRIC,IFRICM
       write(1,*)'  Ice/Soil Friction     ',SFRICMAX,SFRIC,SFRICM
       write(1,*)'  SRL (time = 0)        ',SRLMAX(1),SRL(1),SRLM
c       write(1,*)'  SRL (time = infinity) ',SRLMAX(2),SRL(2),SRL
       write(1,*)'  Spring Compaction     ',SCMAX,SC,SCMIN
       write(1,*)'  Spring Shear          ',SSMAX,SS,SSMIN
       write(1,*)'  Damper RL             ',DRLMAX,DRL,DRLMIN
       write(1,*)'  Damper Compaction     ',DCMAX,DC,DCMIN
       write(1,*)'  Damper Shear          ',DSMAX,DS,DSMIN
       end
```

```
*HEADING, UNSYMM
 14SEPT,1989:MODELLING GROUNDED ICE RUBBLE USING MATERIAL PROPERTY E
*PREPRINT,ECHO=NO,MODEL=NO,HISTORY=NO
********************************************************************
***********************************   NODES
********************************************************************
*NODE
**NOD   XCOORD   YCOORD
  11,     1.0,    0.0
  21,     2.0,    0.0
  22,     2.0,    0.0
  23,     2.0,    0.0
  31,     3.0,    0.0
  32,     3.0,    0.0
  33,     3.0,    0.0
  41,     4.0,    0.0
  42,     4.0,    0.0
  43,     4.0,    0.0
  51,     5.0,    0.0
  52,     5.0,    0.0
  53,     5.0,    0.0
  61,     6.0,    0.0
  62,     6.0,    0.0
  63,     6.0,    0.0
*NSET,NSET=RFLNODES
 11,21,31,41,51,61,62,63
********************************************************************
***********************************   FRICTION ELEMENT
********************************************************************
*ELEMENT,TYPE=GAPUNI,ELSET=FRICT
**  EL     LN     UN
     4,    23,    22
    14,    33,    32
    24,    43,    42
    34,    53,    52
    44,    63,    62
*GAP,ELSET=FRICT
**    GAP     XCOS     YCOS     ZCOS
      0.0,    0.0,     1.0,     0.0
*FRICTION
**    MU      K     FLIM (= LIMIT ON FRICTIONAL FORCE)
     0.71,  1.E12,    0.0
********************************************************************
***********************************   REFROZEN LAYER ELEMENT
********************************************************************
*ELEMENT,TYPE=C1D2,ELSET=MAT1
**  EL     N1     N2
     1,    11,    21
    11,    21,    31
    21,    31,    41
    31,    41,    51
    41,    51,    61
*SOLID SECTION,ELSET=MAT1,MATERIAL=RFL
**  CROSS SECTION AREA
```

```
 1.0
*MATERIAL,NAME=RFL
*ELASTIC
**  E
 1.90E09
*CREEP,LAW=STRAIN
**  A         N         M
 1.31E-25,   3,        0
********************************************************************
***********************************  SHEAR ELEMENT
********************************************************************
*ELEMENT,TYPE=C1D2,ELSET=MAT2
**   EL     N1    N2
      2,    11,   22
     12,    21,   32
     22,    31,   42
     32,    41,   52
     42,    51,   62
*SOLID SECTION,ELSET=MAT2,MATERIAL=SHEAR
**  CROSS SECTION AREA
 1.0
*MATERIAL,NAME=SHEAR
*ELASTIC
**  E
 1.42E08
*CREEP,LAW=STRAIN
**  A         N         M
 1.78E-26,   3,        0
********************************************************************
***********************************  COMPACTION ELEMENT
********************************************************************
*ELEMENT,TYPE=C1D2,ELSET=MAT3
**   EL     N1    N2
      3,    11,   21
     13,    21,   31
     23,    31,   41
     33,    41,   51
     43,    51,   61
*SOLID SECTION,ELSET=MAT3,MATERIAL=COMPACT
**  CROSS SECTION AREA
 1.0
*MATERIAL,NAME=COMPACT
*ELASTIC
**  E
 6.6E05
*CREEP,LAW=STRAIN
**  A           N        M
  4.6E-12,      1,       0
********************************************************************
***********************************  LOADING STEP
********************************************************************
*BOUNDARY
**NOD  DF  RANGE    U
  11,   2,   3,   0.0
```

```
  21,   2,   3,   0.0
  22,   3,   3,   0.0
  23,   1,   3,   0.0
  31,   2,   3,   0.0
  32,   3,   3,   0.0
  33,   1,   3,   0.0
  41,   2,   3,   0.0
  42,   3,   3,   0.0
  43,   1,   3,   0.0
  51,   2,   3,   0.0
  52,   3,   3,   0.0
  53,   1,   3,   0.0
  61,   1,   3,   0.0
  62,   3,   3,   0.0
  63,   1,   3,   0.0
*******************************************
*STEP, CYCLE=30,INC=2,AMPLITUDE=STEP
*STATIC,PTOL=1.0,DIRECT
 1.,1.
*CLOAD
**NOD   DF    FORCE
  11,   1,    267000.
  22,   2,    -54078.
  32,   2,    -54078.
  42,   2,    -54078.
  52,   2,    -54078.
  62,   2,    -54078.
*PRINT,RESIDUAL=NO,FREQUENCY=1
*EL PRINT,FREQUENCY=0
 S,E,CE11
*NODE PRINT,FREQUENCY=1
 U1,RF1,CF1,
*NODE FILE,NSET=RFLNODES
 U,RF
*END STEP
*******************************************
*STEP, CYCLE=10,INC=250
*VISCO,PTOL=2.0,CTOL=1.E-12
 0.1,1.0,1.E-4,1.0
*EL PRINT,FREQUENCY=0
 S,E,CE11
*PRINT,RESIDUAL=NO,FREQUENCY=10
*NODE PRINT,FREQUENCY=10
 U1,RF1,CF1,
*NODE FILE,NSET=RFLNODES,FREQUENCY=10
 U,RF
*END STEP
*******************************************
*STEP, CYCLE=15,INC=25000
*VISCO,PTOL=100.0,CTOL=1.E-10
 100.0,604800.0,1.E-4,250
*PRINT,RESIDUAL=NO,FREQUENCY=50
*EL PRINT,FREQUENCY=0
 S,E,CE11
```

```
*NODE PRINT,FREQUENCY=50
 U1,RF1,CF1,
*NODE FILE,NSET=RFLNODES,FREQUENCY=50
 U,RF
*END STEP
*********************************************
```